



<https://theses.gla.ac.uk/>

Theses Digitisation:

<https://www.gla.ac.uk/myglasgow/research/enlighten/theses/digitisation/>

This is a digitised version of the original print thesis.

Copyright and moral rights for this work are retained by the author

A copy can be downloaded for personal non-commercial research or study,  
without prior permission or charge

This work cannot be reproduced or quoted extensively from without first  
obtaining permission in writing from the author

The content must not be changed in any way or sold commercially in any  
format or medium without the formal permission of the author

When referring to this work, full bibliographic details including the author,  
title, awarding institution and date of the thesis must be given

Enlighten: Theses

<https://theses.gla.ac.uk/>  
[research-enlighten@glasgow.ac.uk](mailto:research-enlighten@glasgow.ac.uk)

**Design criteria for high resolution gamma-ray  
body counting systems.**

**THESIS**

**Submitted For The Degree of  
Master of Science ( M.Sc ) at The  
University of Glasgow**

*By;*

***NOURI ALI DROUGHI***

**The Scottish Universities Research and Reactor Centre  
East Kilbride, Glasgow**

**September 1992**

**© Droughi, Nouri , 1992**

ProQuest Number: 10992229

All rights reserved

INFORMATION TO ALL USERS

The quality of this reproduction is dependent upon the quality of the copy submitted.

In the unlikely event that the author did not send a complete manuscript and there are missing pages, these will be noted. Also, if material had to be removed, a note will indicate the deletion.



ProQuest 10992229

Published by ProQuest LLC (2018). Copyright of the Dissertation is held by the Author.

All rights reserved.

This work is protected against unauthorized copying under Title 17, United States Code  
Microform Edition © ProQuest LLC.

ProQuest LLC.  
789 East Eisenhower Parkway  
P.O. Box 1346  
Ann Arbor, MI 48106 – 1346

Thesis  
9324  
copy 1

GLASGOW  
UNIVERSITY  
LIBRARY

## CONTENTS

MEMORANDUM	I
ABSTRACT	II
LIST OF FIGURES	III
LIST OF TABLES	IV
ACKNOWLEDGEMENTS	V
DEDICATION	VI
ABBREVIATIONS	VII

### Page No.

## CHAPTER 1 INTRODUCTION

1.0	Introduction	
1.1	Standard Man Definition	2
1.2	The biokinetic lung model and exposure limit	3
1.3	Reasons for the research	5
1.4	Literature review	8
	1.4.1 NaI(Tl) detectors	10
	1.4.2 Phoswich detectors	10
	1.4.3 Germanium semi-conductor detectors	11
1.5	Body counting methods	12
1.6	Problems of body counting by in vivo measurements	13
	1.6.1 Background interference	14
	1.6.2 Gamma-ray absorption	14
	1.6.3 The levels of activity to be measured	16
	1.6.4 Distribution of radioactivity and detector response	17
	1.6.5 Detector calibration	18
1.7	Thesis outline	18

## CHAPTER 2 NATURAL AND MAN-MADE RADIONUCLIDES

2.1	Properties of radionuclides in the body	19
2.2	Uranium series	20
	2.2.1 Uranium in the Earth's crust	20
	2.2.2 Uranium decay series characteristics	20
	2.2.3 Uranium in the Body	21
2.3	Thorium series	24
	2.3.1 Thorium in the Body	25
2.4	Potassium-40	27
2.5	Man-made radionuclides	27
	2.5.1 Radiocaesium in the Body	29

## CHAPTER 3 THE THEORY OF COUNTING

3.1	Types of Gamma-ray interactions	32
3.1.1	The photoelectric interaction	32
3.1.2	Compton scattering	33
3.1.3	Pair production	33
3.1.4	Full energy peak	34
3.1.5	Single escape peak	34
3.1.6	Double escape peak	36
3.1.7	Compton edge	36
3.1.8	Backscatter peak	36
3.1.9	Compton plateau	36
3.1.10	Sum peak	36
3.2	Absorption coefficients	38
3.3	The theory of the germanium detection	38
3.3.1	The band energy theory	38
3.3.2	Detection principles and semiconductor detectors	39
3.4	Semi-conductor detector characteristics	40
3.4.1	Detector sensitivity	40
3.4.2	Efficiency calibration	40
3.4.3	Detector resolution (FWHM)	41
3.5	Sodium iodide detectors NaI(Tl)	43
3.5.1	Detection Principles	43
3.5.2	Sensitivity	43
3.5.3	Resolution	44
3.6	Peak-to-Compton ratios	44
3.7	Efficiency and energy calibration	45
3.8	Counting statistics	45
3.8.1	Counting error	45
3.9	Concepts of Minimum Detectable Activity	47
3.9.1	Critical level	47
3.9.2	Detection limit	50
3.9.3	Determination limit	51
3.10	Counting time	52
3.11	Energy Calibration	52
3.12	Efficiency Calibration	53
3.13	Shielding properties	53

## CHAPTER 4 SODIUM IODIDE DETECTOR BODY COUNTING STUDIES METHODS AND RESULTS

4.1	Description of the NaI(Tl) whole-body monitor	56
4.1.1	Mechanical system and electronic components	57
4.2	Data handling and software analysis programs	57
4.3	Investigation of NaI(Tl) body monitor parameters	61
4.3.1	Energy calibration-method	61
4.3.2	Background measurements	61
4.3.3	Minimum detectable activities	63

**CHAPTER 5 SEMI-CONDUCTOR GERMANIUM DETECTOR STUDIES**

<b>5.1</b>	<b>Introduction</b>	<b>68</b>
<b>5.2</b>	<b>Measurement with a 127cm<sup>3</sup> Ge-detector</b>	<b>70</b>
<b>5.2.1</b>	<b>The experimental set up</b>	<b>70</b>
<b>5.2.1.1</b>	<b>Detector and electronics</b>	<b>70</b>
<b>5.2.1.2</b>	<b>Shielding arrangements</b>	<b>70</b>
<b>5.2.2</b>	<b>Experimental method</b>	<b>71</b>
<b>5.2.2.1</b>	<b>Shielding reduction factor</b>	<b>71</b>
<b>5.2.2.2</b>	<b>Build-up the shield</b>	<b>71</b>
<b>5.2.2.3</b>	<b>Collimators effect</b>	<b>74</b>
<b>5.2.2.4</b>	<b>Graded shielding</b>	<b>74</b>
<b>5.2.2.5</b>	<b>Gain settings</b>	<b>76</b>
<b>5.2.2.6</b>	<b>Dead time losses</b>	<b>76</b>
<b>5.3</b>	<b>Analysis of gamma-ray spectra</b>	<b>78</b>
<b>5.3.1</b>	<b>Summation of gamma-ray spectrums</b>	<b>80</b>
<b>5.4</b>	<b>Results and discussion of the background data collected</b>	<b>80</b>
<b>5.5</b>	<b>Background interferences <sup>60</sup>Co and <sup>41</sup>Ar</b>	<b>83</b>
<b>5.6</b>	<b>Potassium-40</b>	<b>85</b>
<b>5.7</b>	<b>Standard source measurements</b>	<b>86</b>
<b>5.8</b>	<b>Calculation of sensitivity and detection limits</b>	<b>86</b>
<b>5.8.1</b>	<b>Background measurements</b>	<b>89</b>
<b>5.8.2</b>	<b>Barium-133 source</b>	<b>89</b>
<b>5.8.3</b>	<b>Thorium Measurement</b>	<b>90</b>
<b>5.8.4</b>	<b>Uranium measurement</b>	<b>91</b>
<b>5.8.5</b>	<b>Phantom measurement</b>	<b>92</b>
<b>5.9</b>	<b>Measurements with the planar Ge-detector</b>	<b>92</b>
<b>5.10</b>	<b>Measurement of standard sources</b>	<b>94</b>
<b>5.11</b>	<b>Calculated sensitivity and limits of detection</b>	<b>96</b>

**CHAPTER 6 FINALISED DESIGN CRITERIA**

<b>6.1</b>	<b>Simplistic comparison of the Ge and NaI(Tl) detectors for whole-body counters</b>	<b>97</b>
<b>6.2</b>	<b>Optimisation of a shield</b>	<b>98</b>
<b>6.3</b>	<b>Comparison of the performance of the Ge and NaI(Tl) detectors relevant to the body counting</b>	<b>98</b>
<b>6.3.1</b>	<b>A quantitative comparison of measured spectra</b>	<b>98</b>
<b>6.3.2</b>	<b>Potassium-40</b>	<b>102</b>
<b>6.4</b>	<b>The utilisation of the planar</b>	<b>105</b>
<b>6.5</b>	<b>Conclusions and general remarks</b>	<b>105</b>
<b>6.6</b>	<b>A proposed design for a high resolution whole-body monitor</b>	<b>107</b>

**REFERENCES**

## MEMORANDUM

The work described in this thesis was performed in the Nuclear Medicine and Health Physics Department of the Scottish Universities Research & Reactor Centre, East Kilbride, during the period from January 1990 to January 1992, under the supervision of Dr. B. W. East, the head of the Nuclear Medicine and Health Physics Department.

This thesis contains the results of some original research by the author, and no part of the material offered has previously been submitted by the candidate for a degree in this or any other university. Where use has been made of the results and conclusions of the other authors in the relevant studies, care has been taken to ensure that the source of information is always clearly indicated, unless it is of such general nature that indication is impracticable.



*Nouri Ali Droughi*

## Abstract

For several decades whole- and partial-body counters have used NaI(Tl) detectors for gamma-ray analysis which have provided good sensitivity but have possessed poor gamma-ray resolution.

With the increasing availability of more efficient germanium semi-conductor detectors, which offer high resolution gamma-ray spectrometry as well as workable sensitivity, body counting techniques are slowly changing over to their use either as an adjunct to or a replacement for NaI(Tl) or phoswich detectors.

This thesis contains a description of preliminary studies to investigate the requirements of germanium detector body counting systems with regard to shielding, background, detector volume and other relevant factors with the ultimate goal of setting up such a system at the Scottish Universities Research and Reactor Centre. Following recommendations made in recent years for the need to monitor members of the population, particularly those living near nuclear installations, the ability to measure the low energy photon emissions from such radionuclides as uranium, plutonium and americium, in addition to the high energy emissions from radiocaesium and other fission products now has a renewed emphasis in the field of body measurements. The thesis outlines some aims and progress towards the design and construction of "shadow-shield" body counting arrangements based on existing NaI(Tl) counter of this type but using a 30% efficient germanium detector and a thin planar germanium detector for trial measurements.

From a literature review combined with the observed data, a design for a whole-body counter is suggested which should enable the traces of natural decay series radioactivities in the body to be quantified in addition to the easily-measured body potassium. The best approach for  $^{241}\text{Am}$ , an indicator for the presence of plutonium, appears to be the measurement of the skull, tibia or knee where the overlying tissue is thin, reducing low energy photon attenuation. For population studies of radionuclides it may be possible to sum individual spectra to obtain adequate sensitivity and precision at the very low levels of activity expected.

## List of Figures

<u>Figure No.</u>	<u>Page No.</u>
1.1 Total mass-energy absorption coefficients bone and water.....	15
2.1 Uranium-238 decayscheme.....	21
2.2 Thorium-232 decayscheme.....	26
2.3 Potassium-40 decayscheme.....	26
2.4 Caesium-137 decayscheme.....	30
2.5 Caesium-134 decayscheme.....	31
3.1 Linear attenuation coefficient in Ge and NaI crystals for the main $\gamma$ -ray interactions.....	35
3.2 Typical gamma-rayspectrum.....	35
3.3 Types of gamma-ray interactions in a detector.....	37
3.4 A schematic diagram of electron energy band structure in a semiconductor crystal.....	37
3.5 Efficiency vs energy curve for 30% Ge-detector.....	42
3.6 Energy vs channel number.....	42
3.7 Graphical representation of critical level.....	49
3.8 Detection limit and its relationship to the critical level.....	49
3.9 A calibration plot of FWHM vs channel number.....	55
4.1 Representation of the Dual NaI(Tl) detector.....	58
4.2 Whole-body counter phantom background spectrum using the upper NaI(Tl) detectors.....	58
4.3 An example of a peak location methods for a given spectrum.....	60
4.4 Thorium-232 $\gamma$ -ray pulse height spectrum.....	66

4.5	Uranium-238 $\gamma$ -ray pulse height spectrum.....	66
5.1	The location of the proposed WBM at the SURRC.....	69
5.2	Electronic equipment lay-out.....	69
5.3	View the experimental set-up.....	72
5.4	Gamma-ray spectrum of open and closed shield.....	73
5.5	Variation of count rate with different wall roof shielding arrangement.....	73
5.6	Collimation effects on count rate.....	75
5.7	Ratios of count rate variations vs collimation factors.....	75
5.8	Gamma-ray spectrum variation with and without cadmium and copper sheets.....	77
5.9	Dead time regression analysis.....	77
5.10	Peak and background calculation methods used by Minigam II.....	79
5.11	Single and summed spectra variations.....	81
5.12	Argon-41 decay scheme.....	81
5.13	Cobalt-60 decontamination levels.....	84
5.14	Potassium-40 count rate inside shield.....	84
5.15	Normal and expanded $\gamma$ -ray spectra.....	87
5.16	Gamma-ray spectrum of mixed alpha source.....	87
5.17	Gamma-ray spectrum of thorium-232.....	88
5.18	Gamma-ray spectrum of uranium-238.....	88
5.19	Gamma-ray spectra of n-type planar Ge-detector inside the shadow-shielding arrangement.....	93
5.20	Effect of collimation on the planar Ge-detector inside the Experimental shielding.....	93

5.21	Normal and expanded gamma-ray spectrum of the mixed alpha source.....	95
5.22	Gamma-ray spectrum of $^{241}\text{Am}$ , $^{57}\text{Co}$ and $^{137}\text{Cs}$ .....	95
6.1	The suggested final shielding design arrangement for the Ge-detector whole-body counter.....	99
6.2	Potassium-40 count rate and its standard deviation inside the shield....	103
6.3	Observed and mathematical prediction for the potassium-40 count rate inside the shield.....	103

## List of Tables

<u>Table No.</u>	<u>Page No.</u>
1.1 Categories of performance criteria for direct bioassay.....	17
2.1 The intake of uranium-238 and thorium-232 series radionuclides by man...21	21
2.2 The mass activity concentration for certain human organs and tissues for $^{232}\text{Th}$ and $^{238}\text{U}$ .....	23
4.1 The main energies and detection sensitivities for NaI(Tl) detector using $^{226}\text{Ra}$ .....	61
4.2.1 The Background levels of the upper NaI(Tl) detector of the whole-body counter.....	62
4.2.2 Calculated detection parameters for the upper detector of the whole-body counter for a 65 hour count.....	62
4.3.1 Calculated detection parameters for the upper detector of the whole-body counter for a two hour count.....	63
4.3.2 Calculated detection parameters for the lower detector of the whole-body counter detector.....	64
4.5.1 Calculated detection parameters for the upper whole-body NaI(Tl) detector using thorium-232.....	65
4.5.2 Calculated detection parameters for the upper whole-body counter using a 1gm uranium-238.....	65
5.8.1 Calculated detection parameters for a two hour background count using the $127\text{cm}^3$ Ge-detector.....	89
5.8.2 Calculated detection parameters for a two hour $^{133}\text{Ba}$ count using the $127\text{cm}^3$ Ge-detector.....	90
5.8.3 Calculated detection parameters for a two hour $^{232}\text{Th}$ count using the $127\text{cm}^3$ Ge-detector.....	90
5.8.4 Calculated detection parameters for a two hour $^{238}\text{U}$ count using the $127\text{cm}^3$ Ge-detector.....	91

5.8.5	Calculated detection parameters for a chest phantom containing homogenous radionuclides using the 127cm <sup>3</sup> Ge-detector.....	92
5.11.1	Calculated detection parameters for a two hour count of a mixed alpha source using the planar Ge-detector.....	96
6.1	Comparison of the main detection parameters between the upper NaI(Tl) detector and the 127cm <sup>3</sup> Ge-detector for the background.....	100
6.2	Comparison of the main detection parameters between the upper NaI(Tl) detector and the 127cm <sup>3</sup> Ge-detector for <sup>232</sup> Th.....	101
6.3	Comparison of the main detection parameters between the upper NaI(Tl) detector and the 127cm <sup>3</sup> of the Ge-detector for <sup>238</sup> U.....	101

## **ACKNOWLEDGMENTS.**

I wish to express my sincerest gratitude to my supervisor, Dr Brian William East, for his expert advice and guidance, detailed criticism and continuous encouragement throughout this research project. I am very grateful to Mr. I Robertson for his kind assistance and the proof reading of the first manuscript which have been of great value for me. My special thanks to Dr T Preston whom I could contact for advice and help whenever I needed.

I am indebted to the late Mr. I Harris who participated in the first stages of research work and his help for me cannot be forgotten by his absence.

Special thanks are due to Mr W Traquair, whom without his assistance especially in the heavy Lead handling, this work would not have been completed. I would like to thank Dr D Sanderson for his scientific guidance and encouragement. Thanks are due to Prof. M Baxter for his early support and stressing the importance of this research project.

I would like to thank all the academic staff, technicians, research assistants and students for their moral support particularly Dr R Scott.

I wish to express my profound gratitude to my parents, brothers, sisters and friends for their great support and encouragement. I wish to acknowledge the moral support of my wife's parents and family.

I am also grateful to the Libyan people and the Secretary of scientific research secretariat for his personal approval of my scholarship. And to Mr M Elnamey for his kind assistance.

Last but not least, I would like to extend my special thank and admiration to my wife Latfia, for her endless patience and continuous support and encouragement throughout the study period.

**Dedication To My Uncle;  
Mohammed Mansour Berrfaad**

## GLOSSARY OF ABBREVIATIONS

<b>ALARA</b>	<b>As Low As Reasonably Achievable</b>
<b>ANSI</b>	<b>American National Scientific Institute</b>
<b>BEIR</b>	<b>Committee on the Biological Effect of Ionizing Radiation</b>
<b>BKGR</b>	<b>Background Radiation</b>
<b>BNF</b>	<b>British Nuclear Fuel Plc</b>
<b>COMARE</b>	<b>Committee on Medical Aspects of Radiation in the Environment</b>
<b>FWHM</b>	<b>Full Width at Half Maximum</b>
<b>IAEA</b>	<b>International Atomic Energy Agency</b>
<b>ICRP</b>	<b>International Commission on Radiological Protection</b>
<b>ICRU</b>	<b>International Commission on Radiological Units and measurements</b>
<b>IEEE</b>	<b>The Institute of Electrical and Electronic Engineers</b>
<b>MCA</b>	<b>Multichannel analyzer</b>
<b>MCB</b>	<b>Multichannel Buffer</b>
<b>MPC<sub>a</sub></b>	<b>Maximum Permissible concentration in air</b>
<b>MPC<sub>w</sub></b>	<b>Maximum Permissible Concentration in water</b>
<b>MPBB</b>	<b>Maximum Permissible Body Burden</b>
<b>NCRP</b>	<b>National Council on Radiation Protection and measurement</b>
<b>NRPB</b>	<b>National Radiological Protection Board</b>
<b>RWMAC</b>	<b>Radioactive Waste Management Advisory Committee</b>
<b>PM</b>	<b>Photomultiplier tube</b>
<b>ADCAM</b>	<b>Advanced Data Collection and Management system</b>
<b>UNSCEAR</b>	<b>United Nation Scientific Committee on the Effect of Atomic Radiation</b>

# **CHAPTER 1**

## **Introduction**

The deleterious effect of ionizing radiation on man was actually observed as early as 1500 when it was recognized there was a high incidence of lung disease among a group of miners in the Schneeberg cobalt pitchblende mine of Bohemia (Morgan,1970). It was not known then, of course, that death among these miners was caused by radon and its daughter products which leaked into the working areas of the mine from the uranium ores contained in the mineral deposits. In 1879 Herting and Hess (Morgan, 1967) performed the first postmortems on diseased miners and noted malignant growths in the lungs. It was not until 1911 that this was first shown by Arnstein (Sikl, 1950), to be lung carcinoma.

About the same time Grubbe (Grubbe,E.H., 1933), a manufacturer of Crooks tubes in Chicago, Illinois, (USA) in 1895 was perhaps the first person knowingly to receive biological damage from ionising radiation thus making the cause and effect link. He was using his equipment which generated ionising radiation, to study the fluorescence of chemicals even before the public press announcement on January 4th 1896 about Roentgen's discovery of X-rays.

The fact that there were hazards associated with exposure to these newly discovered materials and processes began to be apparent and Russ (Russ, 1916) made one of the first studies of the general "radiation protection" problem. Following his study in 1916, the British Roentgen Society unanimously adopted a resolution recognizing the hazards from X-ray examinations and recommended a number of precautionary measures. This was followed by the publication of the general recommendations and measures for x-ray and radium protection.

The first International Congress of Radiology (ICR), established the International Commission on Radiological Units (ICRU) in 1925. At the second

ICRP in 1928, the International Commission on Radiological Protection (ICRP) was formed. In the same year the ICRU took the important step of adopting the Roentgen as the unit of exposure, and the ICRP published the first set of international recommendations for ionizing radiation.

However, due to World Wars I and II, there was no coordination between different countries concerning radiation protection or its standards, even though during this time a great many discoveries had been made, especially the utilization of uranium in fission reactors and weapons. The production and use of fission products had increased markedly, especially in the United States of America and the United Kingdom representing a whole new range of "man-made" radioactive materials. A product of that research period was the first use of atomic technology in war when atomic bombs were dropped on Hiroshima and Nagasaki in August 1945.

From these early days it was recognised that the effects of ionising radiations could be considered to occur in two ways. Firstly by external exposure and secondly by internal exposure resulting from the intake of radio-active materials into the body. In order to understand radioactivity inside the body, much more data about the body's make-up and functioning was required. In 1949 a conference was held at the Chalk River National Laboratory in the USA, often referred to as the "*Chalk River Conference*", or "*The Standard Man Conference*" which was attended by many of the pioneers in the field of radiation protection at the time. They produced the first comprehensive documentation of standard quantities for use in the discipline of internal dosimetry which included among other things, the concept and definition of "Standard Man" and a Biokinetic Lung Model relevant to the intake of radioactive materials via this route.

### **1.1 The Standard Man definition.**

The definition of standard man is considered to be the foundation of internal dosimetry calculations and is a concept which has continued until the present day.

Body parameters such as the weights of organs, quantities of fluids taken in and excreted, rates of growth etc are set out based on average values for normal men, women and children in the population. These data can be used to define the behaviour of radioactive materials in the body and enable radiation doses to be assessed. They are contained in ICRP publications 2 and 23 and revised continually as knowledge advances.

## 1.2 The biokinetic lung model and exposure limit.

A complete lung model was defined and a limit of 0.3 rep (Roentgen Equivalent Physical) per week for the "critical" tissue was set. Also a set of secondary standards following from the limit were derived such as:- the Maximum Permissible Body Burden (MPBB); the Maximum Permissible Concentration in air (MPC<sub>a</sub>) and water (MCP<sub>w</sub>) which allowed the practical application of protection methods for particular radionuclides.

The Chalk River Conference documentation formed the basis of a report in the British Journal of Radiology (Stanford, 1955) which was subsequently expanded, modified and issued as ICRP Publication 2. This was later in turn revised in Publication 6 and became the handbook for radiation protection for unsealed radiation sources until the late 1970's when it was replaced with publication 30 (ICRP 30).

The last major recommendations of the ICRP were given in ICRP 26, published in 1977, and most recently, significant modifications were contained in ICRP 60, published in 1990 in which recommended limits for exposure to ionising radiations were generally lowered to the lowest that they have ever been.

Two other important bodies regularly review the vast amount of data on radiation hazards and produce regular reports. They are - The United Nations Scientific Committee on the Effects of Atomic Radiation (UNSCEAR), whose most recent report was in 1988, and the Committee on the Biological Effects of Ionizing

Radiation (BEIR), which last reported in 1989. Together with other recognised international and national bodies such as the International Atomic Energy Agency (IAEA); the National Council on Radiological Protection (NCRP) in the USA and the National Radiological Protection Board (NRPB) in the UK, the ICRP has been responsible for the evolution of concepts and the introduction of a tremendous amount of data regarding radiation protection dosimetry and standards.

As implied by the concept of internal exposure, one of the requirements for the application of radiation protection principles is a knowledge of radioactivity in the body of the exposed individual. Measurements of radioactivity and radiation in the individual's surroundings and the application of models can provide excellent information when body metabolism and the form of the radioactivity is known, but these factors can only be checked ultimately by direct measurements of body radioactivity content. Biological analysis of body excretions can be very useful for this purpose but is essentially indirect and still dependent on a knowledge of body metabolism. Rather than examining body excretions indirectly, there is always the possibility of more direct measurements for gamma emitting radionuclides which can be observed outside the body with external detectors. Clearly, energetic gamma emitters (above 100 keV) are relatively easy to detect outside the body because their emissions are not attenuated too greatly. Much work has been done on such materials over the decades since World War II.

Detector systems have improved also with time and there is always an interest in applying the latest techniques in order to explore the possibility of obtaining better data. An example here is the much improved resolution of germanium semi-conductor detectors compared with sodium iodide detectors for measuring gamma radiations which can help to separate the signals from mixtures of radionuclides much more easily. As a result of the nuclear fuel cycle which can give rise to the contamination of the surroundings with actinides as well as fission products, considerable interest has developed in recent years in the measurement of the body content of the former materials.

Occupationally exposed individuals have always been of concern in this respect but there is also much more interest in how members of the public at large may or may not be affected by trace amounts. The problem is that the actinides are principally alpha particle emitters undetectable outside the body. Where gamma rays are also emitted these are often of very low energy as are any associated X-rays, and these are not easily measurable outside the body because of severe attenuation. The accurate measurement of actinides and other low energy emitters such as decay series daughters therefore represents a considerable challenge but is also of great interest in the final confirmation of intake models and in the assessment of cause and effect hypotheses. The substance of this thesis is work on semi-conductor germanium detectors applied to the problems of body radioactivity measurement with the aim of providing high resolution facilities and means of measuring actinide elements.

### **1.3 Reasons for the research.**

Facilities for the measurement of radioactivity in people are relatively expensive and therefore are not usually applied widely. There is a continuing need for them in the occupational context in order to monitor radiation workers and to check compliance with rules and regulations under both routine operation or in accident conditions and their cost forms part of the operational picture in these circumstances. In recent years the public awareness of the possible risks involved with exposure to ionising radiations nationally and internationally has increased. Environmental discharges of radioactivity in the UK due to the enrichment, fabrication and reprocessing of fuel for nuclear reactors at Sellafield and the reactor accident at Chernobyl in the former Soviet Union have contributed to this increased awareness. At the same time the pressures against radioactive contamination of the environment have also increased. All this leads to the first reason why the design of improved body monitoring systems has been undertaken in this work.

While monitoring of the environment by field analysis can provide information on radioactive content, the need for developing methods of monitoring of the general public in order to check models would also seem to have become greater. More specifically, in the UK, the apparent existence of clusters of excess cases of leukaemia near atomic energy establishments has focused attention on the possible link with radiation exposure, particularly from traces of plutonium. As a consequence, the British government set up an Independent Advisory Group, chaired by Sir Douglas Black, to investigate whether the leukaemia cluster observed in Cumbria, NW England, could be due to or linked with the frequent radioactive discharges from Sellafield. Their first report entitled "Investigation of the possible increased incidence of cancer in West Cumbria" (Black report, 1984), confirmed an increased incidence of leukaemia, especially among young children. The increase was found to be about a factor of four above the figures for the national incidence. Also the Advisory Group made a number of very significant recommendations to the Government. One of these was to establish a committee, known as the Committee On Medical Aspects of Radiation in the Environment (COMARE) to monitor environmental/medical problems.

The other recommendation (number 6) of the same report suggested that more attention should be directed to the measurement of radiation levels in a wider spectrum of the general public at as sensitive a level as proved to be possible. The use of the word "feasible" in the report is the challenge here in relation to body measurements because whereas  $\gamma$ -emitting radionuclides such as radiocaesium are relatively easy, the measurement of actinides such as plutonium, which is strongly implicated in the causation of cancers, is much more difficult because of its very "soft" electromagnetic emissions. Later, the COMARE committee reviewed more up-to-date data and new scientific findings about the leukaemia clusters, and published its conclusions in 1986 (COMARE report, 1986). Two years later a second report (COMARE reports, 1988) investigated the incidence of childhood leukaemia around Dounreay, the nuclear plant in the north of Scotland and confirmed an increase in the incidence of cases, but could find no evidence of an association with radiation exposures.

The most recent studies of the same phenomena have observed an excess number of affected children around Dounreay and have associated the increase with parental exposure to high doses of radiation (COMARE, 1989) and (Urquhart, *et al.*, 1991). It is particularly the problems of providing answers to some of the questions raised by these findings by means of improved monitoring of the population as originally recommended by Black which provides the principal incentive for the present work, directed towards the investigation of body actinides and related radioactivities by body counting.

A second reason for the work is in relation to natural radioactivity. The contribution from radon to the annual radiation dose received by a member of the general public in the UK is now estimated to be some 47% ( 1270 $\mu$ Sv ) on average ( NRPB report R227, 1989). This value is based on the monitoring of homes by means of integrating dosimeters which record concentrations of radon in the air in Bq m<sup>-1</sup> from which dosimetry is calculated. In some areas of the UK such as Cornwall, annual radiation doses of up to 20mSv can be received.

One method of confirming these values would be to measure radon and its daughters in the body. Radon can, in principle, be measured in exhaled breath but would only be possible soon after exposure. Radon daughter products would be more persistent in the body and could provide a longer term indication of exposure.

However, because of either their soft electromagnetic emissions or their short half-lives, they are very difficult to measure unless sensitive, high resolution detector systems can be used together with other techniques such as spectrum summing from population samples or groups. In addition, the levels of these materials in members of the population are extremely low except possibly in people from high radon areas. While NaI(Tl) detectors can provide high sensitivity they cannot resolve many of the features present in the body spectrum eg the 63.5 keV photopeaks from <sup>234</sup>U and the 93.5 keV from <sup>234</sup>Th ( U&Th decay series ). Germanium detectors could do this provided sufficient sensitivity can be obtained to give acceptable counting times for *in vivo* measurement.

Therefore it would appear that there is a significant need for further investigation ( literature and experimental ) of high resolution systems in order to assess the feasibility of such systems as a method of obtaining solutions to these important problems.

#### 1.4 Literature Review.

The need to detect and ascertain the amount of radio-activity in the human body arose with the first wide spread appearance of artificial or "man-made" radionuclides following the atmospheric atomic bomb tests of the early 1950's. Also the increasingly widespread use of ionizing radiation in various scientific and technological fields, including nuclear energy, has been accompanied by increased external, as well as, internal exposure.

The internal dosimetry field has come to comprise the estimation of the radiation dose to the individual organs and the whole body from radioactive material contained within the body (Traub and Robinson, 1986). It is a well known fact that radioactive nuclides may enter the body by any of the following routes: inhalation, ingestion, injection and absorption through the skin. In order to determine the amount of activity and to estimate the dose delivered to the whole body account has to be taken of the possible concentration of radionuclides in different organs. The effective dose ( $H_E$ ) to the whole-body can be found by modifying the equivalent dose ( $H_T$ ) received by each organ using the respective tissue weighting factor ( $W_T$ ) and summing the weighted equivalent doses as follows;

$$H_E = \sum (W_T \cdot H_T)$$

To assign tissue weighting factors, the ICRP and NCRP have taken into consideration the different mortality risk factors from cancer and severe hereditary effects associated with irradiation of different organs and tissues of the body.

Measurements of body radioactivity can be carried out by two main methods as follows:

i) Biological or *in vitro* analysis.

This method assays radionuclides in biological materials such as excreta i.e urine, faeces, saliva and tissue samples. It will not be dealt with further as it is outside the remit of this research project.

ii) Body counting or *in vivo* analysis.

This involves the direct measurement of penetrating radiation from the radionuclides present within the body by using appropriate detection systems such as whole or partial body counters.

Direct body radioactivity measurement facilities or whole body counters have been in use at a number of major laboratories all over the world (Directory, IAEA, 1970). They frequently consist of one or a number of high efficiency detectors mounted inside a well-shielded low background enclosure. The actual geometrical configuration of these detectors is made to suit the purpose of the measurement carried out i.e whole body or partial body (organ) measurement. They can provide a quick and convenient estimate of activity in the body. As mentioned earlier, this approach is feasible only for those radionuclides emitting radiations with enough energy to escape from the body. In principle, therefore, this technique can only be used for radionuclides that emit X-or  $\gamma$ -rays or positrons detectable by their annihilation radiation. Most alpha-emitting radionuclides such as thorium, uranium and the transuranic elements emit only low-energy photons and soft X-rays in low abundance following their alpha decays and require special systems for their detection. Other  $\gamma$ -ray emitting radionuclides such as  $^{131}\text{I}$ ,  $^{137}\text{Cs}$  and  $^{60}\text{Co}$ , can be detected with comparatively simple detection equipment at low levels of detection (Masse and Bolton, 1970).

Some of the types of detectors which have been in use for many years are as follows:

#### 1.4.1 NaI(Tl) detectors.

Since Marinelli's use of NaI(Tl) detectors for *in vivo*  $\gamma$ -ray spectroscopy studies in the early 1950's, this type of detector has been the most widely used for the measurement of internally deposited  $\gamma$ -ray emitting radionuclides (Toobey, *et al.*, 1983). At present, most whole-body radioactivity measurement facilities, whether high-sensitivity or single systems, use thallium-activated sodium detectors because they have the advantage of high efficiency for the detection of medium and high energy  $\gamma$ -rays because of the large volume of the crystals which can be manufactured relatively cheaply.

#### 1.4.2 Phoswich detectors.

Another detector system in use is the phoswich detector derived from phosphor sandwich, which employs a combination of two dissimilar scintillation materials, NaI and CsI typically, optically coupled to a single photomultiplier (PM) tube. The detector uses the principle that the differences in the fluorescent decay times of CsI and NaI ( 1.1 and 0.25 usec respectively ) can be distinguished electronically. In addition to that, the higher energy photons are principally detected in the thick (50mm) CsI crystal which means they are eliminated from the low energy spectra seen by the thin NaI crystal (Wrenn and Blanchard, 1971).

The scintillators are chosen to have different decay times so that the shape of the output pulse from the PM tube depends on the relative contribution of scintillation light from the two scintillators and therefore can be distinguished by pulse shape difference. Even though they give increased sensitivity for the low energy peaks, their resolution is still poor and extended regions of integration from about 40 keV to 125 keV are necessary in order to capture the full peak width of both the 63 keV and 93 keV photons from natural uranium and  $^{234}\text{Th}$  respectively.

### 1.4.3 Germanium semi-conductor detectors.

Within the last two decades there has been rapid development of semiconductor detectors such as lithium-drifted germanium (Ge(Li)) and hyper-pure germanium (HPGe) detectors (Falk, *et al.*, 1979). NaI(Tl) and phoswich detectors are now being superseded for some purposes by these high resolution detectors which can be especially designed to have high efficiency at low energies (Lane, *et al.*, 1985). King (King, 1987) and, Beger and Goans (Beger *et al.*, 1981) have described an array of high-purity planar germanium detectors for the measurement of plutonium in the lungs through the detection of the  $L_{1\alpha}$  and  $L_{\beta 1}$ -X-rays (Np, 17.2-20.2 keV). Palmer and his colleagues at the Pacific North West Laboratory in the USA have thoroughly investigated the performance of different types of germanium detectors and detector arrangements. They (Palmer *et al.*, 1981), have shown that the superior resolution of germanium detectors, results in an advantageous peak-to-Compton ratio. It results in a narrower spectral regions which can be used for background determination which in turns enhances sensitivity for the measurement of low-level, low-energy photon emitters in different organs of the human body than that achieved using plain NaI(Tl) or phoswich-type detectors (Palmer and Rieksts, 1985). The greater resolution results in lower standard deviation of the background which in turn increases the sensitivity and reduces the background contributed by other body radioactivity i.e potassium-40 (Newman, 1985). Using a number of hyper-pure germanium detectors, Palmer has shown that even though the detection sensitivity of the germanium detectors is lower than the other types of detectors, it is sufficient to identify and even quantify uranium and transuranic radionuclides within the human body which cannot otherwise be measured at low levels by NaI(Tl) and NaI-CsI phoswich detectors.

Significant advances in the measurement of  $^{239}\text{Pu}$ ,  $^{241}\text{Am}$ ,  $^{235}\text{U}$  and  $^{238}\text{U}$  have been made during the last decade due to the availability of these advanced detectors and the improved use of other supporting factors for accurate detection and calibration such as well constructed phantoms which provide realistic monitoring

geometries accurately representing the attenuation properties of human tissue ( Griffith *et al.*, 1978 ). Recently Palmer, (1991) using large area germanium semiconductors in a whole-body monitor, reported promising results for the identification of low-energy photon emitters. The utilisation of these large-area semi-conductor detectors as standard equipment for monitoring classified workers as well as members of the public, could enable precautionary screening to be carried out. This could allow accurate detection and assessment of the long-term accumulation of such radionuclides in the body and, in turn, the evaluation of the dose commitment resulting from low-level, low-energy emitters in the actinide group of radionuclides.

### **1.5 Body counting methods.**

Direct methods of the assessment of internally deposited radioactivity, especially of low concentration, low energy emitters such as uranium and plutonium have been investigated by a number of scientists. Various types of detectors and detector shielding arrangements have been tried over the past two decades. Combinations of large NaI(Tl) crystals with thin (beryllium) casings, housed inside steel room shields are common. The shielded room is preferably made of low activity steel and in the UK pre-1945 naval steel known to be free from artificial radioactivities is recoverable and frequently used. Thicknesses of 12.5cm are typical with the inner surface often lined with 3-5mm of aged lead (Morsy, 1971). Early types of germanium detectors provided excellent resolution even for the low-energy X-and gamma rays but their main drawbacks were much lower sensitivity than NaI(Tl) or gas counters and higher cost. With recent advances in gamma spectroscopy and supporting computer technology the current state-of-the-art detection of actinides is by means of an array of hyper-pure germanium detectors either in planar configurations for low energy photons <100 keV or large volume coaxial arrangements (Palmer and Rieksts, 1991).

One of the most notable differences between NaI(Tl), phoswich, and germanium detectors for in-vivo measurements is the capability of identifying and quantifying

the main background spectral lines, from the radon-progeny peaks in the latter detectors. Because of the low resolution of NaI(Tl) detectors, their background spectral lines for  $^{214}\text{Pb}$  and  $^{214}\text{Bi}$  peaks are masked by the Compton continuum and appear at the best as broad "humps". Any other low energy photopeak in the region will also be masked and unidentifiable.

As well as the advantages of higher resolution, recent advances in data handling such as stripping, spectrum expansion and addition of gamma-ray spectra have made the gamma-ray spectroscopy analysis easier. The detection parameters make it possible to come close to "matching" the latest recommendations of NCRP-30 and the ANSI 13.3 regarding the measurement of activities corresponding to the Annual Limits on Intake (ALI) and the dose commitment of relevant actinides. For example, using an array of hyper-pure germanium detectors in a steel room, Palmer was able to detect the 185 keV gamma photon energy of  $^{235}\text{U}$  down to 0.034nCi (1.3Bq) at 95% confidence. This is equivalent to 2.2mg of total natural uranium.  $^{235}\text{U}$  can also be measured using the same system via the 63 keV or 93 keV  $\gamma$ -rays down to 0.50nCi(19Bq) which is equivalent 1.9mg of  $^{235}\text{U}$ .

#### 1.6 Problems of body counting by *in-vivo* measurement.

Individual monitoring by whole-body measurement can be carried out on exposed workers to demonstrate the maintenance of satisfactory working conditions and provide a warning sign of any departure from normality. It can also be used for screening of the general public, especially for "critical groups" who live near nuclear establishments (high risk group). In order to carry out such monitoring programmes and follow the Black report recommendations, together with those of the NCRP and NRPB, very reliable, sensitive and high resolution detection systems are necessary. In attempting to design a suitable system the following factors need to be considered and studied carefully:

### **1.6.1 Background interferences.**

One of the most important factors requiring consideration is the detector background and its control which greatly affects the detection limit. The sensitivity of counting ( $\gamma$ -ray spectrometry) is inversely related to the square root of the background. Main causes of the background recorded by the detector are natural or artificial radioactive elements distributed in the surroundings and components of the detector and also a considerable contribution of the cosmic radiations. The background can be minimised in two ways; firstly by selecting specially designed detector systems containing components with low levels of radioactivity; secondly by shielding the detection system in a very low background arrangement i.e. an expensive complete steel room. For body counting these ideal requirements must be balanced against the fact that there is always background radiation coming from radioactivity present in the body so that while it can be worthwhile making shielding from external sources of radiation as effective as possible, there may be little point in using "low background" (and expensive) components in the detector assembly itself. Palmer has stated that in his arrangement, about two-thirds of the background comes from the body and only about one-third can be attributed to the detector, shielded room and cosmic-ray interferences.

Once the background has been determined for a particular arrangement another important requirement is that it is kept constant and checked frequently.

### **1.6.2 Gamma-ray absorption.**

As previously mentioned, the transuranic nuclides decay predominantly by alpha particle emission and subsequent electromagnetic emissions often have low-energy as well as low abundance. In body counting considerable attenuation by overlying tissues can result depending on the site of deposition within the body. For instance, when counting low-energy x and gamma rays in the lungs, the chest wall thickness overlying the lungs is critical. A tissue thickness of 10mm will transmit only 25% of the 17 keV  $L\beta_1$  x-ray from  $^{239}\text{Pu}$ . Bone will cause even

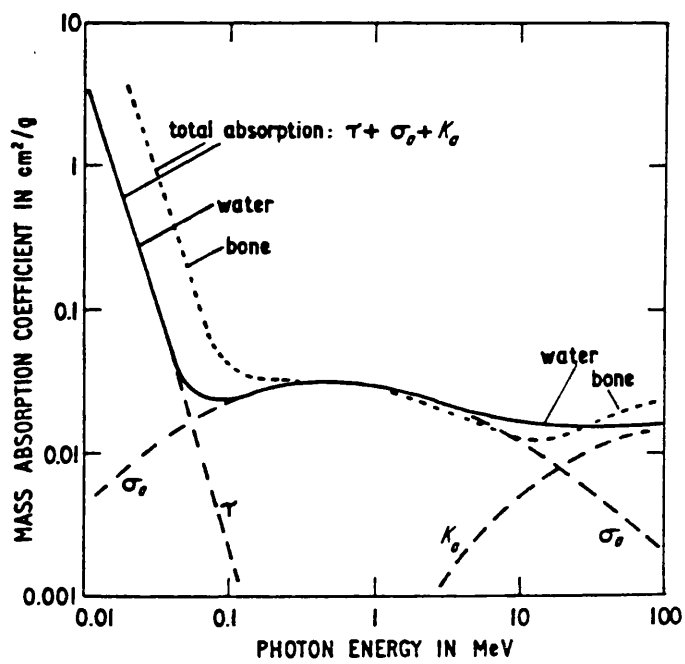


**Figure 1.1 Total mass-energy absorption coefficients for bone and water.**

more attenuation. Figure 1.1 shows the different mass attenuation (absorption) coefficients for water, which constitutes about 80% of body weight, compared with those for bone (Woodard,1975).

### **1.6.3 The levels of activity to be measured.**

Embodied in the system of dose limitation is the concept requiring that all ionising radiation exposure to be As Low As Reasonably Achievable (ALARA), taking into consideration all the economic and social factors. The latest national and international recommendations have resulted in the lowering of all the primary dose limits and secondary derived quantities such as ALI's and DAC's to both the general population and specified workers.

In line with keeping exposure as low as possible the American National Standard Institute have issued their latest performance criteria for radiobioassay (ANSI N13.3, 1990). Its purpose is to provide the required accuracy, precision and the acceptable minimum detectable amount for bioassay by direct *in vivo* and indirect *in vitro* methods. Table 1.1 presents the different categories and performance criteria for the direct bioassay.

In terms of *in vivo* body measurement this has increased the requirement for equipment and methods of higher sensitivity to measure the correspondingly smaller amounts of radioactivity.

CATEGORY	ORGAN	ACCEPTABLE MDA*	NOTES
L X-rays of Transuranim	LUNGS	185Bq (5nCi)	sum of $L_{\alpha}$ , $L_{\beta}$ , and $L_{\gamma}$ X-rays
Americium-241	LUNGS	26Bq (0.7nCi)	-----
Thorium-234	LUNGS	1110Bq (30nCi)	-----
Uranium-235	LUNGS	7Bq (0.2nCi)	-----
Fission and activation products	Lungs	740Bq/abundance (20nCi)	Abundance $\equiv$ number of photons per decay
Fission and Activation product	TOTAL BODY	740Bq/abundance (20nCi)	-----
Radionuclides in Thyroid	THYROID	740Bq/abundance (20nCi)	-----

Table 1.1 Category of performance criteria for direct bioassay (ANSI 13.30).  
 \* MDA-the minimum detectable activity which is the minimum activity of a radioactive isotope that can be identified in the presence of a certain background. It is explained further in Chapter 3.

#### 1.6.4 Distribution of radioactivity and detector response.

The concentrations of the different transuranic nuclides in body organs are not always uniform. Hence, to get accurate measurements of the deposition pattern and distribution levels it is necessary to have either: a multi-detector system whereby different organs are measured at the same time; or a detector arrangement that allows for counting in different body locations. In this way non-uniformity in distribution can be allowed for.

### 1.6.5 Detector calibration.

In order to determine the detector response in terms of counting rate per unit activity ( cpm.Bq<sup>-1</sup> ) it is necessary to calibrate for a given geometry using special models or "phantoms" designed to simulate the human body. The accuracy of the simulation depends upon the overall accuracy required and economic resources available since the models can be expensive to construct. An example of a very detailed torso model is the Lawrence Livermore phantom fabricated from tissue equivalent materials and containing known quantities of the actinides.

### 1.7 Outline of studies.

The main aim of the research project is to investigate the design and optimization of body counting techniques using semi-conductor detectors capable of resolving the natural decay-series daughters, from <sup>238</sup>U etc., and measuring the low energy photons emitted from radionuclides of the actinide group. In order to carry out such studies a thorough investigation of the main characteristics of the two types of available detector is undertaken. A qualitative and comparative examination of background spectra to identify the peaks present i.e natural decay series and <sup>40</sup>K for the 30% germanium and the NaI(Tl) detector is carried out. The requirements for a prototype shadow-shield body counting arrangement for the study of low-energy and low-level radionuclides deposited *in vivo* are assessed, particularly statistical analyses of observed background measurements. Values for the background levels are used to derive critical levels and lower limits of detection for the radionuclides of interest for the various detectors. A final design for a versatile prototype body counting arrangement is suggested, aimed at providing optimum background reduction combined with cost effectiveness.

## **CHAPTER 2**

## **Chapter 2**

### **Natural and man-made radionuclides**

#### **2.1 Properties of Radionuclides found in the body.**

Before measurements of any particular radionuclides in the human body can be attempted, a knowledge of their pertinent radiological characteristics and their body metabolism is necessary. In relation to the work described here, the  $\gamma$ -ray emissions are specially important and details of their emission and attenuations need to be understood. Generally speaking, the naturally occurring radionuclides which would be expected to be found in the body would be the same as those which occur in nature and which could enter the body through the main routes of ingestion and inhalation. However, their intake and retention fractions would be expected to be governed by metabolic and biological factors which would alter their quantitative uptake and retention in comparison to the environment. In addition to the "natural" radionuclides, examples of "man-made" radionuclides in the body would be those entering via contamination of the environment or those handled occupationally and ultimately taken up more directly.

The so-called "primordial" terrestrial radionuclides which are likely to be of most significance are the uranium-238, thorium-232 decay series, and potassium-40. These all have half-lives of the same order as the age of the earth and therefore occur in the earth's crust. Under normal circumstances they or their daughters would be expected to be found in the human body, in trace amounts in the case of the actinide series, and in gramme quantities in the case of potassium which is an essential electrolyte.

The principal "man-made" radionuclides, consist of the fission and activation products from nuclear reactor operations and nuclear weapons production and these can also find their way into the body as a result of contamination of the environment and subsequent human intake, or by occupational use. Some of the

most significant of these are strontium-89, strontium-90, caesium-134, caesium-137, iodine-131 and carbon-14. However, since iodine-131 is short-lived ( $T_{1/2}=8$  days) and strontium and carbon are beta emitters, only the radiocaesium nuclides are left as the main  $\gamma$ -emitters detectable by body counting in the long term.

## 2.2 Uranium Series.30

### 2.2.1 Uranium in the Earth's crust.

According to Katz and Seaborg (1957), uranium is widely distributed in nature. Although a few ores contain a high concentration of uranium of about 40-60%, some 100 mineral species contain in the region of 1% (Katz and Seaborg, 1957). The average concentration of uranium in the earth's crust is about  $4 \times 10^{-4}\%$  and in sea water about  $3.3\mu\text{g}$  per litre (Keen, 1968). For these reasons and because uranium is normally present in soil, building materials (Hamilton, 1970), air (Hamilton, 1971) and drinking water in measurable concentrations, it is considered a really ubiquitous element that together with its daughters irradiates all living creatures on earth.

### 2.2.2 Uranium decay series characteristics.

A simplified diagram of the uranium-238 decay series is given in Figure 2.1. It can be seen that it is divided into four sub-series in which the activity of the precursor controls to a large extent the activity of the decay product;  $^{238}\text{U} \rightarrow ^{234}\text{U}$ ;  $^{230}\text{Th} \rightarrow ^{226}\text{Ra}$ ;  $^{222}\text{Rn} \rightarrow ^{214}\text{Po}$ ;  $^{210}\text{Pb} \rightarrow ^{210}\text{Po}$ .

If no disturbance of the system has occurred such as when separation of daughters occur over geological time due to their different aqueous solubility. Which means that a secular equilibrium will exist between all the members of decay chain so that each member will exhibit the same activity. If disturbances have occurred, then the chain will be in disequilibrium with altered activities and ratios. The various members of the series emit a number of alpha, beta and

gamma radiations which finally decay to the stable radionuclide, lead-206.

### 2.2.3 Uranium in the body.

The metabolism of uranium and its related compounds has been investigated since uranium salts were first used in the treatment of diabetes mellitus during the 19<sup>th</sup> century and also in a number of studies on toxicity of compounds after the construction of the uranium enrichment facilities in the USA.

Table 2.1 gives the mean values of intake via the main routes of ingestion and inhalation of all the sub-series of <sup>238</sup>U and <sup>232</sup>Th. Table 2.2 shows the mass activity concentration values in ( mBq kg<sup>-1</sup> ) of the different sub-series in certain body organs and tissues (UNSECAR,1988).

Source	Annual Intake in (Bq) Inhalation	Annual Intake in (Bq) Ingestion
<sup>238</sup> U Series		
<sup>238</sup> U	0.01	5
<sup>230</sup> Th	0.01	2
<sup>226</sup> Ra	0.01	15
<sup>222</sup> Rn	200000	300
<sup>210</sup> Pb	4	40
<sup>210</sup> Po	0.	40
<sup>232</sup> Th Series		
<sup>232</sup> Th	0.01	2
<sup>228</sup> Ra	0.01	15
<sup>220</sup> Rn	100000	-

**Table 2.1 The Intake of uranium-238 and thorium-232 series radionuclides by man (UNSCEAR 88).**

238U Series

Nuclide	Half-life	Major gamma radiation energies (keV) and intensities	
238U 92	4.51x10 <sup>9</sup> Y		
↓ α			
234Th 90	24.1d	63.5 (5.7 %)	93.5 (3.6 %)
↓ β <sup>-</sup>			
234Pa <sup>m</sup> 91	1.17m	766.6 (0.30 %)	1001.4 (0.60 %)
(99.87%) β <sup>-</sup> IT(0.13%)			
↓ β <sup>-</sup>			
234Pa 91	6.75h	131.2 (20.0 %)	569.5 (10.7 %)
↓ β <sup>-</sup>			
234U 92	2.47x10 <sup>5</sup> Y	53.1 (0.2 %)	
↓ α			
230Th 90	8.0x10 <sup>4</sup> Y	67.8 (0.6 %)	142.0 (0.07 %)
↓ α			
226Ra 88	1602Y	186.2 (4 %)	
↓ α			
222Rn 86	3.82 d	510 (0.07 %)	
↓ α			
218Po 84	3.05m		
(99.98%) α      β <sup>-</sup> (0.02%)			
↓ α			
214Pb 82	26.8m	241.0 (7.6 %)	295.2 (18.9 %)
↓ β <sup>-</sup>			
214Bi 83	19.7m	609.3 (41.2 %)	934.0 (3.8 %)
↓ α			
214Po 84	164us	1120.4 (13.6 %)	1155.3 (2.7 %)
↓ α			
210Pb 82	13m	1238.8 (4.3 %)	1378.1 (4.7 %)
↓ β <sup>-</sup>			
210Bi 83	5.01d	1407.9 (2.7 %)	1764.6 (15.8 %)
↓ α			
210Po 84	138.4d	799.0 (0.014 %)	
↓ α			
210Pb 82	21Y	296.0 (80 %)	795.0 (100 %)
↓ β <sup>-</sup>			
210Bi 83	5.01d	1060.0 (12 %)	1210.0 (17 %)
↓ α			
210Po 84	138.4d	1310.0 (21 %)	
↓ α			
206Pb 82	Stable	46.5 (4 %)	
↓ β <sup>-</sup>			
210Bi 83	5.01d		
(-100%) β <sup>-</sup> α (0.0013%)			
↓ β <sup>-</sup>			
210Po 84	138.4d	803.0 (0.0011 %)	
↓ α			
206Pb 82	4.19m		
↓ β <sup>-</sup>			
206Pb 82	Stable		

Intensities refer to percentage of disintegrations of the nuclide itself, not to original parent of series

Figure 2.1 Uranium-238 decay scheme.

Source	Lungs	Trabecular bone	Kidney	Liver	Other tissues
<b><sup>238</sup>U-Series</b>					
<sup>238</sup> U	15	50	5	3	2
<sup>230</sup> Th	20	70	10	7	0.3
<sup>226</sup> Ra	2.7	170	2.7	2.7	2.7
<sup>222</sup> Rn	100	-	-	-	-
<sup>210</sup> Pb	200	3000	200	200	200
<sup>210</sup> Po	100	2400	200	200	200
<b><sup>232</sup>Th-Series</b>					
<sup>232</sup> Th	20	24	3	2	0.15
<sup>228</sup> Ra	15	50	10	5	0.5
<sup>220</sup> Ra	40	-	-	-	-

**Table 2.2 The mass activity concentration for certain organs and tissues for <sup>232</sup>Th and <sup>238</sup>U in mBq kg<sup>-1</sup> (fresh weight) (UNSECAR 88).**

In terms of body content, Reference Man contains 90 $\mu$ g of uranium with 60 $\mu$ g in the skeleton and 30 $\mu$ g in the soft tissues as a result of ingestion (Reference Man, ICRP 23). Its decay daughters which are of most interest in the present studies are radium-226, bismuth-214 and lead-210 because they emit gamma rays with the possibility of detection outside the body. Details of the emissions of these radionuclides are as follows:

<u>Isotope</u>	<u>Half-life</u>	<u>E<math>\gamma</math> (keV)</u>
Radium-226	1620a	186.21 (3.28%)
Bismuth-214	219h	609.31 (43.3%)
		1764.49 (17%)
Lead-210	22a	46.52 (4.05%)

In the body, radium will not only be derived from the uranium decay, but also from ingestion as a contaminant of calcium in the diet. In Reference Man the total radium content is  $0.031\eta\text{g}$  corresponding to approximately 1 Bq. Of this, the skeleton contains some  $0.027\eta\text{g}$ .

Under ideal conditions of secular radioactive equilibrium, the body will also contain the same activity of the short-lived bismuth-214. Lead-210 found in the skeleton will also be enhanced over the expected amount from uranium by material taken in from the decay products of radon-222 via ingestion and inhalation. Uranium's decay daughters tend to concentrate about 70% in the bone and 30% in the soft tissue. In particular, the kidney is considered to be the critical organ in terms of uranium toxicity. There it concentrates about 10 times more than in other soft tissues (ICRP 23, 1975).

Radon-222 is an inert gas with half-life of 3.8 days which diffuses readily into the lungs through inhalation. Table 2.1 shows the highest annual intake of  $^{222}\text{Rn}$  to be  $2 \times 10^5$  Bq by inhalation compared with only about 300 Bq by ingestion. As it decays by alpha particle emission, its decay energy is dissipated in a close cluster of ionisation along a very short path length. It is this property of alpha particles which causes the radiation dose from radon to be delivered to the lung lining, the bronchial epithelium, which for the quantities indicated is estimated to be  $630 \mu\text{Gy}$  (Hofman and *et.al*, 1986). It is possible that the body  $^{210}\text{Pb}$  content could be related to radon exposure and Holtzman has found evidence of this (Holtzman and *et al.*, 1965). It is to be noted that the greatest problems concerning uranium do not arise from soluble uranium but actually from insoluble enriched uranium. It has been estimated that the lethal intravenous amount of uranium is about 1mg ( UNSCEAR, 1988).

### 2.3 Thorium series.

Igneous rocks and granites contain significant concentrations of thorium whereas sedimentary rocks have a low content. The average mass activity concentration of  $^{232}\text{Th}$  in soil is estimated to be  $25 \text{ Bq.kg}^{-1}$ . A simplified diagram of the

thorium-232 decay series is given in Figure 2.2. It has been divided into three sub-series of 11 radionuclides:  $^{232}\text{Th}$  itself;  $^{228}\text{Ra} \rightarrow ^{224}\text{Ra}$ ; and  $^{220}\text{Rn} \rightarrow ^{208}\text{Pb}$ . Table 2.1 shows the amount of annual intake of  $^{232}\text{Th}$  through inhalation is estimated to be about 0.01Bq. Whereas from ingestion it has been measured recently to be about 2 Bq according to Fisenne (Fisenne *et al.*, 1987). The activity mass concentration of thorium-232 in the body is found to be lower than that of  $^{230}\text{Th}$  by a factor of 2 (Sing *et al.*, 1982). It is known that about 60% of this activity is distributed in the skeleton as shown in Table 2.2. An interesting comparison between  $^{222}\text{Rn}$  from uranium and  $^{220}\text{Rn}$  from thorium can be seen in Tables.2.1 and 2.2 taken from the UNSCEAR 1988 publication. The  $^{222}\text{Rn}$  ( $T_{1/2}=3.82$  days) annual intake is about twice that of  $^{220}\text{Rn}$  ( $T_{1/2}=55.6$  sec) but the average activity concentration in the lung is different by 2.5 times which can mainly be attributed to the difference in their half-lives. The radionuclides which can be used to determine the presence of the thorium series are actinium-228, thorium-228 and thallium-208 which have the following decay modes:

<u>Isotope</u>	<u>Half-life</u>	<u>E<math>\gamma</math> (keV)</u>
Actinum-228	6.8h	338keV(11.1), 911keV(26.35)
Thorium-228	1.9a	131.5keV(0.13%), 215.75keV(0.28%)
Thallium-208	3m	2614.53keV(99.79%)

### 2.3.1 Thorium in the Body.

The investigation of thorium metabolism has been more limited than that for uranium due to its absence in the nuclear fuel cycle. However, it is known that the acute toxicity of all thorium salts by the different routes of intake is low. The uptake value for absorption factors by the gastrointestinal tract is less than  $1 \times 10^{-4}$ . The presence of the members of the decay series given above is probably as a result of the decay of radium-228, a beta emitter, which has been ingested as a contaminant of calcium in the diet, analogous to radium-226.

<sup>232</sup>Th Series

Nuclide	Half-life	Major gamma radiation energies (keV) and intensities	
<sup>232</sup> Th 90	1.41x10 <sup>10</sup> Y		
↓ α			
<sup>228</sup> Ra 88	6.79Y		
↓ β <sup>-</sup>			
<sup>228</sup> Ac 89	6.13h	129.1 (2.1 %)	
↓ β <sup>-</sup>		209.5 (3.5 %)	
		270.5 (2.8 %)	
		328.3 (2.6 %)	
		338.8 (9.3 %)	
		409.8 (1.6 %)	
		463.3 (3.7 %)	
		755.3 (0.81 %)	
		771.8 (1.5 %)	
		795.8 (3.9 %)	
		911.2 (22.4 %)	
		964.0 (3.7 %)	
		968.3 (13.3 %)	
↓ β <sup>-</sup>			
<sup>228</sup> Th 90	1.910Y	84.5 (1.6 %)	
↓ α		216.0 (0.3 %)	
<sup>224</sup> Ra 88	3.64d	241.0 (3.7 %)	
↓ α			
<sup>220</sup> Rn 86	55s	542.0 (0.07 %)	
↓ α			
<sup>216</sup> Po 84	0.15s		
↓ α			
<sup>212</sup> Pb 82	10.64h	238.6 (43.1 %)	
↓ β <sup>-</sup>		300.4 (3.2 %)	
<sup>212</sup> Bi 83	60.6m	39.86 (2 %)	
		727.3 (7 %)	
		1620.6 (1.8 %)	
↓ α (64.0%)			
<sup>212</sup> Po 84	304ns		
↓ β <sup>-</sup> (36.0%)			
<sup>208</sup> Tl 81	3.10m	2614.6 (100 %)	
		860.5 (12.0 %)	
		583.1 (86 %)	
		510.8 (22.5 %)	
↓ α			
<sup>208</sup> Pb 82	Stable		

Intensities refer to percentage of disintegrations of the nuclide itself, not to original parent of series.

Figure 2.2 Thorium decay scheme.

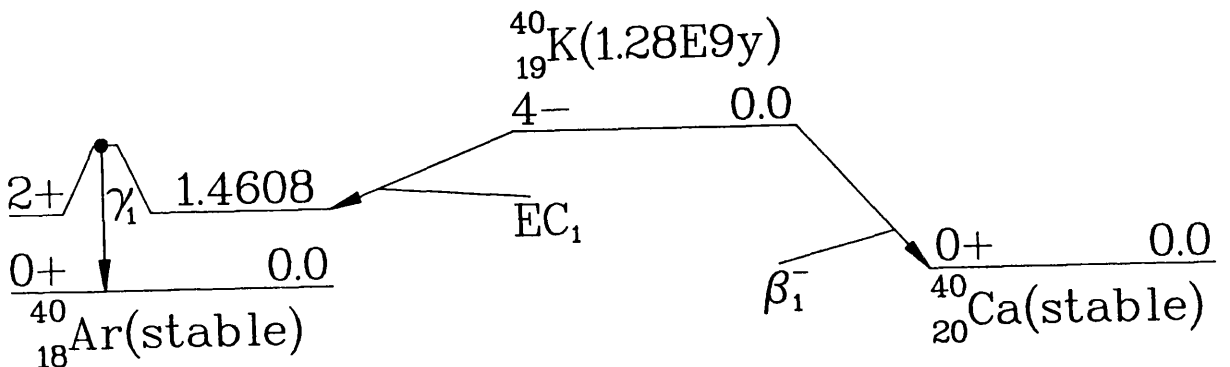


Figure 2.3 Potassium-40 decay scheme ( Spins and parities are shown to the left of the nuclear energy levels ).

Radium-228 has a half-life of 5.75 years and has been reported to be present in the body to the extent of 1.9Bq with 80% of this in the skeleton. It is more available to plant and animals than  $^{232}\text{Th}$ , so the activity concentration of  $^{228}\text{Ra}$  in humans is found to be 15Bq, which is mostly due to dietary intake. Thorium is considered to be a bone seeker and has a long residence time in the skeleton and it is assumed to remain near the bone surface, but in the gastrointestinal tract it has a very low absorption (Cohen, 1977). Other long-lived daughters are transferred to other tissues of the body particularly bone and kidney, with a low percentage as shown in Table 2.2.

#### **2.4 Potassium-40.**

Potassium-40 is present in many rocks and in the body it is present in solution in the cell electrolytes and is maintained in homeostatic equilibrium. The average man contains approximately 140 grammes of potassium and ingests and excretes about 3 grammes per day. The specific activity of  $^{40}\text{K}$  is 32 Bq per gramme and it is the main contributor to the natural radiation exposure of the human body from internal radioactivity which amounts to  $190\mu\text{Sv}$  annually.

The decay scheme diagram for potassium is given in Figure 2.3. This radionuclide has a half-life of  $1.27 \times 10^9$  years and occurs with an abundance of 0.0117%.

The decay of potassium is complex but the significant emission for body counting measurements is the 1.461 MeV gamma-ray emitted in 10.67% of decays (UNSCEAR 88). This corresponds to an emission of 478 gamma photons per second in the body of the average man.

#### **2.5 Man-made Radionuclides.**

The most widely distributed radionuclide contamination is from the explosion tests of nuclear weapons in the atmosphere. Materials from such explosions are known to spread over a large part of world because they are carried in the upper atmosphere, and then return to the earth's surface as radioactive fallout.

Exposure to fallout was considered to be at its highest during the periods 1952-1958 and 1961-1962 when weapon testing was at its most intense. However, since the Test Ban Treaty of 1963, most testing stopped, except that carried out by France and China which has tended to maintain atmospheric contamination levels. When fallout enters the food chain, fission products from the explosions, such as caesium-137 and strontium-90 can be taken into the body. Strontium is a pure beta emitter and so cannot be detected easily outside the body by counting, although for substantial body activities it is possible to measure the bremsstrahlung radiation (East, 1992). Caesium radionuclides are gamma emitters and can be easily measured.

Similar contamination can also result from the nuclear fuel cycle because of the waste resulting from reactor fuel reprocessing. High and intermediate level wastes from reprocessing plants are specially stored to isolate them from the environment because they are so hazardous, but low level wastes are frequently discharged into the environment relying on dilution and dispersion for their ultimate safe disposal. Typically, low level liquid radioactive wastes may be discharged into the sea and as an example British Nuclear Fuel plc "BNF" in the UK, has authorizations for this purpose. According to the Radioactivity Waste Management Advisory Committee (RWMAC) annual report, 1990, BNF at Sellafield was allowed to discharge up to  $1.4 \times 10^{13}$  Bq of alpha-emitting radionuclides into the sea. These radioactivities and others released earlier can be detected around much of the coastline of Britain, right round to East Anglia.

In contrast to atmospheric weapons testing, this type of contamination is much more localised to the vicinity of the plant producing it.

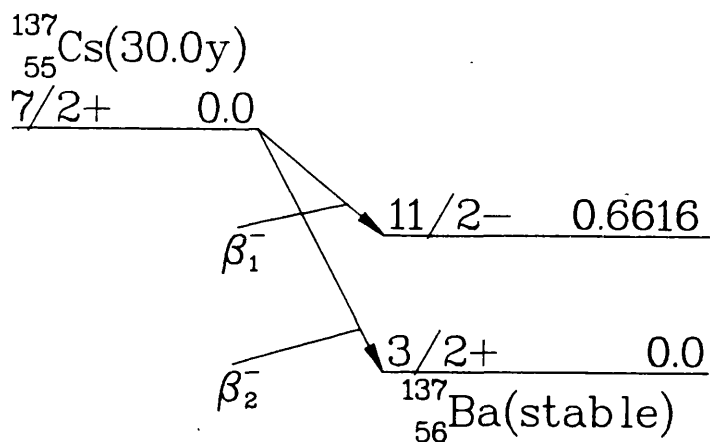
Nuclear power stations themselves produce low-level radioactive wastes consisting of liquid wastes often associated with coolant requirements, and some gaseous materials due to the circulation of air around the reactor core region and activation of primary coolants such as carbon dioxide. Radionuclide contaminants may also escape into the environment in two main ways:

- i) Under normal operating conditions where waste and excess liquid or gaseous radioactivities are discharged into the air or sea.
- ii) Under accident or abnormal conditions, caused by a failure of the safety systems of a nuclear reactor e.g the loss of coolant. The most notable example of this is the Chernobyl accident in 1986 when a reactor exploded and discharged large amounts of fission products and "hot particles" into the atmosphere, severely contaminating the immediate surroundings and causing fallout over large areas of the Northern hemisphere.

Probably the most prominent man-made gamma emitting radionuclide from the nuclear fuel cycle is caesium-137. Its decay scheme is given in Figure 2.4 where it can be seen that the 0.662 MeV gamma photon of its daughter, barium-137, is emitted in 85% of its decays. Similarly, caesium-134 is also a gamma emitter with the decay scheme given in Figure 2.5. This radionuclide is however an activation product resulting from neutron capture in caesium-133 which occurs significantly in nuclear reactors.

### **2.5.1 Radiocaesium in the Body.**

Radiocaesium is principally ingested in milk and meat in the diet after these foods have been contaminated via uptake of deposited radioactivity on grass which is eaten by farm animals. In the body it behaves very similarly to potassium and is found in the muscle cells. It has an effective half-life in the body of 110 days in adults and approximately 30 days in children. Since the atmospheric testing of nuclear weapons, trace quantities of caesium-137 have been detectable in man throughout the following decades by gamma-ray counting. After the Chernobyl reactor accident in 1986, both caesium-134 and caesium-137 could be observed in a large proportion of the world population. Specifically, measurements of members of the Scottish population using the NaI(Tl) whole-body monitor at SURRC showed an average maximum value of 800 Bq some eight months after the release ( East and Robertson, 1988 ).



55-CESIUM-137

HALFLIFE = 30 YEARS

04-MAY-77

DECAY MODE(S):  $\beta^-$

RADIATION	y(i) (Bq-s) <sup>-1</sup>	E(i) (MeV)	y(i)×E(i)
$\beta^-$ 1	9.46E-01	1.734E-01*	1.64E-01
$\beta^-$ 2	5.40E-02	4.246E-01*	2.29E-02

LISTED  $\beta$ , ce AND Auger RADIATIONS

1.87E-01

LISTED RADIATIONS

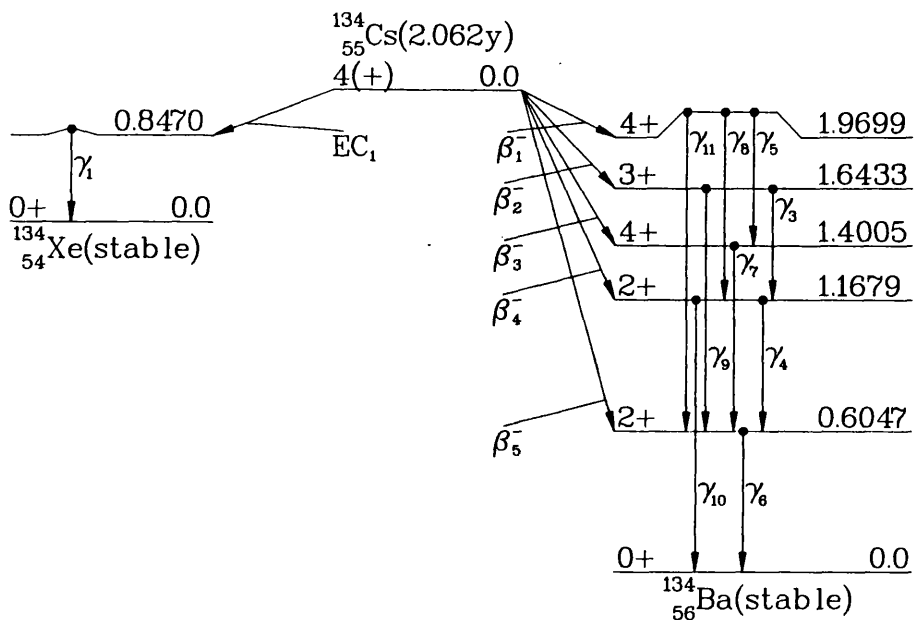
1.87E-01

\* AVERAGE ENERGY (MeV)

BARIUM-137M DAUGHTER, YIELD 9.46E-01,  
IS RADIOACTIVE.

BARIUM-137 DAUGHTER, YIELD 5.40E-02,  
IS STABLE.

Figure 2.4 Decay scheme of caesium-137.



55 - CESIUM - 134

HALFLIFE = 2.062 YEARS  
 DECAY MODE(S): EC,  $\beta^-$

RADIATION	$\lambda(i)$ (Bq-s) <sup>-1</sup>	E(i) (MeV)	$\lambda(i) \times E(i)$				
$\beta^-$ 1	2.74E-01	2.309E-02*	6.32E-03	$\gamma$ 10	1.80E-02	1.168E 00	2.10E-02
$\beta^-$ 2	2.47E-02	1.234E-01*	3.05E-03	$\gamma$ 11	3.04E-02	1.365E 00	4.15E-02
$\beta^-$ 3	7.01E-01	2.101E-01*	1.47E-01				
$\gamma$ 3	1.46E-02	4.753E 01	6.94E-03				1.55E 00
$\gamma$ 4	8.38E-02	5.632E-01	4.72E-02				3.84E-04
ce-K, $\gamma$ 4	5.06E-04	5.258E-01	2.66E-04				1.63E-01
$\gamma$ 5	1.54E-01	5.693E-01	8.78E-02				9.43E-04
ce-K, $\gamma$ 5	1.28E-03	5.319E-01	6.83E-04				1.72E 00
$\gamma$ 6	9.76E 01	6.047E-01	5.90E-01				1.33E-03
ce-K, $\gamma$ 6	4.91E-03	5.673E-01	2.79E-03				
ce-L <sub>1</sub> , $\gamma$ 6	5.64E-04	5.987E-01	3.38E-04				
$\gamma$ 7	8.54E-01	7.958E-01	6.80E-01				
ce-K, $\gamma$ 7	2.21E-03	7.584E-01	1.67E-03				
ce-L <sub>1</sub> , $\gamma$ 7	2.56E-04	7.899E-01	2.02E-04				
$\gamma$ 8	8.73E-02	8.019E-01	7.00E-02				
ce-K, $\gamma$ 8	2.22E-04	7.645E-01	1.69E-04				
$\gamma$ 9	1.00E-02	1.039E 00	1.04E-02				

LISTED X,  $\gamma$  AND  $\gamma_{\pm}$  RADIATIONS  
 OMITTED X,  $\gamma$  AND  $\gamma_{\pm}$  RADIATIONS\*\*  
 LISTED  $\beta$ , ce AND Auger RADIATIONS  
 OMITTED  $\beta$ , ce AND Auger RADIATIONS\*\*  
 LISTED RADIATIONS  
 OMITTED RADIATIONS\*\*

\* AVERAGE ENERGY (MeV)  
 \*\* EACH OMITTED TRANSITION CONTRIBUTES  
 <0.100% TO  $\sum \lambda(i) \times E(i)$  IN ITS CATEGORY.  
 XENON-134 DAUGHTER, YIELD 3.00E-06,  
 IS STABLE.  
 BARIUM-134 DAUGHTER IS STABLE.

Figure 2.5 Decay scheme of caesium-134.

## **CHAPTER 3**

## CHAPTER 3

### 3 The theory of counting

Unlike charged particles ( alpha and beta ) which lose energy continuously along their path by ionization and excitation processes,  $\gamma$ -rays, being uncharged electromagnetic radiation, undergo three major interaction processes with matter, namely: the Photoelectric effect, the Compton effect and Pair Production.

#### 3.1 Types of gamma-ray interactions.

##### 3.1.1 The photoelectric interaction (PE).

In this interaction all of the energy of an incident  $\gamma$ - ray is delivered to a bound electron of an atom of the detector crystal. An electron is ejected with an energy  $(h\nu - E_b)$ , where  $E_b$  is the binding energy of the electron. When these electrons are absorbed by a detector and impart their full energy into the crystal a photopeak or gamma-ray peak is produced in the  $\gamma$ -ray spectrum which corresponds to the incident  $\gamma$ -ray energy. The cross section ( $\tau$ ) of the photoelectric effect increases with increasing atomic number and decreases with increasing energy, ( $PE \propto Z^4 \cdot E^{-3}$ ). When photons are absorbed, characteristic X-rays of the absorbing material are often produced. The strong dependence on  $Z$  indicates that high  $Z$  material is very effective in the absorption of photons. When photons are absorbed, characteristics X-rays of the absorbing material are often produced. Also, the strong dependence on the energy of the incident photons explains the reason why this interaction is the dominant mode of  $\gamma$ -ray interaction at low energies and becomes negligible for high energy photons. This gamma energy dependence is shown clearly in Figure 3.1 for the three different types of  $\gamma$ -ray interactions (Knoll, 1979). The discontinuity shown at 11.1 keV is because of the binding energy of the K-shell electron for germanium and that at 29 keV for sodium iodide detectors because of iodine binding energy.

The other discontinuities occurring at lower energies correspond to the electron binding energies in the higher electron shells. The photoelectric effect is particularly significant for low energy photon interactions.

### 3.1.2 Compton scattering.

This is considered to be essentially an elastic collision between the incident photon and a loosely bound electron of the detector crystal. The energy of the incident photon is shared between the scattered gamma photon and the recoil electron depending on the angle of scattering giving a range of electron energies for photons of a given energy. As the electrons are absorbed in the detector, the  $\gamma$ -ray gives rise to the so called "Compton continuum" from zero energy up to a maximum energy of the recoil electron as predicted by the Compton interaction cross section. The probability for this effect decreases with increasing energy but less rapidly than for the photoelectric effect.

The  $Z$  and  $E$  dependence of the total Compton cross section ( $\sigma$ ) is given approximately by  $\sigma \propto Z.E^{-1}$  and the Compton mass attenuation coefficient is given by  $\mu_{\sigma}/\rho = N_A (Z/A)_e$ . Thus  $\mu_{\sigma}/\rho$  is nearly independent of the nature of the absorber because  $(Z/A)=0.45 \pm 0.05$  for almost all elements. So when comparing NaI and Ge-detectors the interaction events occur in a much shorter time than the generation and decay of the scintillation light pulse for the NaI detector while for Ge-detector most of the Compton events are detected.

Figure 3.1 shows that the Compton cross section becomes comparable with that of the photoelectric absorption at about 150 keV for Ge and 200 keV for NaI detectors and then quickly dominates the total cross section at higher energies.

For both types of detectors, it is the Compton continuum which adds to the difficulty of measuring low energy photopeaks because it results in an additional background.

### 3.1.3 Pair production.

When the incident  $\gamma$ -ray has an energy of 1.02MeV or more and it enters the intense field close to the nucleus of an atom it can give rise to an electron-

positron pair. The photon energy is converted into the rest mass energy and the kinetic energy of the electron-positron pair. Clearly, the photon energy has to be greater than twice the energy corresponding to the rest mass of the electron for the effect to occur i.e. 1.022MeV. The excess energy,  $E_\gamma - 2m_0c^2$ , is shared between the two particles as kinetic energy. As they interact with the adjacent material of the detector crystal, the positrons are finally annihilated and give rise to two  $\gamma$ -rays of 0.511MeV energy. Hence, a peak in the  $\gamma$ -ray spectrum 1.02MeV below the energy of the photopeak may appear due to this process. This annihilation process also results in other additional peaks in the  $\gamma$ -ray spectrum. Thus, one or both of the annihilation  $\gamma$ -rays may escape from the detector without interaction (Adams and Dam, 1970).

The pair production cross section varies approximately as  $Z^2$  and the energy dependence of the linear attenuation coefficient is shown in Figure 3.1 and can be seen to dominate the total cross section above 10MeV.

As a result of these interactions, the  $\gamma$ -ray spectrum which is observed in a detector is complex. In Figure 3.2 an idealised diagram of a typical spectrum from a mono-energetic gamma emitter is given which shows the various peaks and continua. In more detail, each of these features can be described as follows (Debertin, *et al.*, 1988).

#### 3.1.4 Full energy peak.

The full energy peak represents the complete deposition of all the incident  $\gamma$ -ray energy in the detector crystal. Because the detector response is proportional to  $\gamma$ -ray energy this peak occurs at a fixed position. It is used as a signature to identify the different  $\gamma$ -emitting radionuclides.

#### 3.1.5 Single escape peak.

The pair production single escape peak occurs when one of the annihilation photons escapes from the detector crystal without being absorbed i.e. the first escape peak corresponds to  $(E - m_0c^2)$  for energy greater than the 1.02MeV.

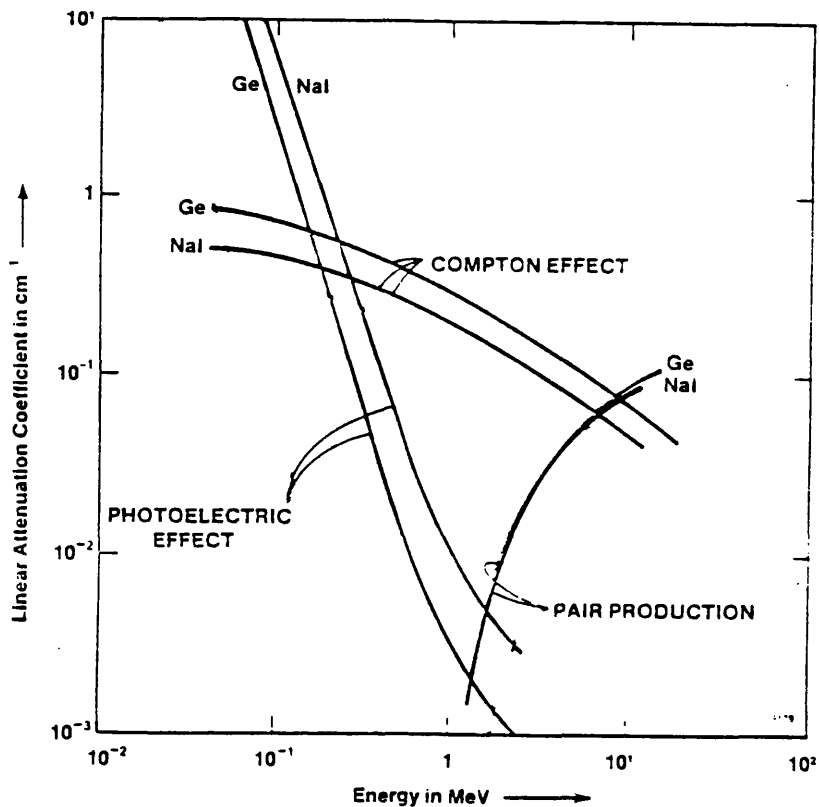


**Figure 3.1 Linear attenuation coefficients vs  $\gamma$ -ray energy for germanium and sodium iodide for the three main  $\gamma$ -ray interactions.**

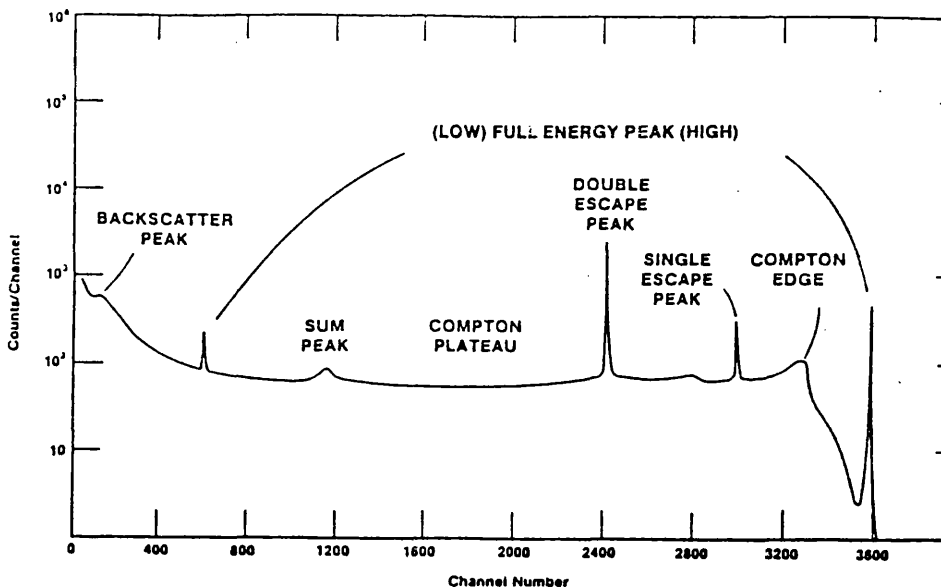


**Figure 3.2 A typical gamma-ray spectrum.**

### 3.1.6 Double escape peak.

This occurs when both annihilation photons escape detection in the detector. Both single and double escape peaks represents a loss of counts from the incident  $\gamma$ -ray.

### 3.1.7 Compton edge.

This is due to scattering of the incident photon at  $180^\circ$  with energy ( $E' = E/1 - 2\alpha$ ), where  $\alpha = m_e c^2 = 0.511$  MeV. It's shape is quite pronounced relative to the broad Compton distribution, and corresponds to the maximum transfer of energy to the recoil electron.

### 3.1.8 Backscatter peak.

This occurs as a result of a collision where maximum energy is transferred to an electron by the incident  $\gamma$ -ray, with the backscattered gamma depositing its energy within the detector crystal.

### 3.1.9 Compton plateau.

In addition to the main peaks due to the primary interaction of the incident  $\gamma$ -ray with the detector material, the  $\gamma$ -ray spectrum may also include a distribution of pulses from externally scattered radiation, mainly due to Compton scattering of  $\gamma$ -rays into the crystal from the surrounding shielding. The peak of this distribution generally occurs at an energy corresponding to  $180^\circ$  Compton scattering of the primary  $\gamma$ -rays, and the photopeak corresponds to the complete absorption of the photoelectron. In addition, Fig 3.3 also shows a practical shielded counting arrangement depicting diagrammatically the behaviour of  $\gamma$ -rays in relation to the detector.

### 3.1.10 Sum peaks.

Random summing occurs within the detector when  $\gamma$ -rays enter simultaneously and are detected as a single event with the recorded pulse being proportional to the sum of the energies of the two  $\gamma$ -rays. Generally summing is only important at high count rates.

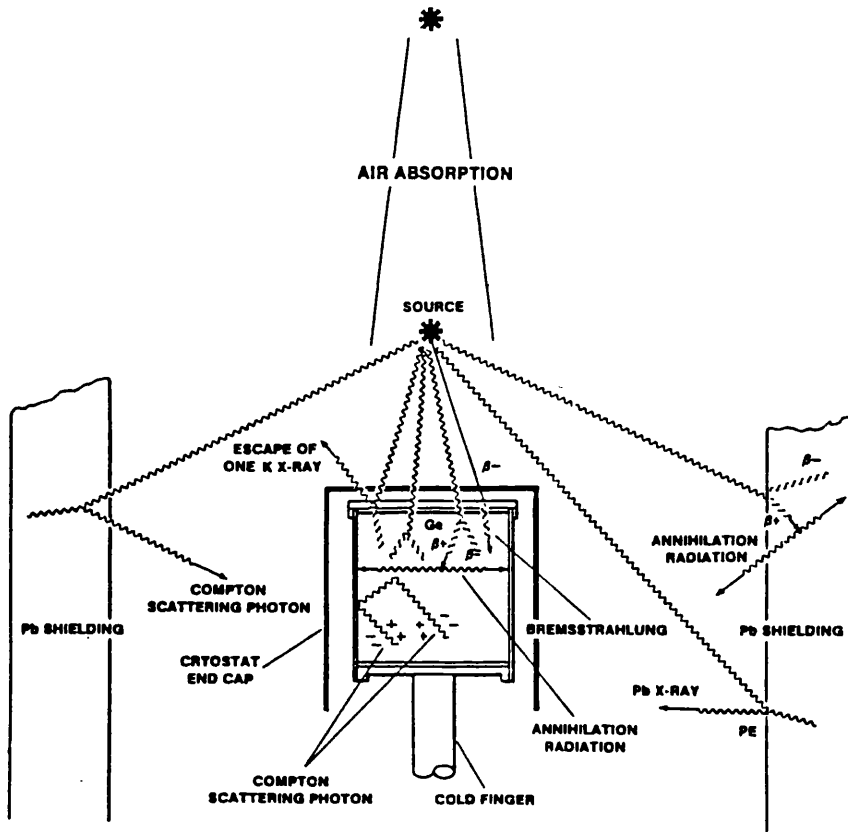


Figure 3.3 Types of  $\gamma$ -ray interactions in a Ge-detector.

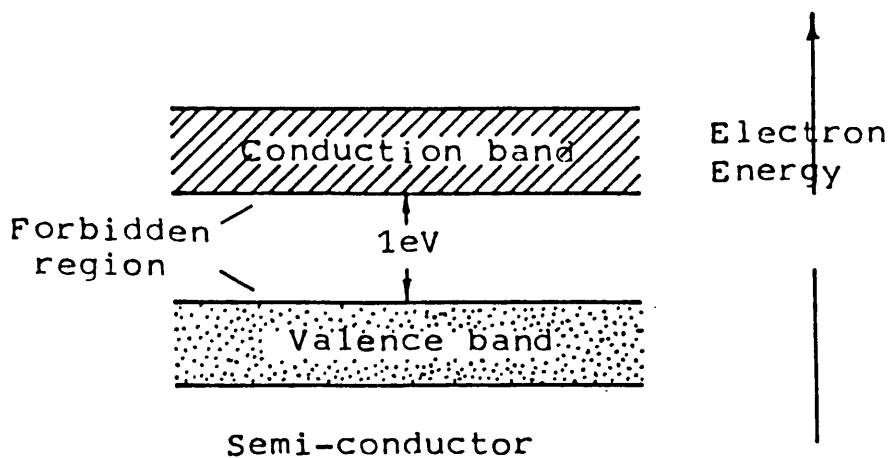


Figure 3.4 A schematic diagram of electron energy band structure in a semi-conductor crystal.

### 3.2 Absorption coefficients.

The probability of  $\gamma$ -ray interacting with matter by one of the three main interaction process is expressed either as a cross section ( $\tau$ ) or as an absorption coefficient ( $\mu$ ). The absorption coefficient contains the cross section of all the interactions involved. The attenuation coefficient for an incident beam of  $\gamma$ -ray is related to the number of  $\gamma$ -rays removed from the beam by the three interaction processes either through scattering or absorption. The attenuation coefficient for each type of interaction can be defined in terms of thickness  $X(\text{cm})$  which is called the linear attenuation coefficient or a "surface weight"  $\rho X (\text{gm} \times \text{cm}^{-2})$ , where  $\rho$  is the density in ( $\text{gm cm}^{-3}$ ), which is called the mass attenuation coefficient. The number of primary photons  $N$  removed from an incident beam of  $N$  photons is  $dN/N = -\mu x$ , which by integration becomes  $N = N_0 e^{-\mu x}$  for the linear attenuation coefficient and  $N = N_0 e^{-\mu/\rho(\rho x)}$  for mass attenuation coefficient (Adams and Dams, 1970).

The total attenuation coefficient is the summation of the partial attenuation coefficients for the three main interaction processes as follows:

$$\mu(\text{total}) = \mu(\text{photoelectric}) + \mu(\text{Compton}) + \mu(\text{pair production}).$$

### 3.3 The theory of germanium detection.

#### 3.3.1 The Band energy theory.

The periodic lattice of crystalline material establishes allowed energy bands for electrons that exist in the solid state. In a single crystal of semiconducting material such as germanium, the energy of these electrons is confined into bands of energy states that are characteristics of the crystal as a whole. In the absence of excitation, the outer electrons are bound in the valence band. The next higher electrons lie in the conduction band and are free to migrate through the crystal. The conduction band is separated from the valence band by the band gap which is of the order of 1 eV for a semiconductor and greater than 5eV for an

insulator. This band gap contains no allowed energy states for the high purity crystal with no impurities such as a high purity germanium detector. Therefore an electron can only be promoted from the valence band into the conduction band by imparting to it an energy which is at least equal to that of the band gap. Electrons reaching the conduction band are free to move under the influence of an externally applied electric field and then can be collected at an electrode. At the same time the vacancy or "hole" created in the valence band as result of the electron excitation can also move in a direction opposite to that of the electron. The mobilities of the holes and electrons are different and the speed with which the two charges move through the crystal is also different (Debertin, *et al.*, 1988). A schematic diagram of the electron energy band structure in a semi-conductor material is shown in Figure 3.4. The semi-conductor detectors are commonly operated at a temperature of 77K and both electrons and holes are collected to form the detector pulses.

### **3.3.2 Detection principles and semiconductor detectors.**

When a photon of a certain energy interacts in the semi-conductor crystal, bound electrons are excited to the conduction band by the primary electrons that are produced by any of the three types of  $\gamma$ -ray interactions. If these electrons carry sufficient energy, they can create additional secondary electrons. The primary electrons initiate a cascading process producing more electrons which are free to be collected at the electrodes of the detector. In order to be able to collect the charges which they constitute, an electric field of about  $1000 \text{ V cm}^{-1}$  or more is required. A bias voltage as it is known, of this order, is applied across the detector electrodes for charge collection. In order to give good peak shapes the bias is however kept to the minimum necessary.

Practical semi-conductors are not totally free of impurities or crystal defects, and they are commonly classified according to the type of charge impurities they carry. With germanium, the effect of impurities with three valence electrons such as boron, aluminium, gallium or indium, is the introduction of free holes within the crystalline lattice. This type of impurity is called an acceptor since the

holes can accept electrons, and the semi-conductor formed is known as p-type material. When impurities with five valence electrons such as phosphorus, arsenic and antimony are introduced into germanium, the converse applies and the material is known as n-type.

### **3.4 Semi-conductor detector characteristics.**

In order to utilize semi-conductor detectors efficiently the main characteristics which affect their operation need to be understood.

#### **3.4.1 Detector sensitivity.**

There are a number of factors which determine the detector's ultimate sensitivity such as full energy peak efficiency, energy resolution, background interference, count rate and counting interval (Cooper, 1970). It is a well known fact that a germanium detector's sensitivity is inversely related to the square root of the number of the counts "background" because it defines approximately the standard deviation of the counts and as the standard deviation decreases the ability to measure more sensitively increases such as:

$$Sensitivity \propto \frac{1}{\sqrt{BKGR}}$$

A further discussion of the counter sensitivity is set out in section 3.8.1 "Counting Error" where expressions are defined from statistical theory. In this work the sensitivity of a counter is taken to be approximately the activity corresponding to two standard deviations of the background.

#### **3.4.2 Efficiency calibration.**

The term efficiency in gamma spectroscopy is the measure of the ratio between the total count rate or the count rate in the full energy peak at a particular energy to the emission rate of photons with that particular energy. It is not a

property of the detector, but is an experimentally determined value for a detector under specific counting conditions. It is a complex function of energy and a number of other factors such as size of the active volume of the detector, its shape (detector geometry), source-detector geometry and the interactions in the shielding material surrounding the detector. For low photon energies it is primarily a function of the exposed active detector area, while for high energies it is a function of the active detector volume because low energies are more rapidly absorbed with depth than higher energies. The full energy peak efficiency is defined as the ratio of the number of measured counts under the full energy peak to the total number of gamma rays emitted from the source (Zimmer, 1977). Its value is also related to the solid angle subtended by the detector, determined by the source-to-detector distance and the source geometry. A typical efficiency vs energy graph for the 30% germanium detector used in these studies is shown in Figure. 3.5.

It is worth noting that the relative efficiency for a semi-conductor detector is usually defined in terms of its detection efficiency at 1.332 MeV ( $^{60}\text{Co}$ ) relative to that of a standard 7.6cm diameter x 7.6cm length NaI(Tl) cylindrical scintillation detector. The test procedure for germanium detectors for the measurement of ionizing radiation is described in IEEE Standard Test Procedure (ANSI/IEEE-325, 1986). Once the absolute efficiency of the detector is determined it is divided by  $1.2 \times 10^{-3}$ , which represents the absolute efficiency of a standard (7.6cm x 7.6cm) NaI(Tl) detector at 25cm from the  $^{60}\text{Co}$  standard source. The value quoted by the manufacturer of the HPGe-detector used in this study is 30%. Generally, the efficiency of germanium detectors is low when compared to that of NaI(Tl) detectors.

### 3.4.3 Detector resolution (FWHM).

The resolution of germanium detectors is usually specified as the full width at half maximum at the 1332 keV peak of  $^{60}\text{Co}$ . For good detectors this value is 1.8 -2.0 keV ( $\approx 0.16\%$ ). During spectrum analysis the resolution is also calculated

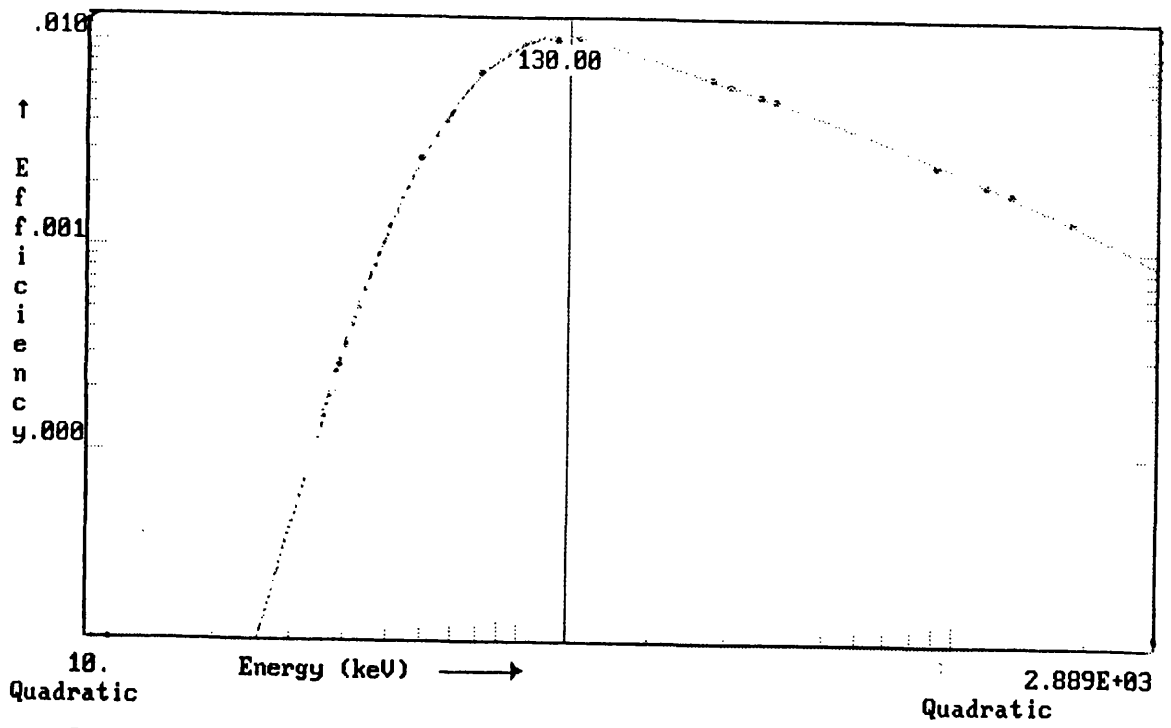


Figure 3.5 Efficiency vs energy plot for 30% efficiency germanium detector.

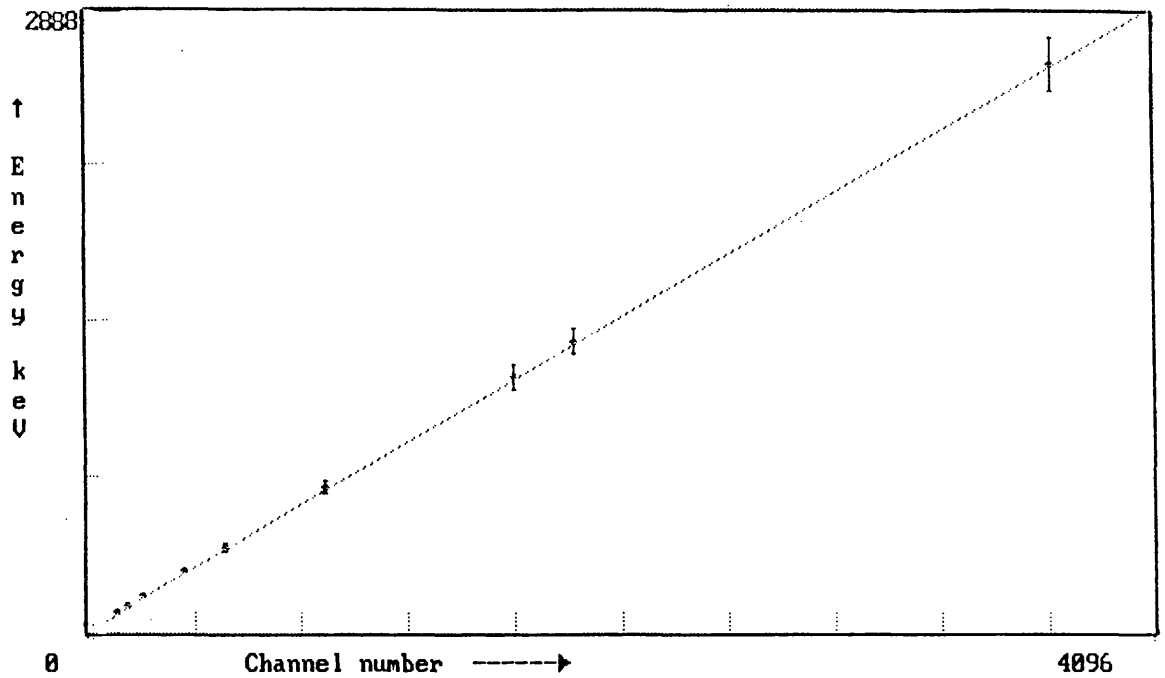


Figure 3.6 Energy vs channel number

at other peak energies which are of interest and provides an indication of correct detector performance. An example of the variation in resolution in a spectrum is shown in Fig 3.6.

The resolution of germanium detectors is high compared to sodium iodide and is good enough to avoid the problem of peak convolution when integrating over a region in which there are closely spaced peaks. As the resolution of the germanium detector improves (sharpens) fewer background counts are obtained under the peak which in turn improves detection sensitivity.

### **3.5 Sodium iodide detectors NaI(Tl).**

#### **3.5.1 Detection principles.**

The thallium-activated sodium iodide (NaI(Tl)) responds to the  $\gamma$ -ray by producing a pulse of light; a "scintillation". These scintillations occur when scintillator electrons excited by energy absorption from the incident photons, return to their ground state i.e a de-excitation of molecular states. The average energy required to produce a light photon is about 100eV.

The detector crystal is mounted on a photomultiplier "PM" tube in a closed light-free arrangement. The PM tube converts the scintillations to an electrical pulse that can be measured. The PM tube consists of a photocathode, a focusing electrode, and usually 10 or more dynodes which multiply the number of electrons to give amplification factors of a million times or so. The magnitude of the final electronic pulse collected at the anode is proportional to the original incident  $\gamma$ -ray energy.

#### **3.5.2 Sensitivity.**

The basic factors that generally affect the sensitivity of germanium detectors apply also to NaI(Tl) detectors. The main difference is determined by the properties of the iodide crystal. Because of the high atomic number  $Z$  of iodine (53) compared to that of germanium (32), there is better absorption of medium and

high energy  $\gamma$ -rays. As for germanium detectors, the absolute peak efficiency of a NaI(Tl) detector is defined as the ratio of the counts under the full energy photopeak to the total number of gammas emitted from the source for a given gamma energy (Berger *et al.*, 1981).

### 3.5.3 Resolution.

The resolution of the NaI(Tl) detectors governs their ability to distinguish two gamma-ray peaks which are close together in energy. It can be calculated from the pulse height spectrum in terms of channels, by applying the following equation;

$$R = \frac{\Delta}{C_0} \times 100\%$$

Where;

R= The resolution in percent

$\Delta$ = The number of channels in the full width at half maximum of the photopeak (FWHM) which is a measure of the spread of the peak at one half the maximum peak height.

$C_0$ = The channel number of the centroid of the photopeak. The resolution of NaI(Tl) detectors is normally taken as that at the caesium-137 photopeak at 0.662 MeV and a good detector will have a value of around 8%.

Generally NaI(Tl) detectors are renowned for their high detection sensitivity at the expense of rather poor energy resolution.

### 3.6 Peak-to-Compton ratio.

The peak-to-Compton ratio is a useful measure of a detector's performance because it is one way of stating the signal-to-noise ratio of the detector system.

A value for the ratio can be deduced from the true net peak height and its associated average Compton height. This is usually obtained by dividing the height of the 1.332 MeV peak ( $^{60}\text{Co}$ ) by the average Compton plateau between

1.040 and 1.096 MeV. The peak-to-Compton ratio value for the germanium detector used in these studies is 47:1. For the NaI(Tl) detector the corresponding value is 6. A number of factors adversely affect i.e reduce, this value such as smaller detector size, poorer detector resolution, irregular source shape, smaller source-to-detector distance and the materials surrounding the detector. It can be concluded that the higher the ratio, the lower the signal-to-noise ratio of the detector and therefore, the better the detector performance. In considering the use of germanium detectors for body monitoring purposes where high sensitivity is necessary, the improved signal-to-noise capability which offsets reduced sensitivity compared to NaI(Tl) crystals, is an important factor.

### **3.7 Efficiency and energy calibration.**

The energy and efficiency calibration procedure carried out for the detectors used in these studies will be outlined in more detail in following sections.

### **3.8 Counting statistics.**

Radioactive decay is a random process and therefore any measurement which is based on observing the radiation emitted from a source or the detection of trace amounts within a human body is subject to statistical fluctuations. This inherent fluctuation process represents an unavoidable source of uncertainty in all types of nuclear decay measurements, and results in a statistical error which influences detection precision. Therefore, in order to carry out statistical analysis, the following terms and statistical concepts have to be defined:

#### **3.8.1 Counting error.**

The standard deviation ( $\sigma$ ) of a count is generally taken as an indication of its error.

If a total of (G) gross counts is observed in a counting time (T), and if (T) is short compared with the radioactive half-life which is always the case for the

radionuclides discussed in this study, the error of the count can be shown to be approximately  $\pm \sqrt{G}$  and the standard deviation of (G) is given by ;

$$\sigma = \sqrt{G} \dots\dots\dots 1$$

Now the counting rate which is the parameter generally used in practice is given

$$R = \frac{G}{T}$$

by;

so that the standard deviation of R is given by;

$$\sigma_R = \frac{\sqrt{G}}{T}$$

$$\sigma_R = \frac{\sqrt{RT}}{T} = \sqrt{\frac{R}{T}} \dots\dots\dots 2$$

When a sample is measured the total counting rate,  $R_G$ , is corrected by subtracting the background rate to give the net sample counting rate,  $R_s$ :

$$R_s = R_G - R_B$$

The standard deviation of  $R_s$  is obtained from:

$$\sigma_s^2 = \sigma_G^2 + \sigma_B^2$$

i.e.,

$$\sigma_s = \sqrt{\sigma_G^2 + \sigma_B^2} \dots\dots\dots 3$$

assuming the counts have Poisson distributions then, for the background count:

$$\sigma_B = \frac{\sqrt{B}}{T_B} \dots\dots\dots 4$$

where ; B is the background count in time  $T_B$

Therefore,

$$\sigma_B^2 = \frac{B}{T_B^2}$$

For the gross count ;

$$\sigma_G = \frac{\sqrt{G}}{T_G} \dots\dots\dots 5$$

where ; G is the gross count in time  $T_G$

Therefore,

$$\sigma_G^2 = \frac{G}{T_G^2}$$

It follows that,

$$\sigma_S = \sqrt{\frac{G}{T_G^2} + \frac{B}{T_B^2}} \dots\dots\dots 6$$

### 3.9 Concept of the Minimum Detectable Activity (MDA).

#### 3.9.1 Critical level.

The critical level can be defined as the sample counting rate (the net counting rate after correcting for the background) which must be exceeded for the sample

to be taken as containing measurable radioactivity above the background. Very often the convention is adopted by taking the standard deviation  $\sigma_s$  of the count, or multiples of it i.e  $2\sigma_s$  or  $3\sigma_s$ , as the critical level. To define the Critical level more precisely the work of Currie, summarised by Lochramy, can be used.

In Fig 3.7, the normal definition of a mean sample count rate of zero, corrected for background, is shown graphically.

If the critical level is  $L_c$  then it can be seen from the above figure that;  $L_c = K\sigma_0$  where  $\sigma_0$  is the standard deviation of the sample (zero) net count rate and K is the confidence constant factor. K can be chosen so that 95% of the measurements of the sample (zero) net count rate fall below  $L_c$  and for this condition,  $K=1.65$ . Sample count rates above  $L_c$  are taken to be positive while those below indicate that the total counts in the sample are not statistically different from the background counts at the 0.05 level (for  $K = 1.65$ ) ( Currie, 1968 ).

If the background and sample counting times are known then:

$$L_c = K\sigma_B \left[ 1 + \frac{T_B}{T_G} \right]^{1/2}$$

and:

$$L_c = 1.65\sigma_B \left[ 1 + \frac{T_B}{T_G} \right]^{1/2} \dots\dots\dots 7$$

However , if the sample and the background counting times are equal i.e  $T_B = T_G$

Then:

$$L_c = 1.65\sigma_B\sqrt{2}$$

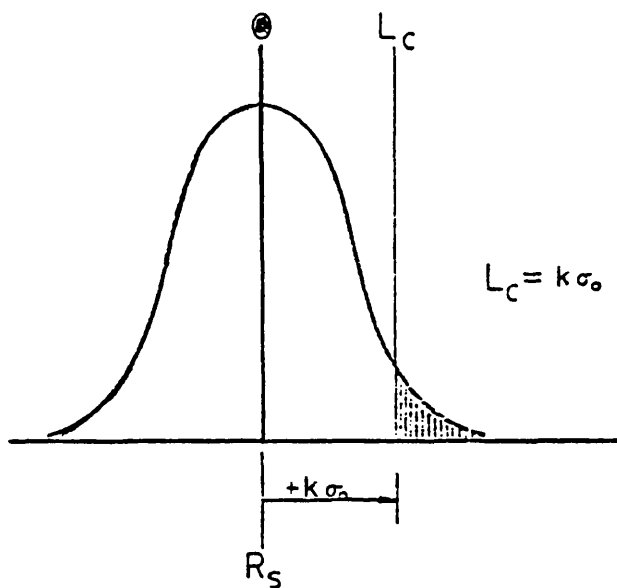


Figure 3.7 Critical level  $L_c$  graphically

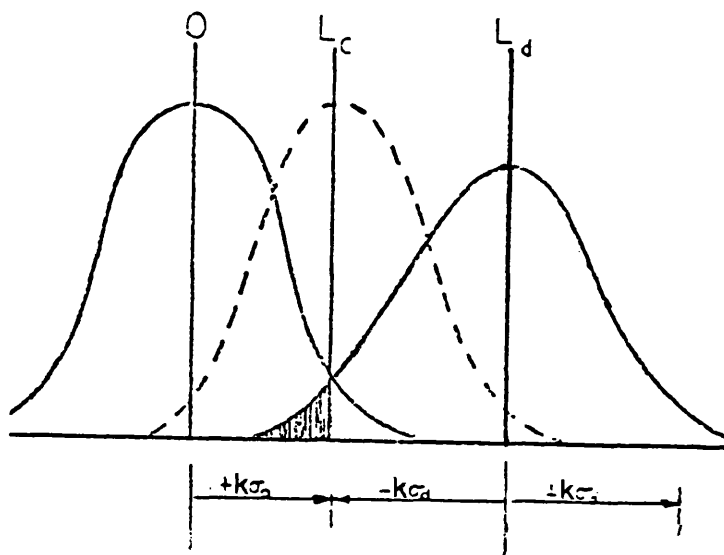


Figure 3.8 The Detection Limit and its relationship to Critical level.

and:

$$L_C = 2.33 \sigma_B \dots \dots \dots 8$$

Thus, it can be seen that the assumption of "twice the standard deviation of the background" as the critical level of detection is not unreasonable for the 95% confidence level.

### 3.9.2 Detection limit. ( $L_D$ )

The detection limit can be defined as the least quantity of radioactivity which can be detected at a specified confidence level. It is a very important parameter in *in vivo* counting studies, and it is useful to set the detection limit so that at low levels, the radioactivity will be detected 95% of the time when carrying out counts. Figure 3.8 shows the concept of the detection limit  $L_D$  graphically, together with its relationship to the critical level  $L_C$ ;

$$L_D = L_C + K \sigma_D$$

From the above figure, where,  $K$  is the confidence factor constant and  $\sigma_D$  is the standard deviation of the net sample counting rate equal to the detection limit.

For detection of the radioactivity with 95% confidence,  $K=1.65$  and, in terms of the standard deviation of the background, the detection limit  $L_D$  is given by:

$$L_D = K^2 + 2K\sigma_B \left[ 1 + \frac{T_B}{T_G} \right]^{\frac{1}{2}}$$

substituting for the corresponding values;

$$L_D = 2.72 + 3.3 \sigma_B \left[ 1 + \frac{T_B}{T_G} \right]^{1/2}$$

For equal background and sample counting times at 95% confidence detection limit;

$$L_D = 2.72 + 4.67 \sigma_B \dots \dots \dots 9$$

Which means that  $L_D$  is inversely proportional to the sample counting time and therefore the longer the counting time the better (lower) the detection limit. (Lochamy, 1976).

### 3.9.3 Determination Limit.

The determination limit can be defined as the lowest net count rate which can be detected at specific confidence level. It is usually expressed as;  $L_Q = K_Q \sigma_Q$ . Where;  $L_Q$  is the true value of the net signal,  $\mu_s$ , having a standard deviation  $\mu_Q$ . In terms of the standard deviation  $L_Q$  can be expressed as :

$$L_Q = K_Q \sigma_Q = K_Q [L_C + \sigma_0^2]^{1/2}$$

which when solved yields :

$$L_Q = \frac{K_Q^2}{2} \left[ 1 + \left( 1 + 4 \frac{\sigma_0^2}{K_Q^2} \right) \right]^{1/2} \dots \dots \dots 10$$

For 95% confidence limit and  $K_Q = 10$ , the above equation becomes :

$$L_Q = 50 \left[ 1 + \left( 1 + \frac{\mu}{12.5} \right) \right]^{1/2} \dots \dots \dots 11$$

### **3.10 Counting time.**

The counting of any radioactive decay over a period of time is governed by the normal distribution i.e the longer the counting time the less the scatter of the data and consequently the lower the uncertainty of the measurement. Equation 8 shows the relationship between the critical measured level and the standard deviation of the background when the counting time for background and sample is equal. For the purpose of whole-body counting it represents an ideal case.

However, since the measured subject has to be either completely or partially shielded while measurement is carried out, the measurement time of the subject will be restricted to the length of time for which the subject can comfortably remain in the position for counting. From the experience gained at SURRC using the NaI(Tl) whole body monitor it was found that a counting period of half an hour was readily accepted by almost all subjects. To compensate for lower sensitivity when using high purity germanium detectors, the plan is to measure for double that length of time i.e an hour. If necessary the subject can be measured again for another hour after a period of relaxation. These collected spectra could be added using the summation computer program and used in the final analysis.

### **3.11 Energy calibration.**

A radium-226 standard source which has a range of  $\gamma$ -ray energies was counted to obtain an adequate number of counts in the main peaks; this data being stored as an "SPC" file using the Mastero II computer program. Only two peaks are required for calibration, one at the lower end of the spectrum and the other at the higher energy end. A note is made of their position in the spectrum in terms of channel number and this is related to their  $\gamma$ -ray energy to give a linear calibration curve from which other  $\gamma$ -ray energies can be obtained. In practice, a calibration computer program is used to calculate the exact peak position taking into account peak shape and adjacent backgrounds. Peak shape is also checked by assessment of resolution in terms of the FWHM. Also the analysis program

uses the energies and shapes of the peaks together with their corresponding spectra positions to produce two types of calibration plots namely; Energy vs Channel number and FWHM vs Channel number, typical examples of these plots are shown in Figures 3.6 and 3.10.

### 3.11.1 Efficiency calibration.

Also the efficiency calibration procedure has been made simple by the utilization of the calibration programme. All that is required is an energy calibrated spectrum and a nuclide library containing all the relevant data about the nuclides in the reference standard source. There are a number of different mixed-nuclide standard sources prepared commercially. For the purpose of whole-body counting efficiency, calibration requires an anthropomorphic phantom, usually made of tissue equivalent materials, which contains certain standard radioactive sources.

### 3.12 Shielding properties.

Adequate thicknesses of suitable shielding materials are required to reduce the ambient background radiation. Lead is the most common material used especially for  $\gamma$ -rays because of its high atomic number ( $Z$ ) and high density. The required thickness depends on the amount of attenuation required for  $\gamma$ -rays of a specific energy. For the application of whole-body counters which covers the energy range from 0 up to 2 MeV, usually a thickness of 10 cm (4") of lead is sufficient. The half-value thickness ( the thickness required to reduce a certain gamma dose rate to half its original value ) of lead for 1 MeV  $\gamma$ -ray is 0.85cm, which really means that the intensity of a beam of 1 MeV  $\gamma$ -ray will be attenuated by a factor of 3400 when passing through a 10cm thickness of lead. In the case of a 2MeV beam of  $\gamma$ -rays the intensity will be reduced by a factor of 175. However, when using planar germanium detectors for the detection of low-energy nuclides e.g uranium and plutonium, the reduction of lead K, X-rays is highly desirable. Therefore, a graded  $Z$  shielding arrangement is required and

this can be achieved by using materials with decreasing atomic number towards the detector. This arrangement absorbs the lead X-rays produced photoelectrically and results in the emission of a secondary X-ray of lower energy. A typical graded Z shield is lead-cadmium-copper as the combination of shielding materials for the detector system. The thickness required for the graded-Z material is also explained in terms of the half-value thickness of the shielding material used. Cadmium has a half-value thickness of 0.3mm at 80keV (Pb K X ray), therefore using 3mm layer would reduce this peak by a factor of 1000. It is known that the cadmium sheet will also provide an additional 20% attenuation at 80 keV.

## **CHAPTER 4**

## Chapter 4

### Sodium iodide detector body counting studies methods and results.

#### 4.1 Description of the NaI(Tl) Whole Body Monitoring Equipment.

Sodium iodide detector body monitoring facilities have been in operation at the SURRC, East Kilbride, since 1963. The early design of the shadow-shield whole body counter had a single NaI(Tl) crystal (7.6cm x 7.6cm) connected to a 100 channel T.M.C. Gammascoppe multichannel analyzer (Boddy 1967a). During 1967 a larger NaI(Tl) detector was installed in the monitor. This much larger cylindrical crystal (29.2cm diameter x 10.0cm length) utilised seven low background photomultiplier tubes and was housed in a 10cm thick lead shield positioned above the subject.

The shadow-shield arrangement has the benefit of providing a high standard of detector shielding for the minimum cost both in money and weight. With the thickness of lead used, backgrounds similar to those of much more expensive shields, such as steel rooms, can be achieved. Additionally there is less claustrophobic effect for the measured subject.

This shadow-shield counter was widely used in clinical studies for the measurement of total body potassium. Later, an *in vivo* neutron activation analysis facility was developed (Boddy, *et al.*, 1972) utilising a scanning bed geometry for irradiation and detection. To meet the higher sensitivity requirement of this system, the whole body monitor was modified to accommodate a second NaI(Tl) detector (29.2cm x 10.0cm) positioned below the subject and directly opposite the first detector. A diagram of this dual detector monitor, with its two vertically opposed detectors is shown in Fig 4.1. The instrument provides simultaneous bilateral monitoring with consequent improvements in detection, uniformity and counting sensitivity over the single-detector monitor (Boddy, *et al.*, 1975). Because the arrangement was principally used for the measurement of mixtures of neutron-induced radionuclides, there was little interest in background radioactivities other than potassium-40 which

is present in the body. In the present work the possibility of examining in more detail the background activities due to the natural decay series which are present in the body has been studied more closely.

#### **4.1.1 Mechanical system and electronic components.**

The two detectors are separated by a distance of 36cm with a motorised bed passing between them on which the supine subject is scanned. The scan speed is altered by means of gears and the distance of travel is controlled by adjustable actuators mounted on the bed to give an "overscan" of 10cm at the head and feet of the subject. The actuators operate microswitches which enable and disable the counter ADC. This arrangement, can operate over a height range of 140-190cm, and provides optimum scan times appropriate to the height of each subject.

On each detector the signals from the seven photomultipliers are combined and fed into a unity-gain preamplifier, which acts as an impedance matching unit ( Boddy, *et al.*, 1975). The separate signals from each detector are handled by two EG&G Ortec ACE multichannel analyzer cards mounted in the data management computer (IBM, PC XT model 286). The accumulated data can be displayed as 2048 channel spectra for each detector. The computer system is used for data handling and analysis and both printed hard copies and floppy disk files are used for data storage.

#### **4.2 Data handling and software analysis programmes.**

By employing the latest "state-of-the-art" technology for gamma-ray spectroscopy the detector system used in these studies utilizes the EG&G concept of Advanced Data Collection And Management "ADCAM" system. All the data handling procedures have been made simple and very efficient. It represents the integration of a suite of computer-controlled instruments and functions are controlled by a personal computer (PC) and appropriate software. Using a programme called " MAESTRO II ", as multichannel analyzer software, the ADCAM system may be configured using a multichannel buffer ( MCB 918A ).

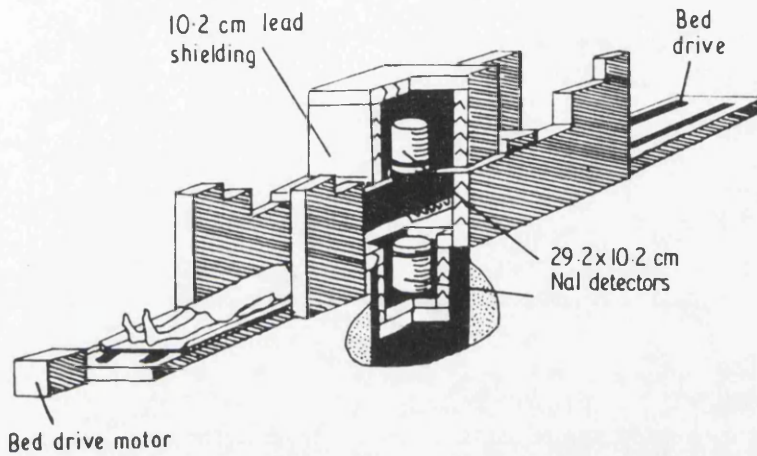


**Figure 4.1 Dual NaI(Tl) detector arrangement.**

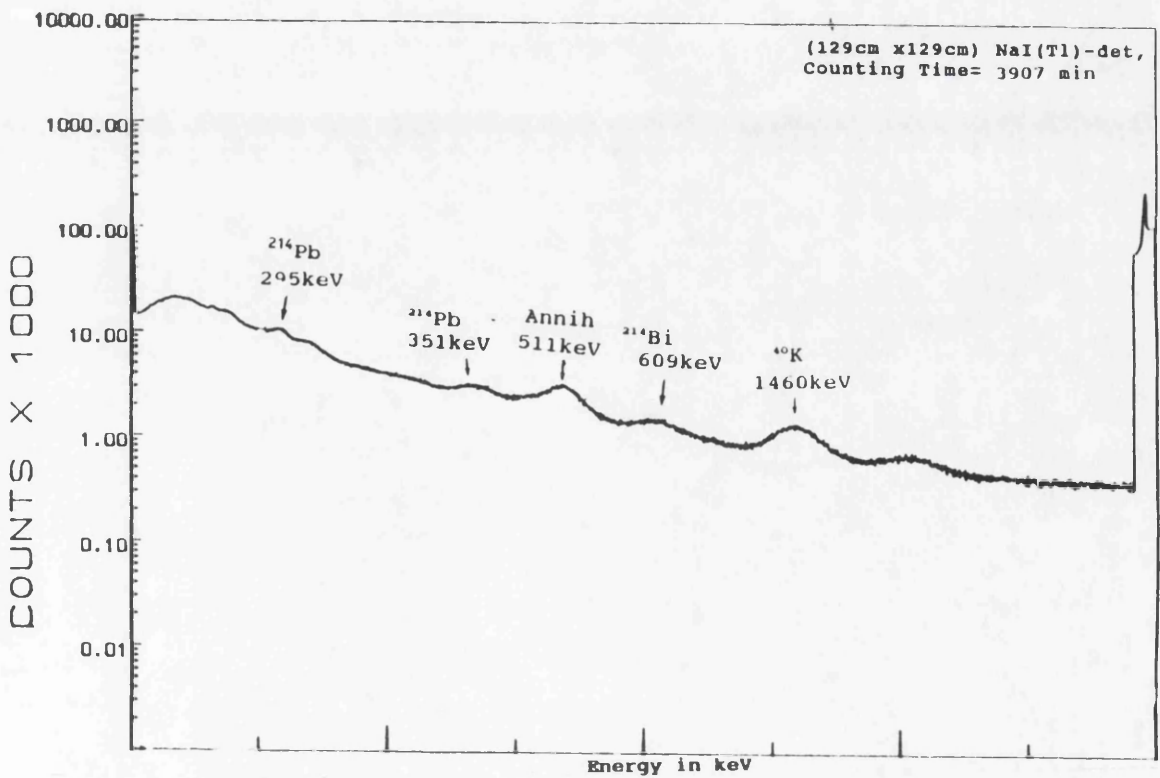


**Figure 4.2 Whole-body counter phantom background spectrum using the upper NaI(Tl) detector.**

Also by using the Multiplexer system, several detectors may share the same MCB. The MAESTRO II MCA Emulation programme provides control of the hardware, spectral display, and a wide range of semi-quantitative analysis routines. However the utilization of another programme "MINIGAM™ II" (EG & G Software manual ), gives the experimenter complete menu-driven and full quantitative analysis supported by high quality graphics. Routinely the following operations are carried out on the collected data obtained from each spectrum;

1- All data are collected in 4096 channel pulse height spectra and each spectrum is and stored as a "CHN" file.

2- Analysis of the stored spectrum file, to determine the energies and areas of the peaks and the nuclides that may be present, is carried out by transferring the "CHN" file to an "SPC" file which also stores the energy calibration file.

3- A second analysis procedure is carried out to determine the areas of the peaks associated with the identified nuclides which were not fitted in the first analysis. It also calculates the activity associated with each nuclide peak. Using the Minigam software, it is possible to carry out two types of peak search. The first, using a library-directed analysis provides the optimum sensitivity analysis.

This peak-search technique is based on the Mariscotti method for the identification of peaks in the presence of background (Mariscotti, 1976). He developed a peak location method that involves the second derivative of the spectrum. As shown in Fig 4.3, when taking the second derivative a large negative peak and two smaller positive peaks form the signature indicating the presence of a peak. By applying a smooth background a constant first derivative and then a zero second derivative are obtained. In order to take meaningful derivative a selection criteria, based on the statistics of the data is used which suppresses the statistical fluctuations and thus locates peaks in the spectrum.

The second type of search is not library directed, it is usually carried out for unidentified sample analysis.

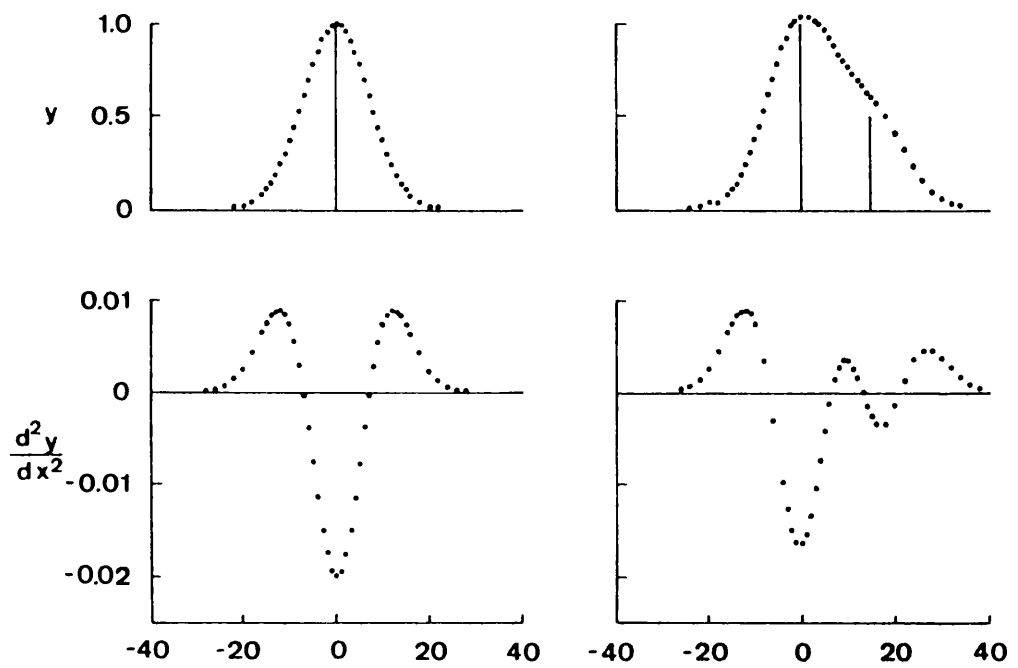


**Figure 4.3** An example of a peak location methods for a given spectrum and its second derivative in the region of single peak and doublet peak (Debertin and Helmer, 1988).

### 4.3 Investigation of NaI(Tl) body monitor parameters

#### 4.3.1 Energy calibration method.

The energy calibration of the detector is carried out simultaneously using a  $^{226}\text{Ra}$  standard source in fixed geometry. The main gamma-ray emissions used are shown in Table 4.1 in which typical responses of the upper (first two rows) and lower detectors (lower rows) are also given.

Energy keV	Channel range	Energy Range keV	Net cpm	Sensitivity cpm/Bq	FWHM keV
609	340-408	570-684	24180	0.131	50.34
1765	980-1120	1646-1881	10200	0.055	116.95
609	340-408	550-667	23040	0.125	57.98
1765	980-1120	1642-1880	7560	0.041	114.16

**Table 4.1** The main energies and detection sensitivity used for calibration of the two (WBM) NaI(Tl) detectors using  $^{226}\text{Ra}$  standard source.

#### 4.3.2 Background measurements.

The counter background is obtained by measuring a water-filled phantom and then subtracted from the measured spectrum of the radionuclide-containing phantom or the subject whole-body spectrum as appropriate. The water-filled model is intended to simulate the scattering characteristics of the human body which will affect the observed background in the monitor. In comparison with an "air" background, the counts observed with a water phantom tend to be higher throughout the spectrum as presented in Table 4.2.1 .

Figure 4.2 shows a typical water phantom background spectrum from the upper detector of the whole-body counter collected for 65 hours with the phantom static and central in the counter. Various features can be seen over the energy range and five photopeaks can be identified as indicated, with others being much less well defined.

In Table 4.2.2 details of the detected radionuclides and the observed counting rates in the identified photo-peaks are given. These data were obtained using the Mastero II programme which also calculated value for the full width at half maximum. For the poorly defined photopeaks little weight can however be given to the FWHM values.

When examining the NaI(Tl) detector backgrounds only a limited number of peaks could be clearly identified as shown in Table 4.2.1 below.

Energy keV	Isotope	NaI(Tl) cpm	FWHM keV
295	<sup>210</sup> Pb	77	11
351	<sup>214</sup> Pb	124	31
511	Annihilation	118	41
609	<sup>214</sup> Bi	110	17
1460	<sup>40</sup> K	84	90

**Table 4.2.1** Details of the water phantom background spectrum collected for 65 hours in the upper NaI(Tl) whole-body monitor.

Nuclide	E <sub>γ</sub> keV	BKGR cpm	σ <sub>B</sub> cpm	L <sub>C</sub>		L <sub>D</sub>		L <sub>Q</sub>
				cpm	Bq	cpm	Bq	Bq
<sup>214</sup> Bi	351	124	0.18	0.42	0.66	3.55	5.6	156
<sup>214</sup> Bi	609	110	0.17	0.39	0.39	3.54	3.6	101
<sup>40</sup> K*	1460	84	0.15	0.35	0.11	3.41	1.1	31

**Table 4.2.2** Background, standard deviation and detection parameters for a 65-hour counting time in the upper NaI(Tl) detector of the whole-body counter.

\*Units in gramme of <sup>40</sup>K.

### 4.3.3 Minimum detectable activities

Using equations 8, 9, and 11 described in chapter 3, and assuming the theory for paired observations ( Currie, 1967-paired observations being specifically a background and a sample counted for similar times ) the standard deviation of the background, critical level, the minimum detectable activity and the determination limit for a number of background energy peaks are calculated for the upper NaI(Tl) detector and presented in Table 4.3.1 and 4.3.2. These calculations were based on the sensitivities obtained for the selected energies with a  $^{226}\text{Ra}$ - standard source. The measured background levels along with the calculated parameters were carried out for counting times of 65 and 2 hours respectively in order to demonstrate the marked improvement on the  $L_C$  and  $L_D$  for longer counting time. It can be seen because of the lower background standard deviation for the longer counting times, the corresponding critical and minimum detectable levels are markedly different. Interestingly the determination limits for both counting times are however similar.

Nuclide	$E_\gamma$ keV	BKGR cpm	$\sigma_B$ cpm	$L_C$		$L_D$		$L_Q$ Bq
				cpm	Bq	cpm	Bq	
$^{214}\text{Bi}$	351	124	1.02	2.38	3.72	7.45	12	160
$^{214}\text{Bi}$	609	110	0.96	2.24	2.26	6.95	7.0	103
$^{40}\text{K}^*$	1460	84	0.84	1.96	0.60	6.62	2.0	31

**Table 4.3.1 Background, standard deviation and detection parameters for a two-hours counting time in the upper.**

\* Units: gramme of potassium.

It must be noted that these particular times were chosen because 2 hours could be considered a maximum possible counting time for a subject and 65 hours could be achieved by the summation of a series of counts.

As mentioned, the values calculated are for paired observations. In routine use the background value could become "well known" and the various detection parameters would be improved i.e have lower values.

In Table 4.3.2 the measured and calculated levels of the main peaks of the background of the lower NaI(Tl) detector are presented. In comparison with the upper detector the background counting rates are higher because the lower detector has effectively poorer shielding and also the critical and detection levels are higher.

Nuclide	$E_\gamma$ keV	BKG cpm	$\sigma_B$ cpm	$L_C$		$L_D$		$L_Q$ Bq
				cpm	Bq	cpm	Bq	
$^{214}\text{Bi}$	351	197	1.28	2.98	4.66	8.66	13.6	161
$^{214}\text{Bi}$	609	133	1.05	2.48	2.51	7.59	6.77	103
$^{40}\text{K}^*$	1460	213	1.33	3.09	0.95	8.9	2.73	33

**Table 4.3.2 Sensitivity, background standard deviation and detection parameters for a two-hour background count using the lower NaI(Tl) detector of the whole-body counter.**

\*Units: gramme of potassium.

#### 4.4 Measurements of radioactive decay series using the NaI(Tl) detector (WBM).

In order to assess the sensitivity of the NaI(Tl) detection for Th & U, as a preliminary experiment, known sample solutions were prepared by dissolving weighed amounts of thorium  $\text{Th}(\text{NO}_3)_4 \cdot 4\text{H}_2\text{O}$  and uranium  $\text{UO}_3(\text{NO}_3)_2 \cdot 6\text{H}_2\text{O}$  salts in 500ml normal hydrochloric acid. The solutions were placed in 500ml cylindrical containers and sealed securely in order to prevent "contamination" leakage.

The sample solutions were positioned against the face of the upper detector of the whole-body counter using an adjustable laboratory jack. The observed spectra are shown in Figures 4.5, 4.6.

Nuclide	$E_\gamma$ keV	cpm/ mg	$\sigma_B$ cpm	$L_C$		$L_D$		$L_Q$ mg
				cpm	mg	cpm	mg	
$^{212}\text{Pb}$	238	1.93	1.0	2.33	1.21	7.36	3.8	53
$^{228}\text{Ac}$	338	0.47	0.9	2.09	4.46	6.89	15	215
$^{208}\text{Tl}$	583	0.88	0.9	2.09	2.38	6.89	7.8	116
$^{212}\text{Bi}$	727	0.28	0.8	1.86	6.66	6.43	23	364

**Table 4.5.1 Sensitivity, Background standard deviation and detection parameters for a two-hour counting time of 60mg  $^{232}\text{Th}$  using the upper detector of the NaI(Tl) whole-body counter. (Gamma energies taken from Knoll, 1988.)**

Nuclide	$E_\gamma$ keV	cpm/ gm	$\sigma_B$ cpm	$L_C$		$L_D$		$L_Q$ mg
				cpm	mg	cpm	mg	
$^{234}\text{Th}$	93	144	0.95	2.21	15	7.13	49	708
$^{226}\text{Ra}$	186	129	0.98	2.28	18	7.27	56	791
$^{234}\text{Pa}$	766	131	1.1	2.45	19	7.59	58	779
$^{234}\text{Pa}$	1000	230	0.93	2.17	10	7.03	30	442

**Table 4.5.2 Sensitivity, Background standard deviation and detection parameters for a two-hour counting time for 1 gm  $^{238}\text{U}$  using the upper NaI(Tl) detector of the whole-body counter.**

For thorium it can be seen that only four photopeaks could be easily picked out for assessment. The sensitivities for each of the attributed daughters are given in Table 4.5.1 in (cpm mg<sup>-1</sup>) thorium. Using data from the counter background sensitivities determined previously a preliminary estimate was made of the  $L_C$ ,  $L_D$  and  $L_Q$  for thorium. As it can be seen from the above Table that the lowest calculated values for these parameters are for the daughter  $^{212}\text{Pb}$ (238keV) and  $^{208}\text{Tl}$  (583 keV) respectively.

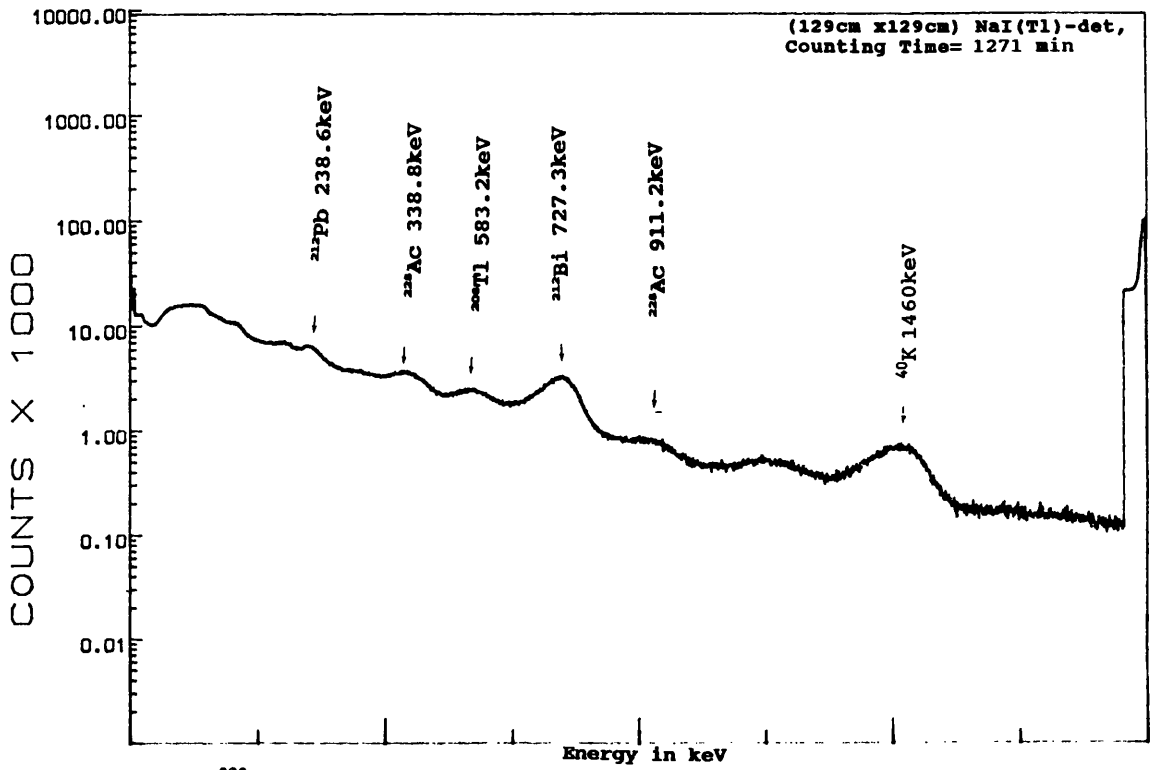


Figure 4.5  $^{232}\text{Th}$   $\gamma$ -ray pulse height spectrum.

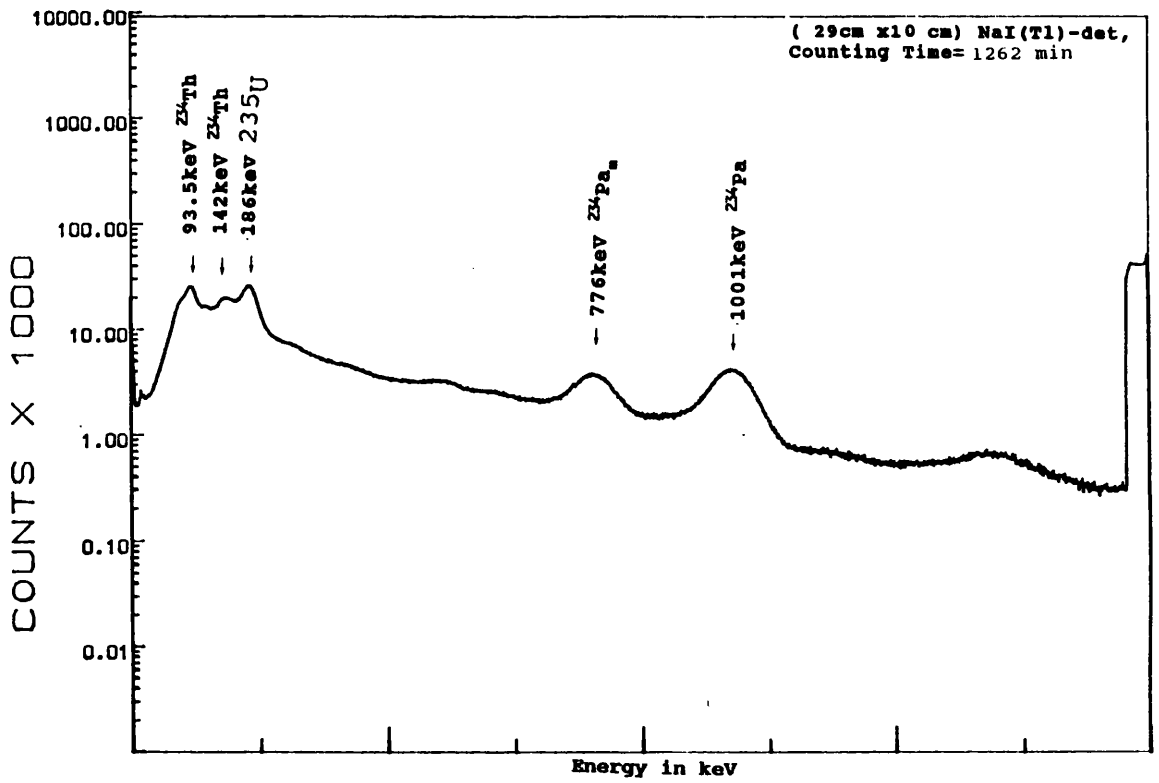


Figure 4.6  $^{238}\text{U}$   $\gamma$ -ray pulse height spectrum.

As the sample was placed in contact with the detector these values represent the best detection geometry which might be obtained. In order to determine sensitivity for thorium in the human body further experiments would be required using Thorium-loaded phantoms which would be expressed to give lower sensitivities but of the same order of magnitude. Thus in relation to expected quantities in the body, the counter performance would appear to be poor.

However it must be noted that these calculated values are only for the upper NaI(Tl) detector. Therefore when operating both of the detectors simultaneously the sensitivity of the detection will be increased by at least 35%.

By the same method of measurement and analysis the natural uranium sample was measured. Table 4.5.2 presents the calculated values of detection sensitivity  $L_C$ ,  $L_D$  and  $L_Q$  for the main energy peaks of the uranium daughters. It seems that the best energy line is the 1000keV of  $^{234m}\text{Pa}$ , which gives the lowest possible detection limit of 442mg uranium at a 95% confidence limit. These data were also collected using the upper detector only with the 500ml container in contact with detector surface. This demonstrates the limitation of this type of detectors for natural background elucidation resulting from its low resolution.

## **CHAPTER 5**

## **Chapter 5**

### **Semi-conductor germanium detector studies.**

#### **5.1 Introduction.**

The reasons for investigating the use of germanium detectors for body counting have been outlined in the first chapter and a more detailed discussion of the advantages and disadvantages in comparison to NaI detectors is given in chapter 6. The use of a "shadow-shield" arrangement for the new semi-conductor body counter was specified, based on the economic factor of minimum cost for acceptable background reduction and two decades of practical experience at the Scottish Universities Research & Reactor Centre (SURRC) with such an arrangement using sodium iodide detectors. The proposed location in the SURRC for the prototype semi-conductor detector whole body arrangement is shown in Fig 5.1. It is adjacent to the operating NaI(Tl) whole body monitor discussed in the previous chapter making it convenient for parallel studies. It was decided to obtain the data required for the optimisation and for the prediction of the performance of a counter experimentally by assembling various "shadow-shield" configurations, installing test semi-conductor detectors and determining the backgrounds and sensitivities to relevant radionuclides.

Two germanium detectors were available for use; a 127 ml high purity crystal and a planar type for low energy photon measurements. The following chapter describes the apparatus and experimental methods for semiconductor detector investigations, the results obtained and the criteria derived from them to be used for counter design. Calculations of expected body counter sensitivity and performance are also made, based on these observations.



## 5.2 Measurement with a 127 ml Ge-detector.

### 5.2.1 The Experimental set-up.

#### 5.2.1.1 Detector and electronics.

The detector (EG&G Ortec) was an intrinsic germanium p-type with a sensitive volume of 127 cm<sup>3</sup> and an efficiency of 30% relative to a 7.6cm x 7.6cm NaI detector. The nominal resolution was 2.3 keV FWHM at the 1332 keV <sup>60</sup>Co peak. The detector characteristics along with the electronic settings used are given below:

Detector type	GEM-231	Preamplifier Gain	= 20.75
Crystal diameter	=54.0mm	Shaping time	= 6μsec
Crystal length	=55.3mm	Amplifier Gain	= 50.07
End cap-crystal	=3.0mm	Bias voltage	= 2800 Volts
Volume	=127cm <sup>3</sup>	Polarity	positive

The electronic counting channel consisted of EG&G Ortec equipment set up as shown in Figure 5.2. It has to be noted that the shaping of 6μsec because it was found that this gave the best resolution. The longer time constant allows the system to average noise more efficiently while at the same time the counting rate in the whole-body is very low so that there will be no random summing effects.

#### 5.2.1.2 Shielding arrangements.

Standard chevron-shaped, low activity lead bricks (Graviner) of 5 and 10 cm thicknesses were used to construct various shielding configurations around the detector. Since the detector was mounted in a vertical configuration on its cryostat, concrete blocks were required to support the necessary lead shielding at the correct height. Beneath the detector dewar the floor was lined with 10 cm lead, upon which steel tables were nested to support an annular collar and collimators which provided shielding for the bottom and sides of the detector. This arrangement resulted in a conical field of view for the detector in the upwards direction, the exact angle of the cone being adjustable by means of the demountable lead rings forming the collimator. Vertical 10cm thick lead walls and a top cover could be built around the collimated detector to test the effect

of various shielding arrangements and in order to accommodate a human in the counter, two walls were positioned symmetrically 36cm apart to a height of 40cm and a length of 120cm around the detector. A 12mm thick steel plate was positioned across the walls to support a "roof" over the counting space which was covered with 10 cm lead bricks.

The clearance between the detector and the roof was 35.8cm which is sufficient to accommodate a human body laying supine inside the lead shield. A diagram of the arrangement is given in Fig 5.3.

In order to study the effectiveness of the shield, bricks could be removed or added and the depth of collimation around the detector could be adjusted. A code for the formation of the shield from the (10cm) lead bricks was used so that "W4XL12" meant four bricks high by twelve bricks long. All the Figures contain a key code for further clarification. A final whole-body counting arrangement would be constructed in a highly secure manner in order to secure patient safety.

## **5.2.2 Experimental method.**

### **5.2.2.1 Shielding reduction factor.**

At the outset, the detector background was examined with no shielding where the cosmic-ray and environmental background components are normally dominant and conversely with maximum shielding (10 cm lead) which reduced these components as shown in Figures 5.4.(a) and 5.4.(b).

### **5.2.2.2 Build-up of the shield.**

The building up of the whole configuration was carried out progressively in stages and simultaneously (wall and roof) starting with the detector in the centre of the shield. The height of the wall was, from the beginning, made to be not less than 40cm so as to be adequate for accommodating a human body, and minimize any claustrophobic effect on the measured person. Long measuring times were necessary to collect acceptably accurate data for the most prominent background peaks. Figure 5.5 shows the effect of the different roof and wall configuration on the measured levels of the

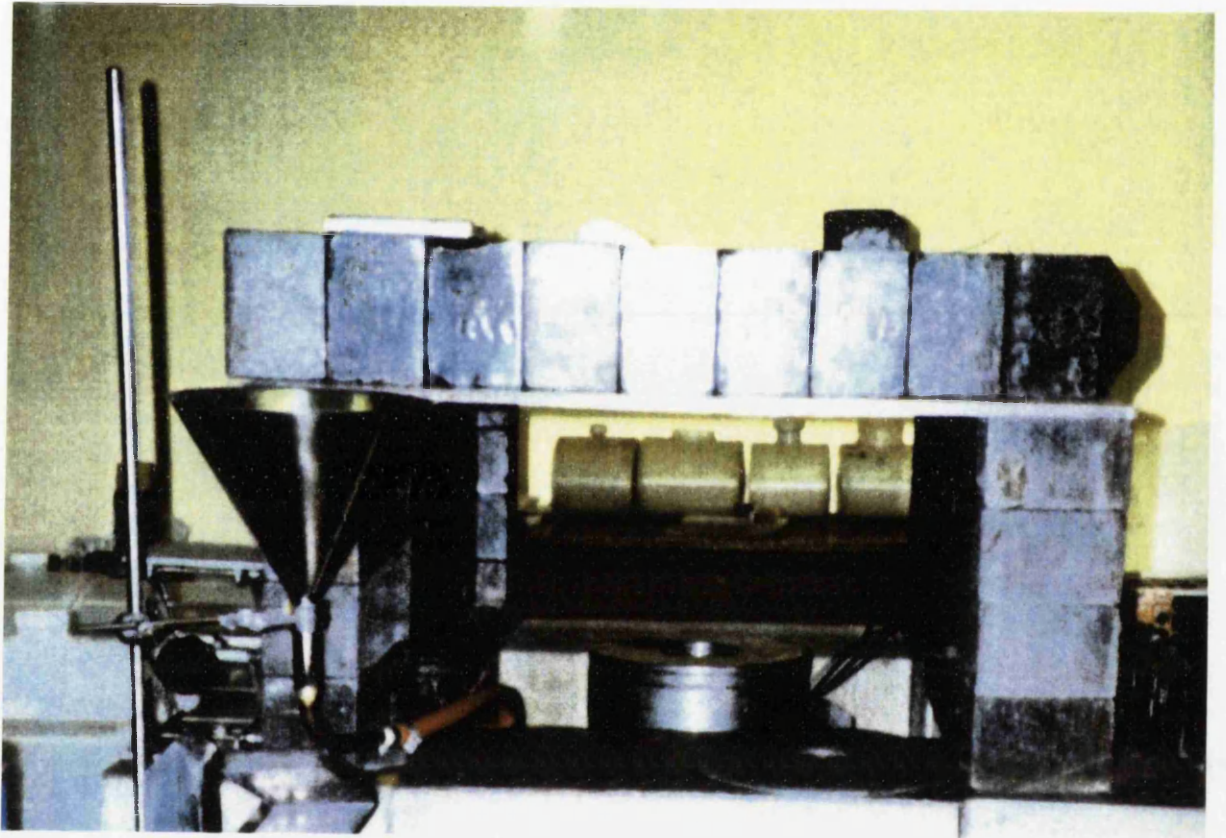


**Figure 5.3** View of the experimental set-up showing the concrete support, the collimator surrounding the  $127\text{cm}^3$  germanium detector and the development of the lead shadow-shield.

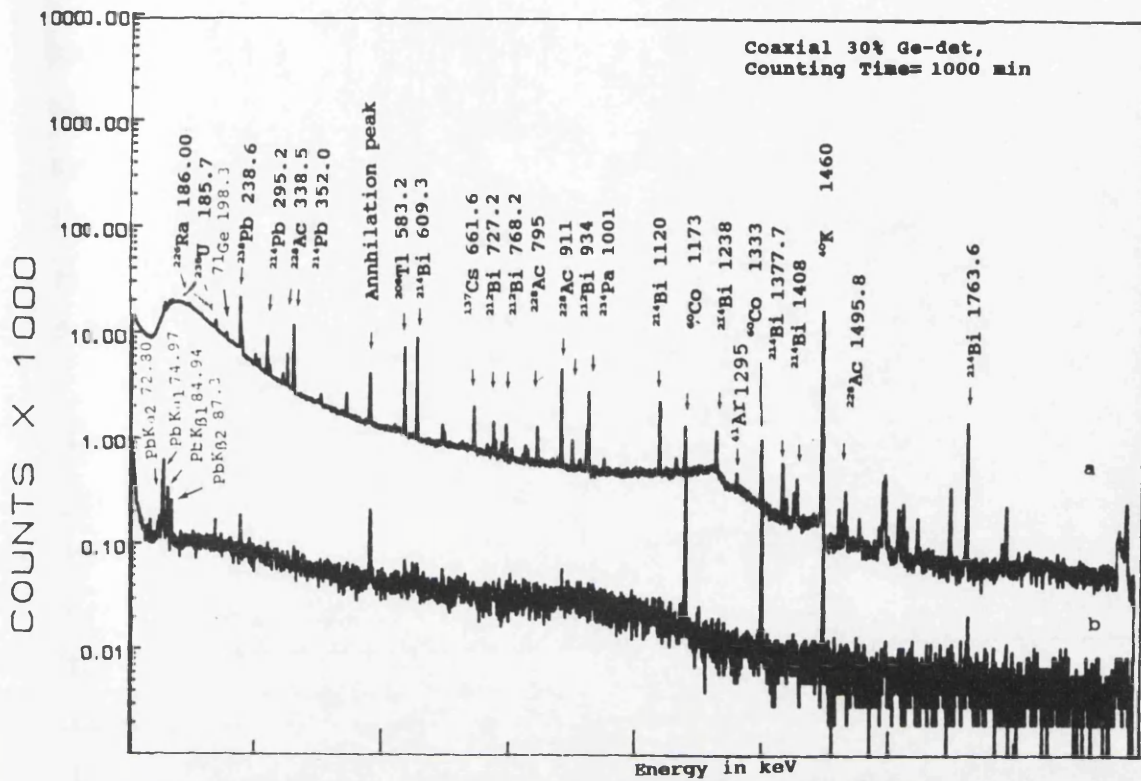


Figure 5.4 (a)  $\gamma$ -ray spectrum of complete open detector.  
(b)  $\gamma$ -ray spectrum of maximum shielded detector.

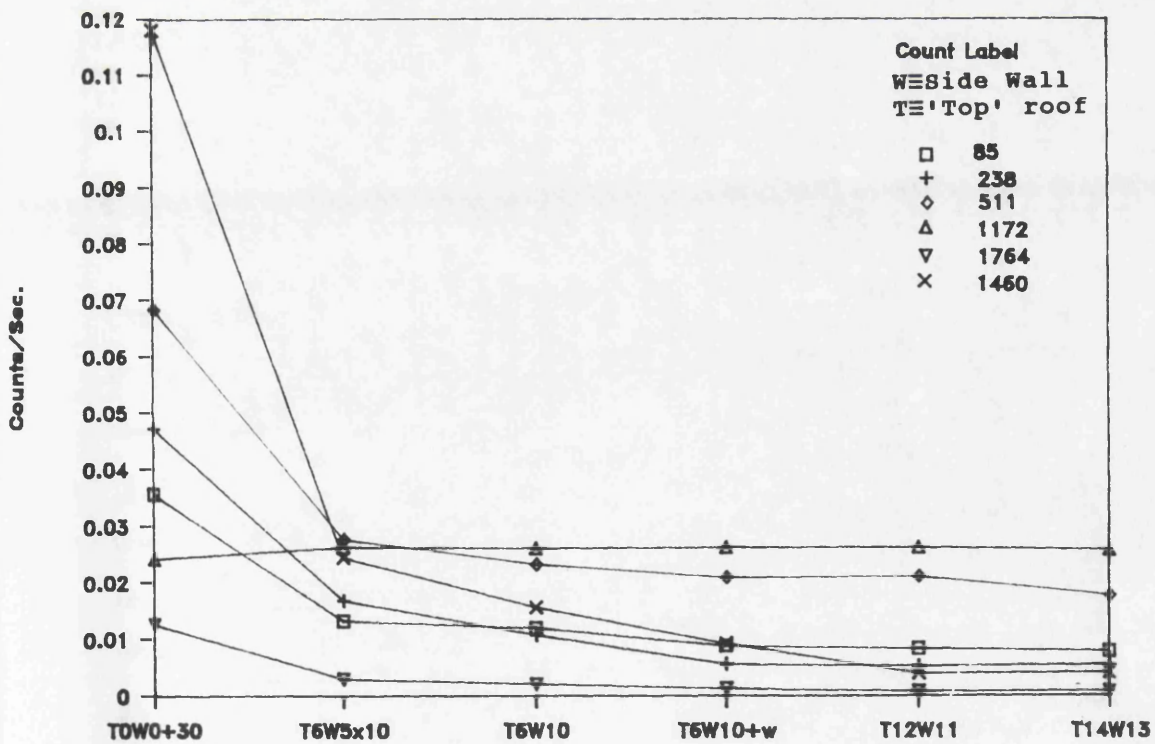


Figure 5.5 Variations of count rate (cps) using different roof and wall arrangements.

main background energy peaks. The coding used to specify the configuration of bricks indicates the number of bricks forming the walls and the roof: T6 means "Top" 6 bricks; W5X10 means "Wall" contain 5 bricks of 10 centimeter thickness; and in some the degree of detector collimation is indicated by (+30) means.

#### **5.2.2.3 Collimator effect.**

The collimation factor is very important for any type of radiation detector in general. The amount of collimation around the detector crystal determines the solid angle of detection which in turn affects how much of the active area of the detector crystal is "seen" by the measured source. Fig 5.6. shows the number of the detected counts per second for a number of gamma-ray energies for various degrees of collimation of the detector crystal. Figure 5.7 shows the ratios of the counts per second (cps) of three collimation settings (-6mm, +30mm & 48mm), to the count rate (cps) obtained with the detector in of the completely closed detector arrangement. Using this detector to measure an internally deposited radioactive nuclide the highest sensitivity will be achieved when the detector is closest to the measured body.

#### **5.2.2.4 Graded shielding.**

Cosmic-ray and secondary gamma-ray interactions produce characteristic X-rays in the detector shielding. For lead these X-rays appear in the lower part of spectrum at 77 keV and 84 keV. These X-rays can be minimised by means of "graded shielding" in which selected elements in the form of metallic foils are used to absorb them. In the present set-up the detector was shielded with 3mm thick sheets of cadmium and of copper, placed around it in the lead shield. The effect of this graded shield can be demonstrated by the difference in unshielded gamma-ray spectrum shown in Fig 5.8(a) and (b) where the lead X-rays at 75 and 85 keV have been significantly attenuated. The cadmium absorbs the Pb X-rays but re-radiates its own X-rays at 23 keV which are in turn absorbed by the copper giving the reduction sought.

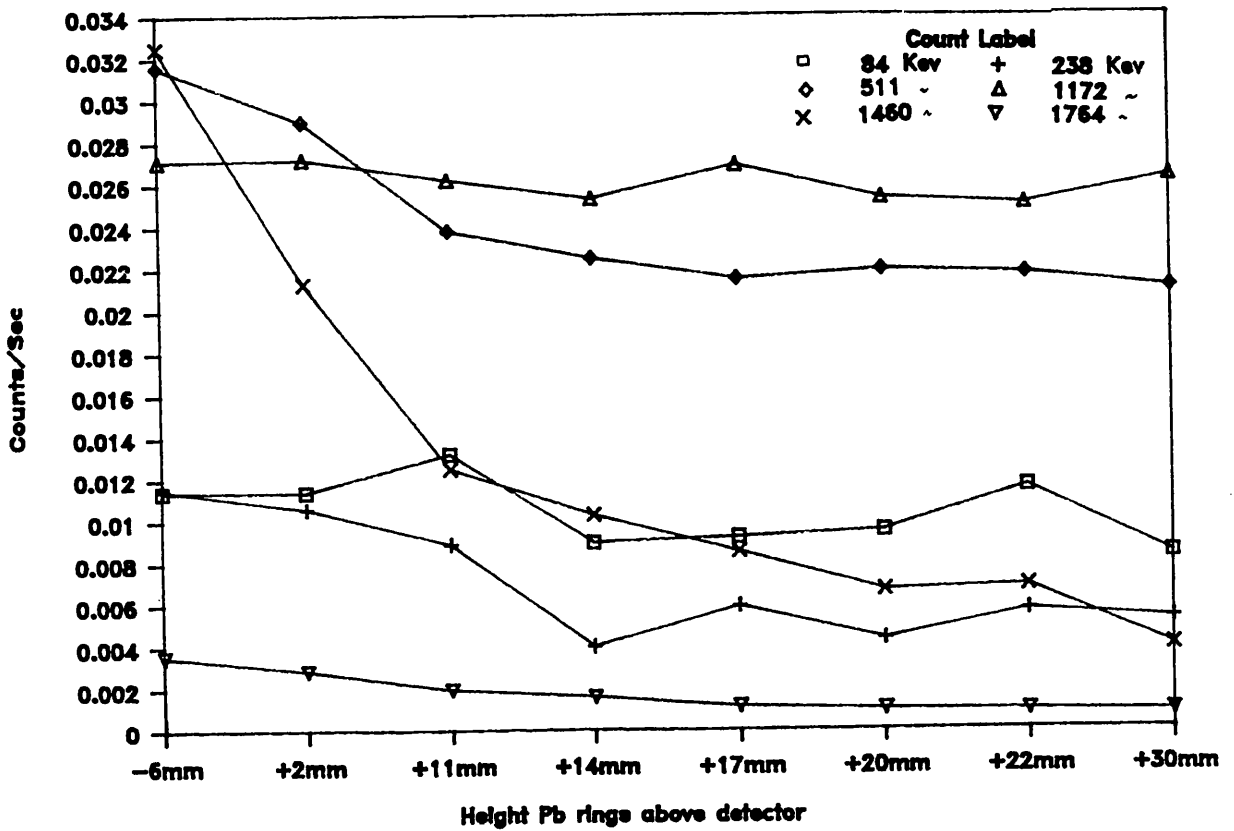


Figure 5.6 The collimation factors vs the count rate (cps) effects on main energy lines.

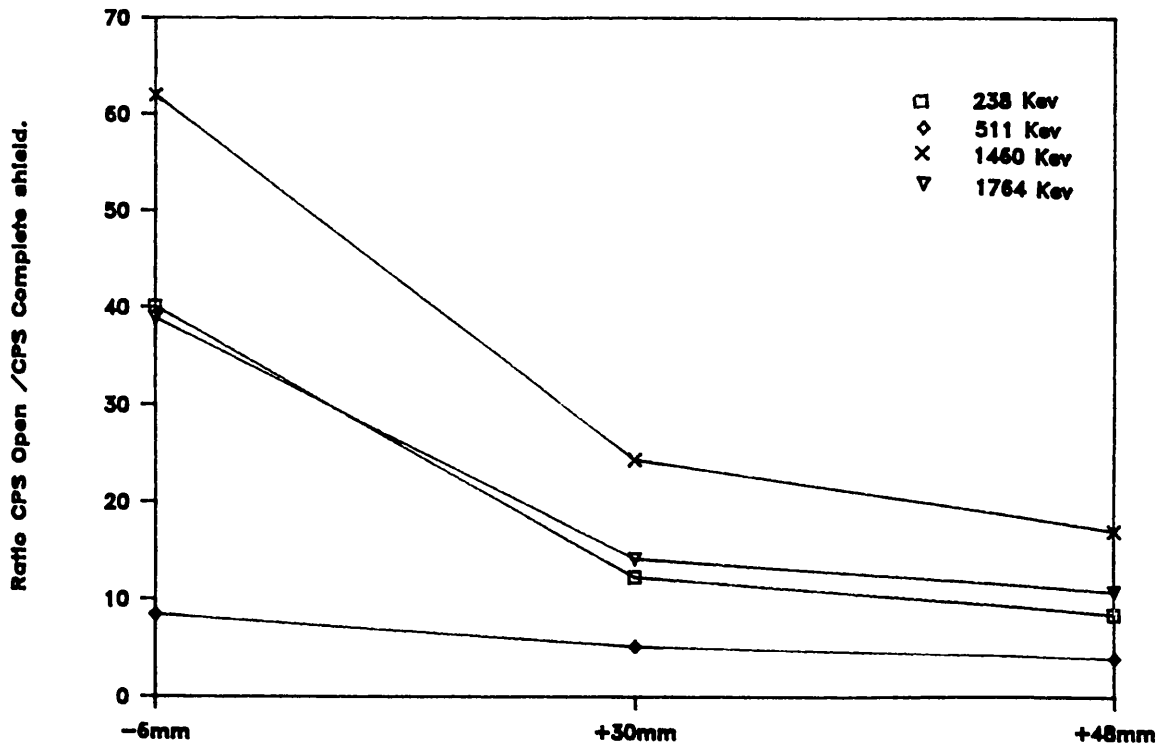


Figure 5.7 Ratios of count rate (cps) using different collimation to the complete closed arrangement.

#### 5.2.2.5 Gain settings.

During the course of measurements two gain settings were used with the main purpose of covering the most abundant natural energy lines around both ends of the gamma spectrum. During the first part of the experimental measurements the gain setting was set at 0.497 keV per channel which extended the lower end of the spectrum to measure down to 40 keV to include the 46 keV gamma from  $^{210}\text{Pb}$ , while the upper energy range was up to 2000 keV only.

In the second stage of the experiment the gain was reduced to give 0.701 keV per channel which extended the upper end of the spectrum to 2800 keV which covered up to 2615 keV  $\gamma$ -ray from  $^{208}\text{Tl}$ . However by doing this, the lower end of the spectrum was suppressed and only energies greater than 60 keV could be identified clearly. Since a planar detector was also available to measure the low energy photons, the use of this higher range in the coaxial germanium detector was appropriate.

#### 5.2.2.6 Dead time losses.

The effect of dead time in  $\gamma$ -ray spectrometry can lead to the loss of counts from the full energy photo-peak at high count rates. It occurs mostly in the analog-to-digital converter of the pulse height analyzer because when it is busy processing a pulse, the analyzer is incapable of accepting a further pulse for a given time interval. Experimentally the dead time of the coaxial germanium detector was studied using a number of  $\gamma$ -ray sources, measuring them separately and then adding them one by one. It was noticed that as the activity increased the dead time also increased progressively and the counts for the main  $^{137}\text{Cs}$  source used to check count losses decreased.

Figure 5.9 shows the experimental graph produced by dead time measurement for the  $^{137}\text{Cs}$  source. From the graph it can be seen that for up to 40% dead time the correction for the counting losses can be taken to be minimal due to the fast processing capabilities of the detector electronics. In addition most of the measurements for body counting would be at low levels and therefore no corrections for dead time would be needed.

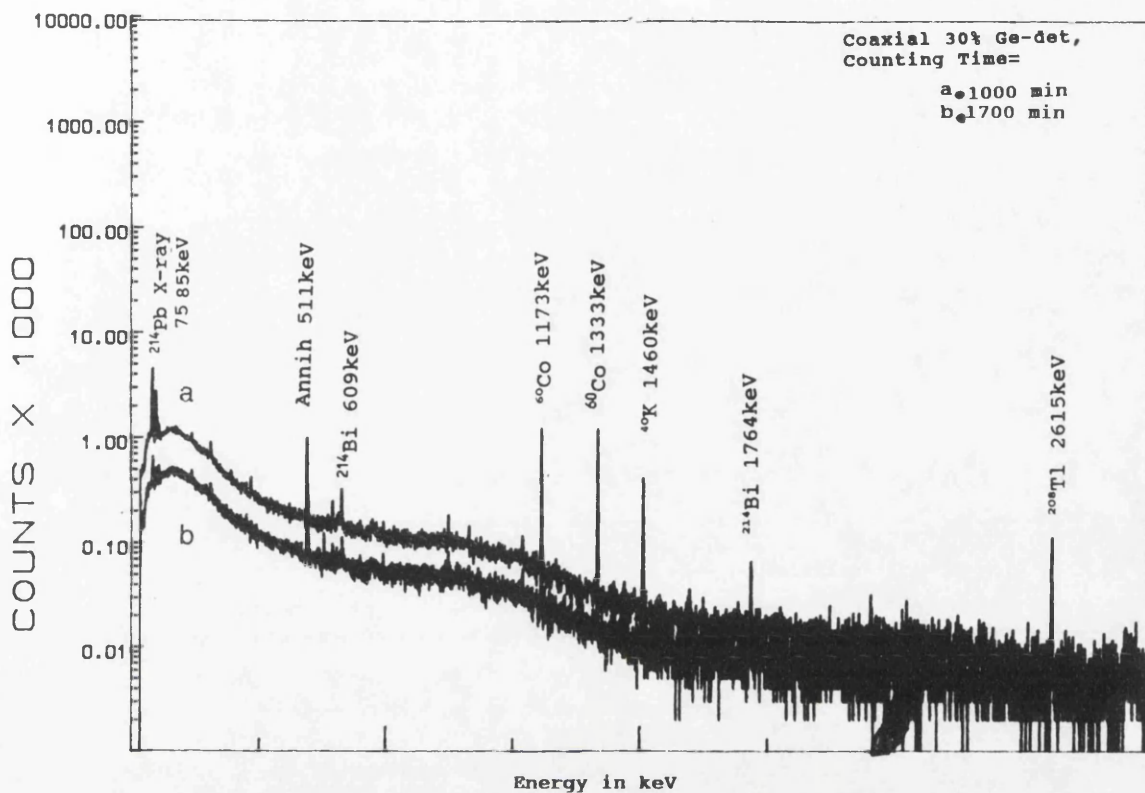


Figure 5.8 (b)  $\gamma$ -ray spectrum without Cd and Cu sheets.  
 (a)  $\gamma$ -ray spectrum with Cd and Cu sheet shield.

POLYNOMIAL REGRESSION FOR DEAD TIME  
 USING CS137 CSOURCE

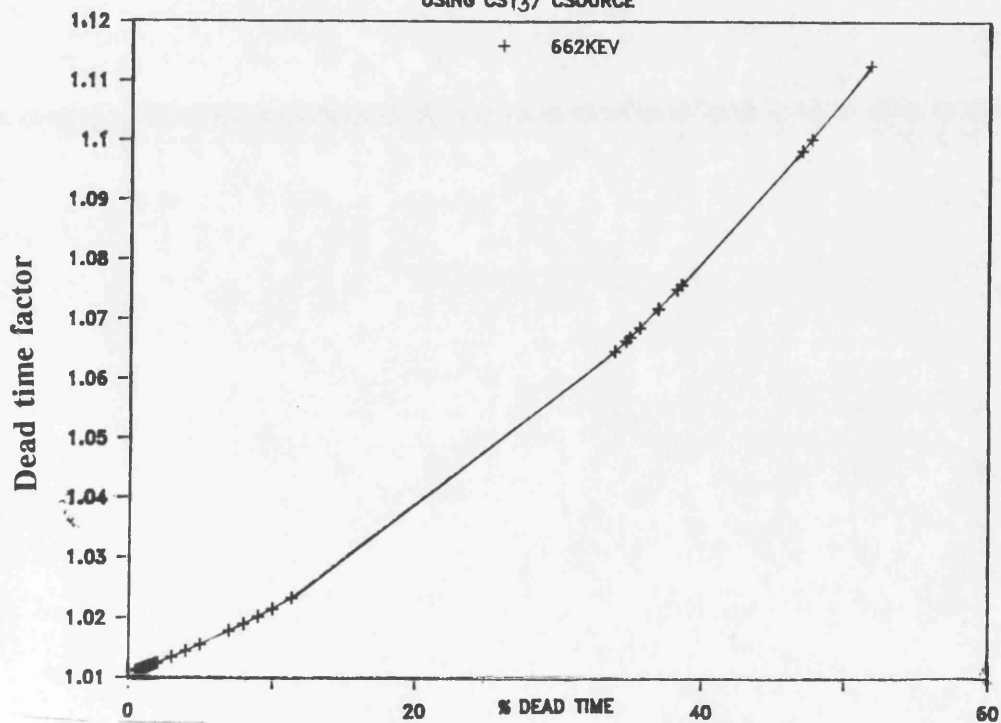


Figure 5.9 Regression analysis for dead time experiment

### 5.3 Analysis of gamma-ray spectra.

As explained earlier, a "Minigam" program (Ortec) was used to analyze the spectra. The program was based on a peak search algorithm employing a smoothed "second-difference" method to locate the peaks. After location of the peaks, their centroids were determined more precisely by a Gaussian fitting technique. The Minigam calculates the peak area in the spectrum by first calculating the background at points above and below the peak centroid but clear of the peak centroid as shown in Figure 5.10(a). Then in order to calculate the peak a 5-point sliding average of the channel contents is calculated for the region ranging from the peak centroid channel to the channel which is three times the calculated FWHM using the calibration data. If the minimum average value is however within one sigma of the actual spectrum data, a 3-point sliding average is used instead to calculate the new minimum value. It is then compared with the actual data and accepted if it is within one standard deviation. If not, then this value is used as a background value. It must be noted that the same process is repeated for the higher energy side of the peak and the background under the peak is taken as a straight line between these two points as shown in Figure 5.10 (b).

Two methods of peak analysis could be used - "library-directed" and "peak-search directed". All the spectrum peaks used for the calculation of activity were validated in the program by a number of criteria as follows;

- (a) exceeding the preset sensitivity level: 30% was the level set for most peak analyses.
- (b) passing a peak shape test to determine the interference level.( i.e of adjacent peaks).
- (c) passing a peak centroid test compared to the energy peaks in the program library.

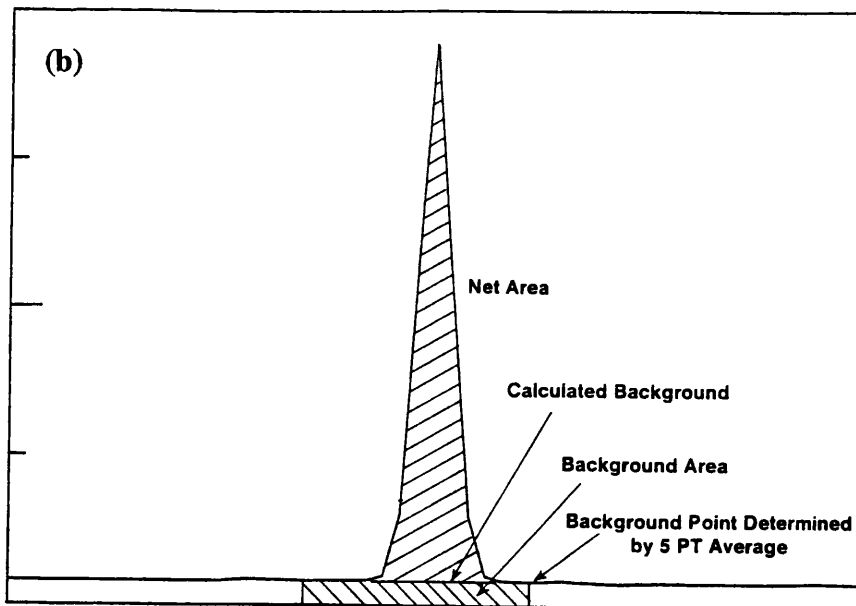
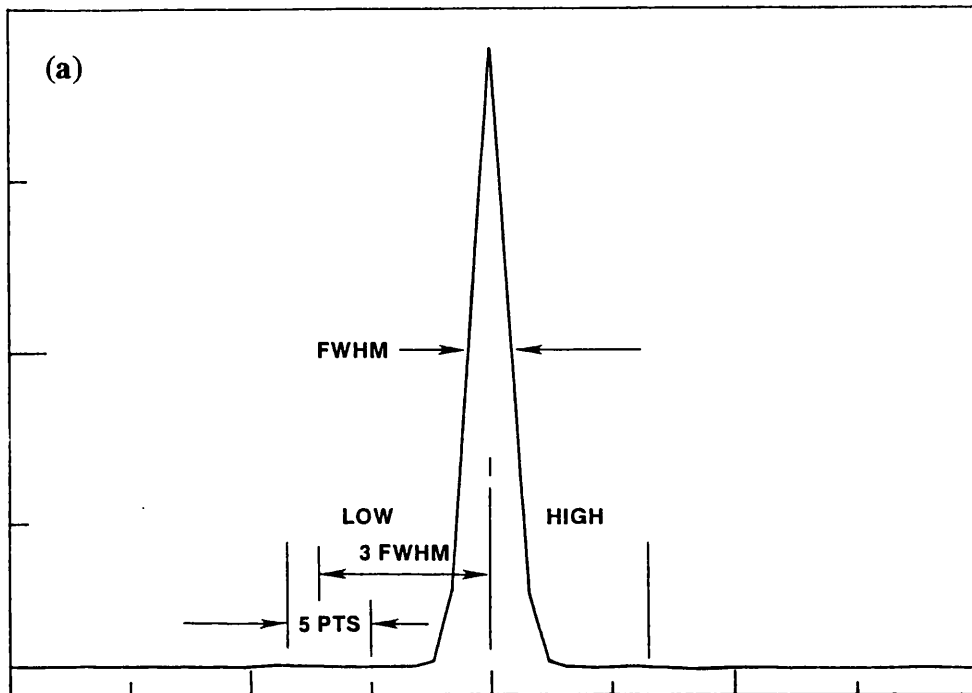


**Figure 5.10 Peak and background calculation methods used by Minigam II computer programme. (a) Peak calculation. (b) Background and net peak area (EG&G manual, 1988).**

### 5.3.1 Summation of gamma ray spectra.

A summation programme was developed (Harris,I. 1990) for data handling capable of summing up to 200  $\gamma$ -ray spectra of 4096 channels each. A requirement was that spectrum files should have matching energy calibrations, especially the first and last spectra summed. This program was utilized successfully to sum a number of recorded matching spectra. Its use is illustrated by comparing a single spectrum with ten summed spectra as shown in Figure 5.11 (a) and (b).

### 5.4 Results and discussion of the Background data collected.

The average exposure rate of natural radiation in the detector vicinity was measured to be approximately (  $60\text{nSv.hr}^{-1}$  ) and outside the building was the same. Thus the building construction did not alter the level appreciably.

The  $\gamma$ -ray spectra shown in Figure 5.4 (a) and (b), are typical of the  $\gamma$ -rays recorded under the two extreme conditions i.e bare detector and complete shielding configurations. A major reduction can be seen in spectrum (b) where the significant reduction of cosmic flux and the ambient sources of  $\gamma$ -rays in the background is demonstrated. The whole spectrum of Fig 5.4.b looks markedly depressed due to the shielding effects even though some of peaks seem to be unaffected. The calculated reduction factor of a number of these peaks is in the range of 100-200.

It is also noted that in the same spectrum (b) some new peaks have emerged which probably represent the interaction of natural cosmic rays with the lead shield and the materials surrounding the detector assembly producing lead X-rays at 74 keV and 84 keV. Also the annihilation peak at 511 keV which is due to pair production is clearly seen.

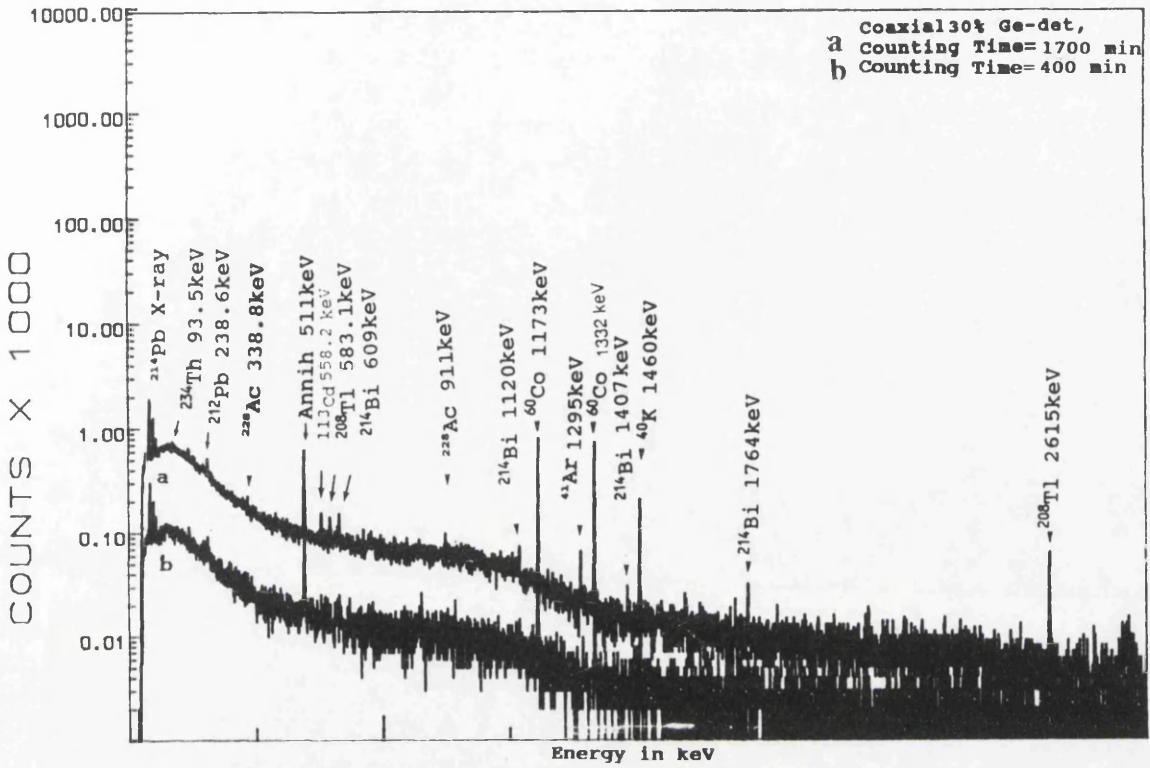


Figure 5.11 (b) single  $\gamma$ -ray spectrum.  
 (a) Ten summed  $\gamma$ -ray spectra.

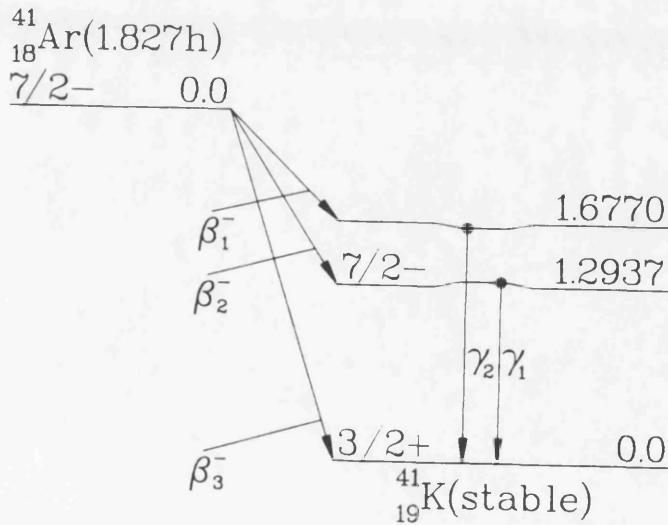


Figure 5.12 Argon-41 decay scheme.

The principal peaks which are clearly identifiable and present in most of the recorded spectra are all members of the thorium, uranium-radium decay series whose main daughter radionuclides are shown in Figures 2.2 and 2.3.

The thorium series is represented by  $^{212}\text{Pb}$  (238.6 keV)  $^{228}\text{Ac}$  (338.8 keV),  $^{208}\text{Tl}$  (583.1 keV),  $^{228}\text{Ac}$  (911.2 keV) and  $^{208}\text{Tl}$  (2614.6 keV).

The gamma energy peaks, corresponding to the uranium series are  $^{210}\text{Pb}$  (46.5 keV)  $^{234}\text{Pa}$  (63.5 and 93.5 keV),  $^{214}\text{Pb}$  (295.2 and 352.0 keV),  $^{214}\text{Bi}$  (609.3 and 1120.3 keV), and can also be seen.

A prominent and recognisable peak at 1460 keV is present in all the  $\gamma$ -ray spectra due to  $^{40}\text{K}$ . Also a measurable amount of the background can be attributed to traces of radioactive gas or dust particles carrying  $^{222}\text{Rn}$  (186.2 keV) or  $^{220}\text{Rn}$  (241 keV) which emanate from uranium and thorium.

In addition to the natural activity, analysis of the recorded gamma energy peaks indicates the presence of traces of  $^{134}\text{Cs}$  (604.7 and 795.8 keV) and  $^{137}\text{Cs}$  (661.66 keV). Also  $^{60}\text{Co}$  is present (1172keV & 1332keV) which was discovered to be due to radioactive contamination. This problem is discussed further in the next sections.  $^{60}\text{Co}$  frequently occurs in the vicinity of nuclear reactors as a contaminant resulting from neutron activation of traces of cobalt in steel components.

A number of other peaks can also be identified in the gamma spectra in the final shielding configuration. These peaks are mainly attributed to the neutron activation process and prompt neutron capture  $\gamma$ -rays mainly with the detector shield and detector material itself. These gamma peaks can be accounted for by interactions of different components of cosmic rays, mainly particles such as neutrons, pions and mesons with the materials surrounding the detector and with the detector crystal itself. These produce  $^{75\text{m}}\text{Ge}$  (138.9 keV),  $^{77}\text{Ge}$  (215.8 keV) and also the 557.8keV of  $^{113}\text{Cd}$  due to the  $(n,\gamma)$  reaction.

The application of the summation program of a number of background measurements is shown in Figure 5.11 (b) from which it can be seen that a number of energy peaks which could not be easily identified before the

summation. They become very clear, more pronounced and easily identifiable in the summed spectrum. These peaks are as follows: 338 keV of  $^{228}\text{Ac}$ , the three distinguished closely sited peaks namely the 557.8 keV, 583 keV and 609 keV. Also the peaks at 1120 keV and 1407.9 keV from  $^{214}\text{Bi}$  can be seen clearly in the summed spectrum.

### 5.5 Background interferences - $^{60}\text{Co}$ and $^{41}\text{Ar}$ .

Two main interferences were observed in a number of the recorded  $\gamma$ -ray spectra mainly due to  $^{60}\text{Co}$  and  $^{41}\text{Ar}$  which gave peaks at 1172 and 1332, and 1295 keV respectively. Both these radionuclides are commonly encountered on a nuclear site.

As far as the  $^{60}\text{Co}$  interference is concerned this could only be explained in terms of an unknown source of contamination occurring on the detector housing before it was relocated for the present work. A number of background measurement were taken before its removal from the previous location which showed no presence of traces of  $^{60}\text{Co}$  contamination at that stage.

However as work on the effect of the shielding was progressing it was noticed that a higher than normal background level of  $^{60}\text{Co}$  was present. For the processing of background analyses this  $^{60}\text{Co}$  was subtracted from the spectra. In order to trace the source of  $^{60}\text{Co}$  contamination a number of measurements were carried out on each element of the detector shielding assembly. It was found very difficult to pin-point the exact location of the contamination. Initially, the detector crystal housing was thought to be the main cause, but after a thorough examination the most contaminated area was found to be the inner part of the lead annular collimators. The inner surface of the collimators was cleaned using "emery" cloth grade 200, and then decontaminated with concentrated "Decon" solution. The same cleaning process was carried out for the detector crystal housing. As demonstrated in Fig 5.13 the levels of  $^{60}\text{Co}$  peaks throughout the decontamination process fluctuated at first and then were reduced to the previous background levels.

The second much lesser degree of interference namely that from  $^{41}\text{Ar}$  could be attributed to the location of the detector assembly. The designated room for the

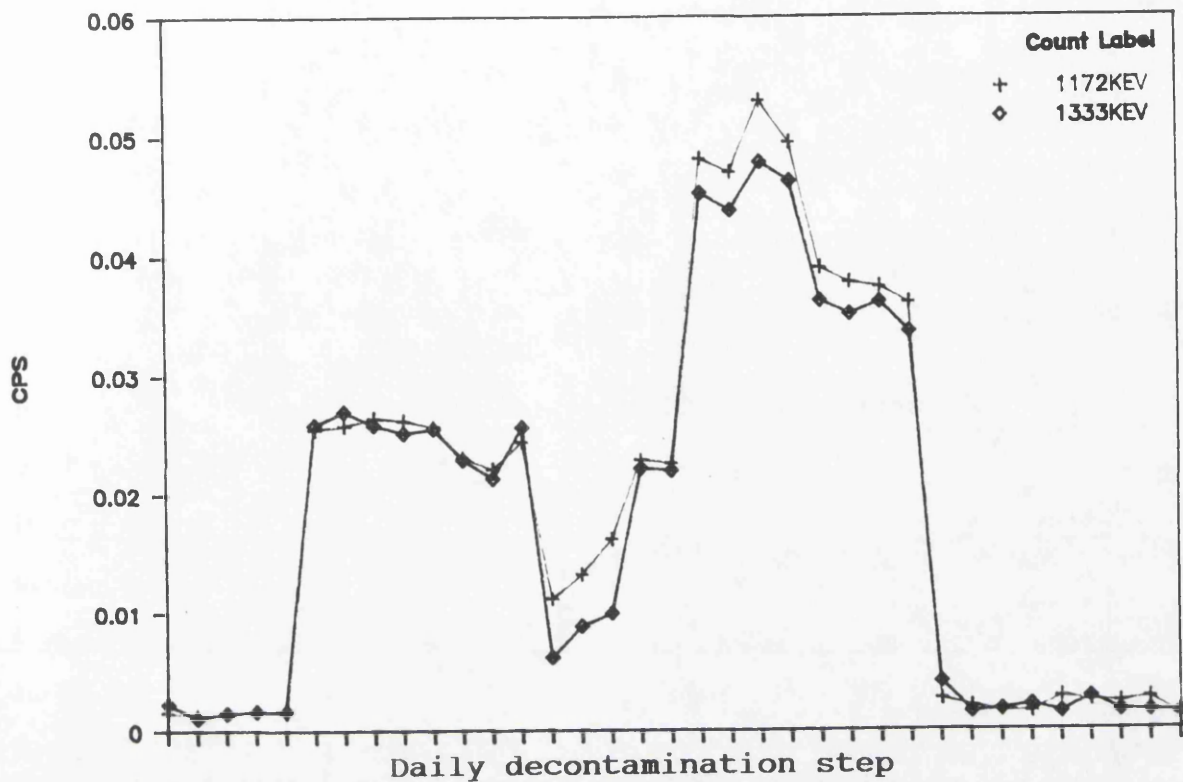


Figure 5.13. The  $^{60}\text{Co}$  detection level before, during and after the decontamination procedures.

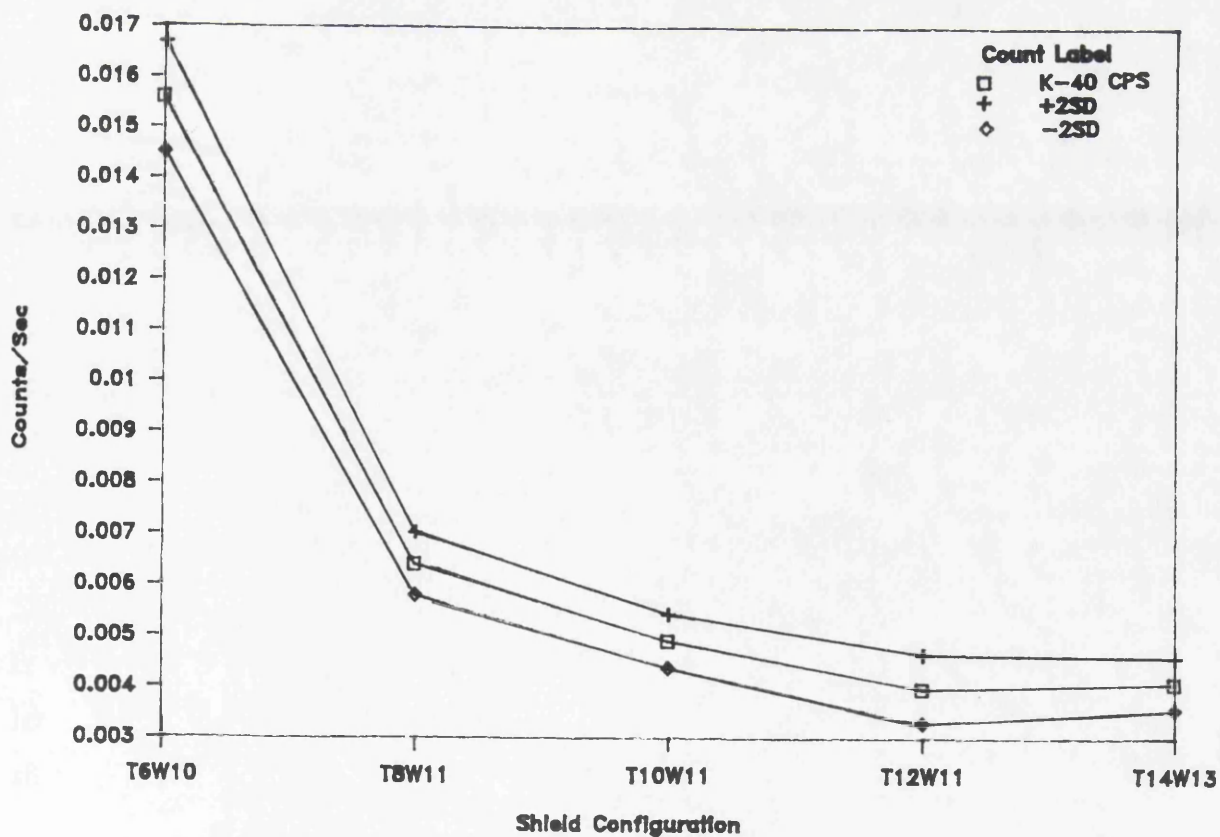


Figure 5.14  $^{40}\text{K}$  cps vs shield configuration.

semi-conductor whole body monitor (SCWBM) shown in Figure 5.1, was situated in the block adjacent to the reactor hall which houses the 300 kwatt nuclear research reactor of the SURRC. Clearly this is not an ideal location for having a low level counting system, but is a factor which has to be accepted under the circumstances. From background measurements it was noticed that on certain days of reactor operation,  $^{41}\text{Ar}$  with a gamma energy of 1295 keV, could be observed depending on the weather conditions. This radionuclide is produced by neutron activation of the air passing through the reactor core;  $^{40}\text{Ar}$  undergoing neutron capture:  $^{40}\text{Ar}(n,\gamma)^{41}\text{Ar}$ , a decay scheme of  $^{41}\text{Ar}$  is shown in Figure 5.12. The summed activity on certain days is shown in Fig 5.11(a) and clearly demonstrates the presence of the 1295 keV peak from  $^{41}\text{Ar}$ . Again because of the high resolution of the Ge-detectors this peak could be easily resolved from others in the spectrum. The same peak appears clearly in Fig. 5.4(a) which is typical of the open background count measurement which continued for a number of days during the reactor operating hours.

#### 5.6. Potassium-40.

Since potassium-40 is one of the main background components in the environment and is present *in vivo* when measuring human subjects, it is useful to take its spectral presence as an indicator for various degrees of shielding around the detector. First, the results for various collimator thicknesses in relation to the reduction of the count rate (cps) of the energy peak of 1460 keV of  $^{40}\text{K}$  are given in Figure 5.14. It can be seen that initially there is a continuous reduction of counts which then levels off between a collimator depth of 20mm and 22mm.

Similarly, different wall and roof configurations were examined and it can be seen from Figure 5.5 that increasing numbers of bricks gave reductions until a roof length of 120 cm and a wall length of 110 cm had been reached. Beyond these sizes little further reduction in the background was observed.

## 5.7 Standard source measurements.

The same prepared sources which were used for the NaI(Tl) counter measurements (Th, U) were measured using the final shadow-shielding configuration to examine the detection capabilities of the detector under this particular arrangement. Also other calibrated point sources were used, particularly  $^{241}\text{Am}$ ,  $^{57}\text{Co}$ ,  $^{137}\text{Cs}$  and a mixed alpha source of  $^{241}\text{Am}$ ,  $^{244}\text{Cm}$  and  $^{241}\text{Pu}$ . All the collected  $\gamma$ -ray spectra of the different available sources are shown in Figures 5.15, 5.16, 5.17 and 5.18. As has been explained earlier the high energy resolution of this detector permits the energy peaks to be clearly identified.

Using the capability of expanding the pulse height spectra, it can be seen in Fig 5.15(a) that even the closely located X-ray peaks of the  $^{241}\text{Am}$  and  $^{241}\text{Pu}$  can be broadened and can be distinguished clearly from one another.

In addition to these sources, 45.6mg of  $^{133}\text{Ba}$  solution was also diluted in 500ml acid solution and measured close to the surface of the detector. Table 5.1 shows the calculated sensitivity, critical level and the limits of detection.  $^{133}\text{Ba}$  provides a series of useful gamma-ray peaks both at low and intermediate energies allowing efficiency and sensitivity to be assessed. The minimum detectable activity at low energies seems to be low and for the medium energy range, i.e around 300-800 keV, becomes considerably lower.

## 5.8 Calculated sensitivities and limits of detection.

Using the derived equations 4, 8 and 9 in chapter 3, the standard deviation of the background, the critical level, the minimum detection limits and the determination level at 95% confidence limit were calculated for the main  $\gamma$ -ray peaks of the background and for a number of radioactive sources. These quantitatively are presented in the Tables of following subsections:

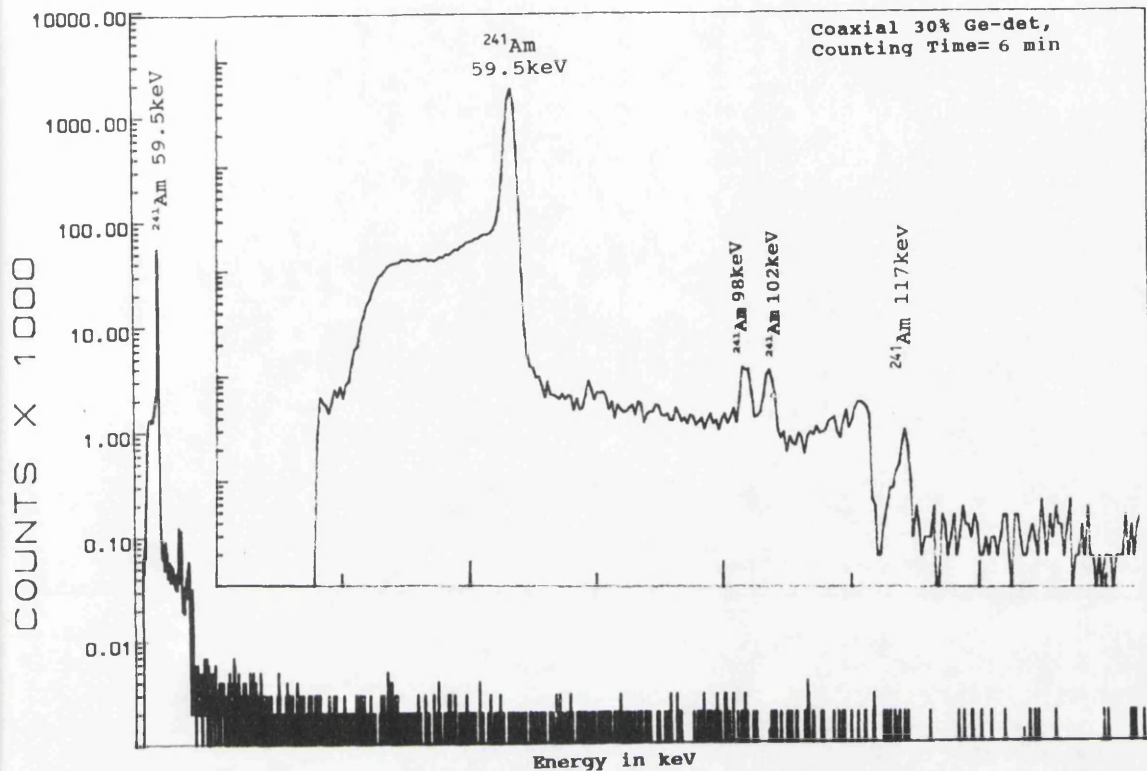


Figure 5.15 (a) Expanded  $\gamma$ -ray pulse height spectrum of  $^{241}\text{Am}$ .  
 (b) Normal  $\gamma$ -ray spectrum of the same source.

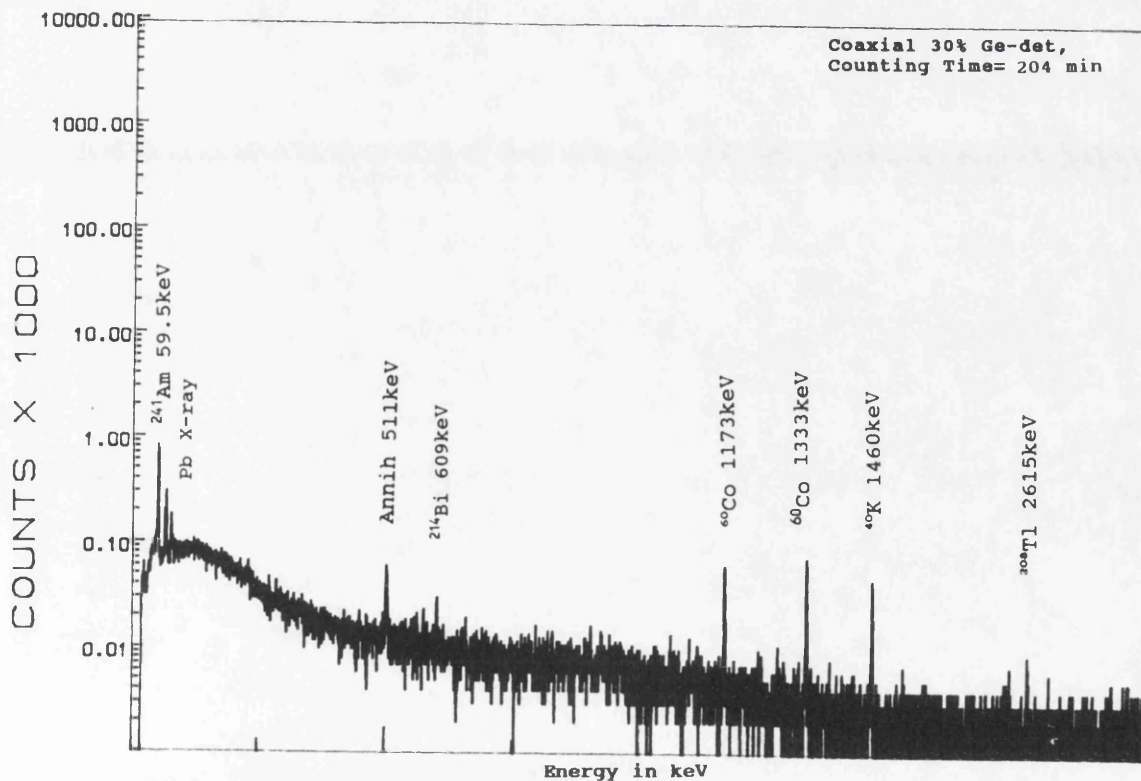


Figure 5.16  $\gamma$ -ray spectrum of the mixed alpha source.

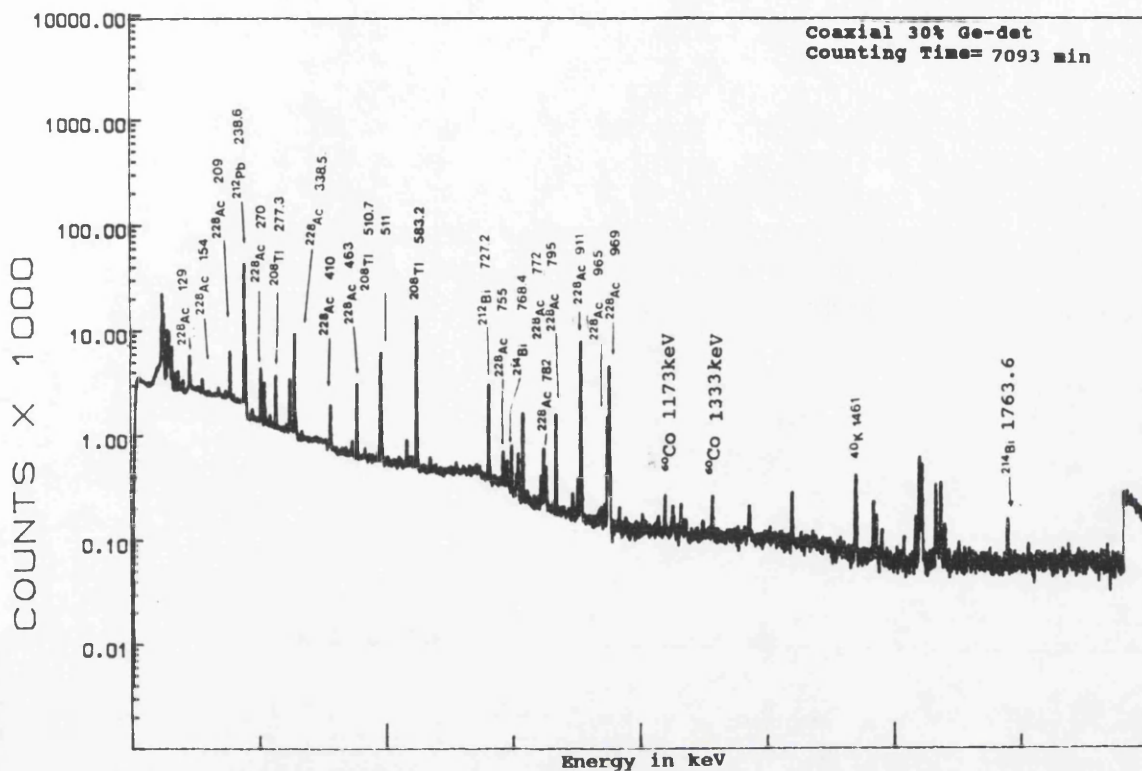


Figure 5.17  $\gamma$ -ray spectrum of  $^{232}\text{Th}$ .

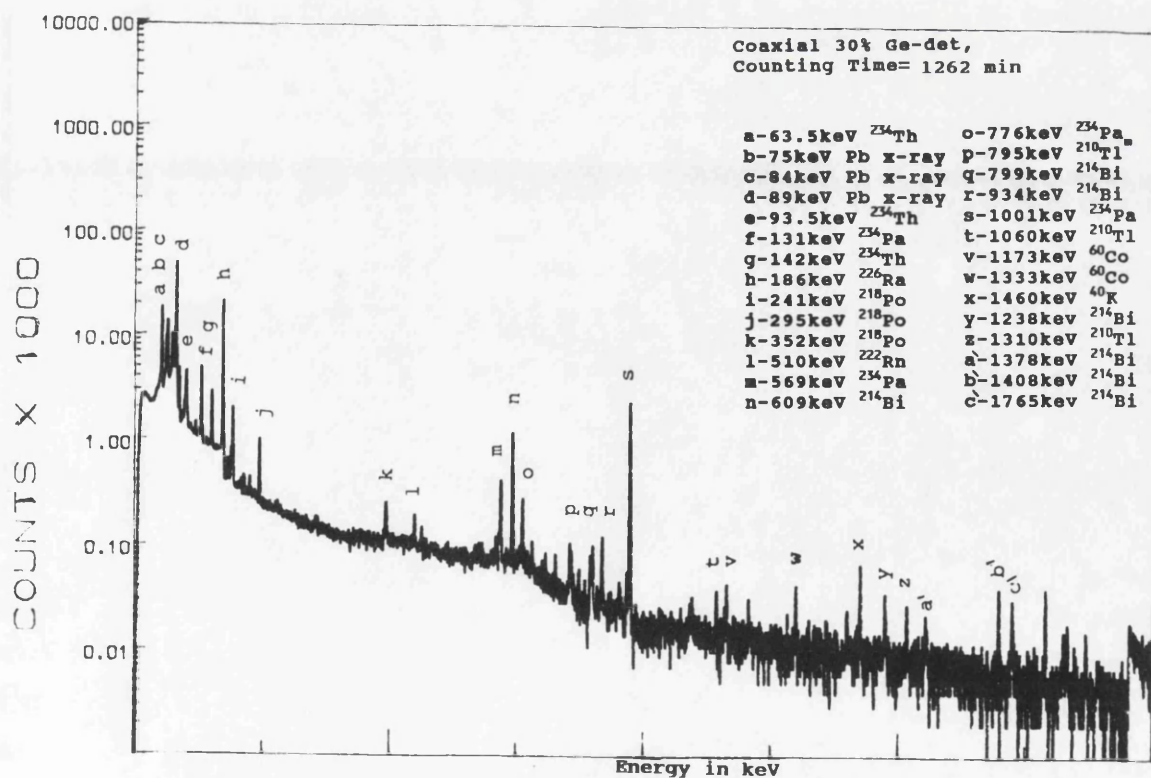


Figure 5.18  $\gamma$ -ray spectrum of  $^{238}\text{U}$ .

### 5.8.1 - Background measurements.

The measured background data for the germanium detector are collected and presented in Table 5.8.1. Due to the high resolution of the detector many peaks can be seen in the background even when the background was recorded with the optimised shielding arrangement. All the natural nuclides are present and can be determined with a considerable sensitivity, especially for the medium energy peaks. The corresponding limits of detection appear to be of a useful magnitude while the determination limits for a 95% confidence limit are as expected, high.

These background levels were measured with the final design of shielding configuration using the 22mm deep lead collimator described previously.

Nuclide	$E_\gamma$ keV	cpm/ Bq	$\sigma_B$ cpm	$L_C$		$L_D$		$L_Q$ Bq
				cpm	Bq	cp	Bq	
$^{234}\text{Th}$	186	0.011	0.19	0.44	40	3.57	325	9091
$^{234}\text{Pa}$	242	0.019	0.15	0.35	18	3.41	179	5263
$^{214}\text{Pb}$	295	0.041	0.13	0.31	8	3.31	81	2439
$^{214}\text{Bi}$	351	0.069	0.09	0.21	3	3.12	45	1449
$^{214}\text{Bi}$	609	0.053	0.07	0.15	3	3.02	57	1887
$^{214}\text{Bi}$	1120	0.011	0.05	0.11	10	2.94	267	9091
$^{214}\text{Bi}$	1238	0.004	0.03	0.08	20	2.87	718	25000
$^{214}\text{Bi}$	1764	0.008	0.03	0.06	8	2.83	354	12500

**Table 5.8.1 Sensitivity, background standard deviation and detection parameters for a two-hour background counting time of the final shielding arrangement of the 127cm<sup>3</sup> Ge-detector.**

### 5.8.2 Barium-133 source.

Table 5.8.2 shows the results of the measured sensitivity and all the calculated values for measuring 100mg of barium-133 labelled powder mixed in a 500ml acid solution. The four main  $\gamma$ -ray energy peaks are present and the calculated values for critical level is in the range of 0.1-1.0 Bq, whereas the minimum detectable activity is in the range of 1.0-9 Bq which is considered to be very high and useful for the measurement of this isotope.

### 5.8.3 Thorium measurements.

Table 5.8.3 shows the calculated values for the same parameters as above for 60mg of  $^{232}\text{Th}$  in a 500ml container measured close to the detector surface. It can be seen that many of the thorium and daughter peaks are present and can be identified. However the best  $\gamma$ -ray peaks sensitivity and lower limits of detection are for the 238, 338, 583 and 911 keV. These peaks could be potentially be used as a clear indication of the presence or absence of thorium even when counting a human subject as they have a substantial energy range and as well as higher abundance.

Energy keV	BKGR cpm	$\sigma_{\text{BKGR}}$ cpm	cpm/Bq	$L_C$ 2hr Bq	$L_D$ 2hr Bq	$L_Q$ 2hr Bq
53	0.75	0.08	0.02	9.32	154	5000
81	3.68	0.18	1.73	0.24	2.43	58
276	1.89	0.13	0.39	0.79	8.72	263
302	1.56	0.11	0.97	0.26	3.32	103
356	1.15	0.10	2.85	0.08	1.12	35
384	1.10	0.95	0.041	54	174	2483

Table 5.8.2  $^{133}\text{Ba}$  calculated values of sensitivity  $L_C$  and MDA for a two-hour count.

ENERGY keV	BKGR cpm	$\sigma_{\text{BKGR}}$ cpm	cpm/mg	$L_C$ 2hr mg	$L_D$ 2hr mg	$L_Q$ 2hr mg
238	5.3972	0.21	0.392	1.25	9.4	255
300	2.5485	0.15	0.023	15.19	148	4350
338	2.6893	0.15	0.077	4.54	44.25	1299
410	2.133	0.13	0.012	25.24	276	8336
463	1.4809	0.11	0.023	11.14	140	4349
583	1.5570	0.11	0.126	2.03	25.57	794
727	0.8006	0.08	0.025	7.46	123	4001
860	0.502	0.06	0.015	9.32	199	6667
911	0.4409	0.06	0.081	1.73	36.9	1235

Table 5.8.3 Background and calculated sensitivity for 127cm<sup>3</sup> Ge-detector for the main gamma-ray peaks of a  $^{232}\text{Th}$  60mg sample for a Two-hour count.

#### 5.8.4 Uranium measurement.

One gramme of natural uranium was dissolved in a 500ml acid solution. The measured and calculated values for the sensitivity, critical level and the minimum detectable activity are given in Table 5.8.4.

Even though a large number of gamma-ray peaks can be identified, the lowest detectable amount of activity is found to be that for the more abundant energy peaks mainly 93, 185.6, and 766 keV. Due to the type and volume of the detector used the best energy range is 63-186keV. In this range the critical limit was from 2 to 9mg for the geometry used (i.e one gramme in a 500ml container at 22mm from the detector). It was noted that the levels at which the detector gives a reliable quantitative determination i.e 95% confidence ( $L_Q$ ) are high even for the close geometry used. However, for initial studies of uranium in the body, such demanding accuracy would not be necessary at the outset.

ENERGY keV	BKGR cpm	$\sigma_{BKGR}$ cpm	cpm/ gm	$L_C$ 2hr mg	$L_D$ 2hr mg	$L_Q$ 2hr mg
63	3.74	0.18	46.9	8.9	76	2133
93	3.86	0.18	153.9	2.7	23	650
98	1.69	0.12	65.9	4.2	50	1518
121	2.68	0.15	9.9	35	341	10015
144	3.41	0.17	12.9	31	270	7709
186	3.41	0.17	66.9	6	52	1495
205	2.45	0.14	3.9	84	842	25100
766	0.71	0.08	4.9	37	686	22275
1001	0.78	0.08	9.9	19	309	10011

**Table 5.8.4 Background and different sensitivity values calculated for the main uranium peaks for a two-hour measurement using the 127cm<sup>3</sup> Ge-detector.**

### 5.8.5 Phantom measurements.

In order to determine the sensitivity of the germanium detector for *in vivo* measurements a number of anthropomorphic hollow polyethylene phantoms simulating the human chest were counted. These phantoms were filled with aqueous solutions containing known quantities of  $^{40}\text{K}$ ,  $^{134}\text{Cs}$  and  $^{137}\text{Cs}$  and measured above the detector inside the experimental shield ( Standardised radiocaesium was obtained from Amersham International PLC ).

Nuclide	$E_\gamma$ keV	BKGR	$L_C$		$L_D$		$L_Q$ Bq
			cpm	Bq	cpm	Bq	
$^{137}\text{Cs}$	662	0.07	0.17	7.0	3.1	127	4167
$^{134}\text{Cs}$	604	0.07	0.16	6.27	3.1	117	3847
	795	0.06	0.14	6.88	2.9	148	4951
$^{40}\text{K}^*$	1460	0.07	0.16	0.49	3.1	9.3	31

**Table.5.8.5 Chest sections of different phantoms containing a homogenous radionuclides using  $127\text{cm}^3$  Ge-detector.**

\* Units: gramme of potassium.

The results are set out in Table 5.8.5.

The limits of detection for  $^{134}\text{Cs}$  and  $^{137}\text{Cs}$  are similar and in the range 120- 150 Bq. This can be compared with the corresponding values of 25 Bq obtained by NaI(Tl) whole-body counting using a counting time of 25 minutes. The critical level for  $^{40}\text{K}$  is equivalent to 15mg of potassium while 1gm can be detected with 95% confidence after 2 hours counting.

### 5.9 Measurements with a low energy photon n-type planar germanium detector.

For the measurement of low energy photons experiments were carried out with an n-type germanium planar detector designed for the purpose and operating over the range of 12-700 keV as shown in Fig 5.18. Silicon detectors are also very useful over this energy range but were not available for appraisal.

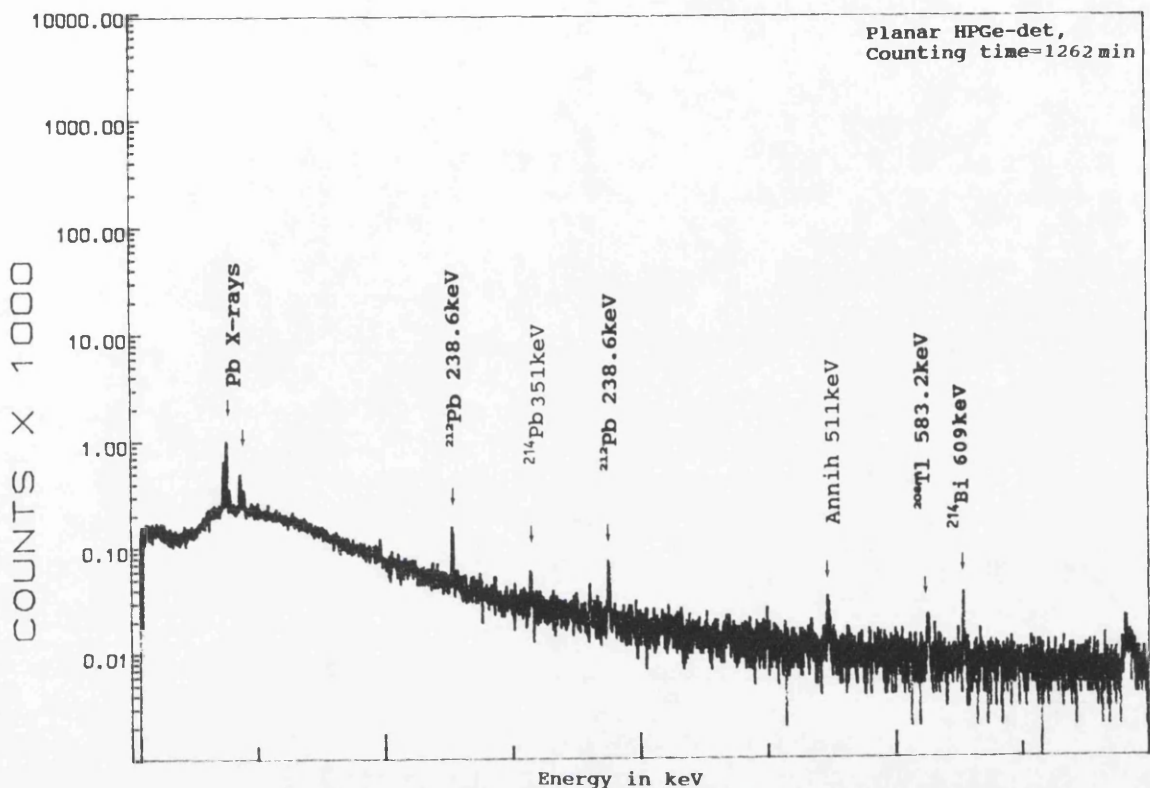


Figure 5.19 Background  $\gamma$ -ray pulse height spectrum using the planar germanium detector inside the shadow-shield.

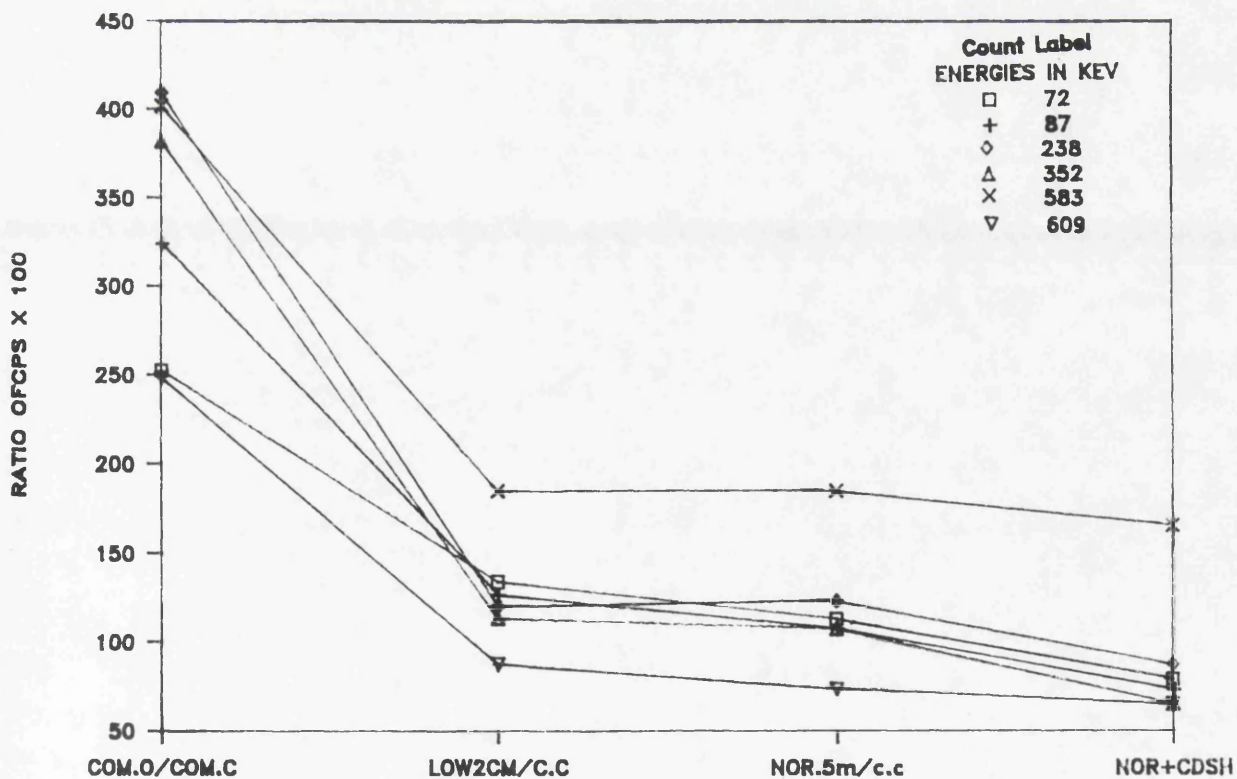


Figure 5.20 Effect of collimation on the detection levels of the main  $\gamma$ -ray energy peaks of the background using Ge-planar.

The eventual aim for low energy counting was to devise counting configurations for the head, the tibia and the kneecap where radionuclides such as americium-241 could be measured with low photon absorption through the minimum thickness of overlying tissue. A semi-portable low energy photon detector was therefore used to investigate suitable arrangements for this type of partial body counting. Using small lead collimator rings around the crystal housing, it was possible to examine various detector positions (note that COM.O  $\equiv$  complete open, COM.C  $\equiv$  complete closed, LOW2cm  $\equiv$  detector lowered by 2cm, NOR.5cm  $\equiv$  detector in normal position of .5cm, C.C  $\equiv$  complete closed and CDSH  $\equiv$  cadmium sheet over detector) as shown in Figure 5.20. It is seen clearly that the detector crystal is very easy to shield and the detected background levels did not change significantly as the collimation levels changed. It can also be seen that the low energy peaks are well detected in contrast to the p-coaxial-type detector which is used for the high energy range. The low energy tail of the gamma spectrum is shown quite clearly with high resolution.

This detector was fitted with a small dewar of capacity 1.2 litres of liquid nitrogen and so its utilization was limited to short background counts on a daily basis only.

The detector was inserted from the upper area of the top shielding through an aperture in the roof cover facing the lower detector cryostat. Because of the short length of the crystal housing its movement inside the shielding configuration was limited. It was connected to the same electronic equipment that shown in Figure 5.2.

### 5.10 Measurement of standard sources.

A number of standard sources were counted using the planar germanium detector under the shadow shielding arrangement. The respective  $\gamma$ -ray pulse height spectra for each of them is shown below.

From the above spectra the lower X-ray energies of plutonium-239 and americium-241 can be seen clearly and separately. Figure 5.22 presents the  $\gamma$ -ray spectrum obtained when three standard point sources of  $^{241}\text{Am}$ ,  $^{57}\text{Co}$  and  $^{137}\text{Cs}$  were counted simultaneously.

All the main energy peaks of three isotopes are clearly identifiable. It should be noted that the 661.6 keV of  $^{137}\text{Cs}$  is the highest energy range that can be measured by this detector with any usefulness with the gain settings used.

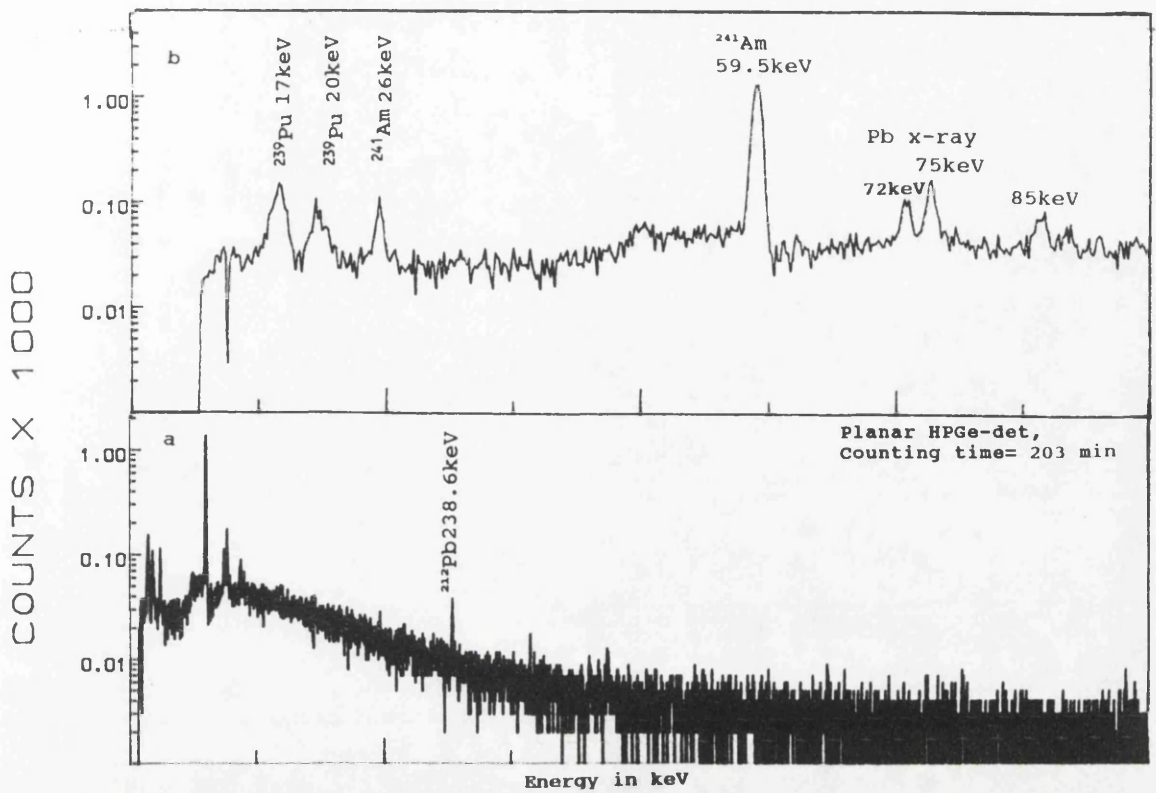


Figure 5.21 (a) Normal  $\gamma$ -ray spectrum of mixed alpha source of  $^{241}\text{Am}$ ,  $^{244}\text{Cm}$  and  $^{239}\text{Pu}$ .  
 (b) Expanded view of the lower end of same spectrum.

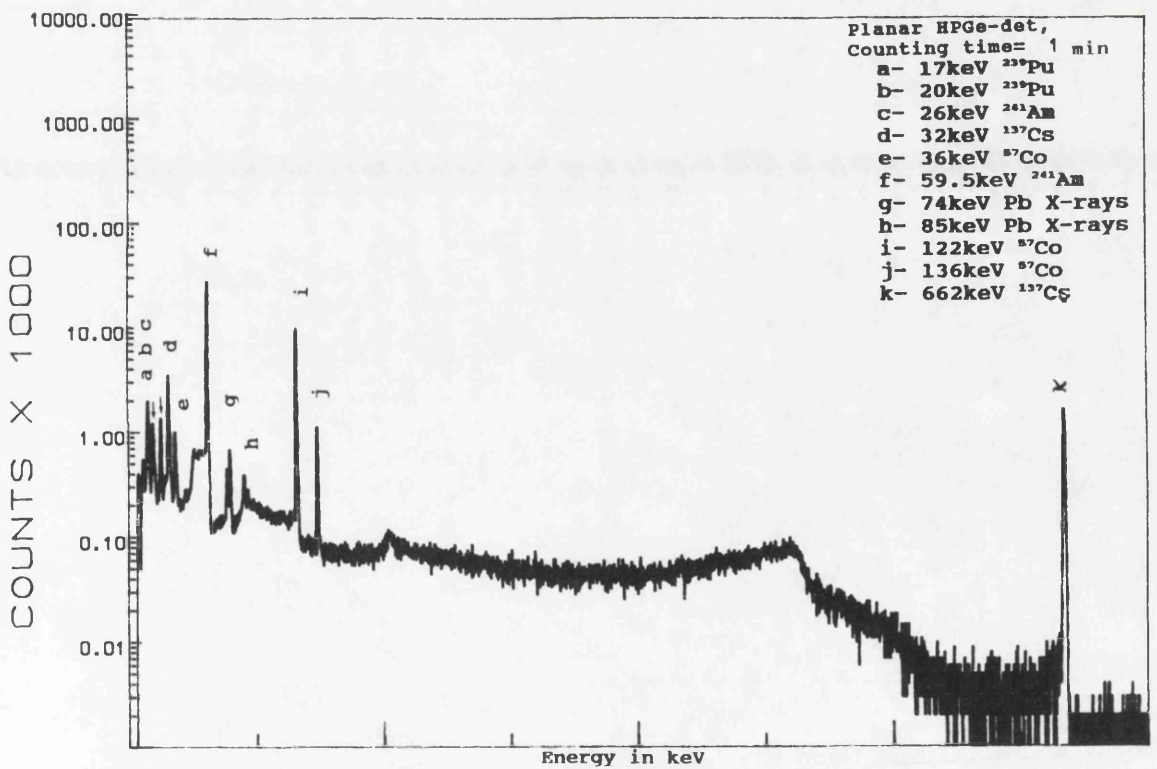


Figure 5.22 Gamma-ray spectrum of  $^{241}\text{Am}$ ,  $^{57}\text{Co}$  and  $^{137}\text{Cs}$ .

### 5.11 Calculated sensitivity and limits of detection.

Using the collected data from the measured standard sources and using equations 8, 9 and 11 from chapter 3, the background, standard deviation, critical level and minimum detectable activity were calculated and tabulated as follows;

Table 5.10.1 shows the calculated values for background sensitivities, critical level, the minimum detectable activity and the determination limits of the gamma energy peaks of the mixed alpha source. The lowest detectable quantity of activity for the 59.5 keV peak from  $^{241}\text{Am}$  is about 11 Bq while the critical limit is about 2Bq. For the lower energy  $^{241}\text{Am}$  peaks the sensitivity seems to be offset because of the low rate of emission and the possible absorption by air and other material.

ENERGY keV	BKGR cpm	$\sigma_{\text{BKGR}}$ cpm	cpm/ Bq	$L_C$ 2hr Bq	$L_D$ 2hr Bq	$L_D$ 2hr Bq
17	18	0.387	0.056	16	81	1850
20	14	0.342	0.029	27	143	3341
26.35	7	0.242	0.022	28	174	4551
59.54	25	0.456	0.482	2.2	11	208

**Table 5.11.1** The calculated background standard deviation and all the other detection parameters for mixed PuAmCm-source for two hour counting time.

## **CHAPTER 6**

## Chapter 6

### Finalised design criteria.

#### 6.1 Simplistic comparison of the Ge and NaI(Tl) for body counters detectors on a volume, cost and peak-to-Compton ratio basis.

From the dimensions of the NaI(Tl) detector crystal used in the whole-body monitor the volume was calculated to be 6.605 litres. The body monitor utilized two crystals of the same dimensions so the total detector volume was 13.21 litres. The 127cm<sup>3</sup> germanium detector used in these studies has an efficiency of 30% relative to the efficiency of a (7.6cmx7.6 cm) NaI(Tl) detector which in turn has a volume of 0.34 litres.

The volume ratio of the detectors is therefore calculated to be  $(13.21/0.345) = 38.3$  times. Because of the 30% relative efficiency of the detector the number of these detectors on this basis which would provide the sensitivity equivalent to that of the present dual detector (NaI) monitor would therefore be given by  $(3.3 \times 38.3) = 127$  germanium detectors. A simple cost comparison can be made since NaI(Tl) crystals cost about £18,000 each at current prices so for two it would be £36,000. The cost of a 30% germanium detector is about £10,000 so it follows that 127 such detectors would cost £1,270,000. The difference in cost is obvious.

However, when considering the superior energy resolution of the 30% germanium detectors and taking into account the different peak-to-Compton (P/C) ratios, the above cost differential can be offset to a large extent. The P/C values for a NaI(Tl) detector are about 6 whereas they are about 50 for a germanium detector. Hence the ratio for P/C values of the two detectors becomes  $(50/6) \approx 8$ . This means that in the germanium detectors the distribution of event between the photopeak and the Compton continuum is approximately 8 times better than that of the NaI(Tl) detectors. This compensates substantially for the inferior sensitivity value of germanium detectors. Therefore, when comparing the sensitivity of both detectors roughly 8 times fewer germanium detectors than have been calculated earlier would be necessary on the basis of sensitivity factors alone i.e about 16 detectors of 30% relative efficiency. Since it is possible to obtain Ge-detectors with relative efficiencies of

100% or more, a further factor of 3 can be applied so that around 5 Ge-detectors with 100% efficiency could give at least an equivalent performance to the large crystal body monitor costing approximately 5 times the sodium iodide cost. This brief analysis illustrates clearly that it is possible to contemplate developing a whole-body monitor based mainly on the use of germanium detectors with the advantages of high resolution which they offer.

## **6.2 Optimisation of a shield.**

The best values for the height and length of the shielding configuration were reached after a complete investigation of the various factors affecting the background measurements had been carried out. The shadow-shielding arrangement arrived at, shown in Fig 5.3 and redrawn in Fig 6.1 took into consideration the compromise between the lowest possible background contribution and the minimum degree of claustrophobic effect on the subject to be measured. Within the volume above the detector and under the shielded space, a stationary or scanning bed arrangement can be used to measure the whole body or different organs of the body by suitable positioning. It has to be noted that because of this shielding configuration and the collimation used, there is no direct unshielded path between the germanium detector crystal and the natural radiation of the building material or that emitted by other sources in the vicinity of the room.

The final configuration of the shielding assembly expressed as (T14W13), represents 14x10cm thick lead bricks (140cm) for the roof and 13 similar bricks for the side walls (130cm).

## **6.3 Comparison of the performances of the Ge and NaI(Tl) detectors relevant to body counting.**

### **6.3.1 A quantitative comparison of measured spectra.**

In order to study the NaI(Tl) background spectrum and to assess its detection capabilities it is of interest to compare it with that obtained with the 30% germanium detector. Figures 4.2 and 5.3 show separate  $\gamma$ -ray pulse height spectra obtained from the upper NaI(Tl) detector of the whole body counter and from the 30% coaxial hyper-pure germanium detector respectively. The two background spectra were collected for about the same length of time (65 hours) and there are significant differences which can be deduced.

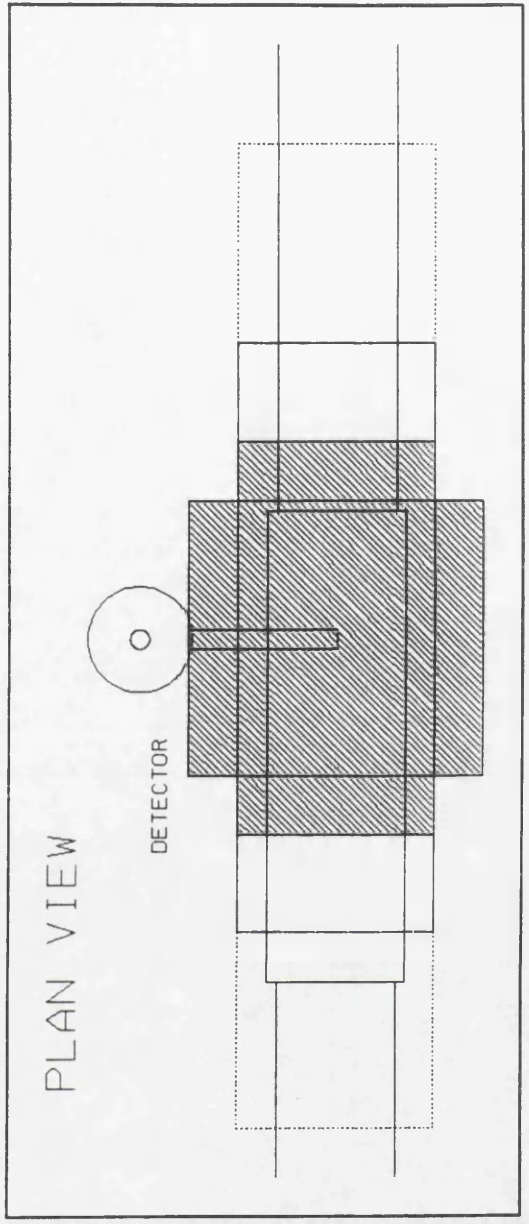
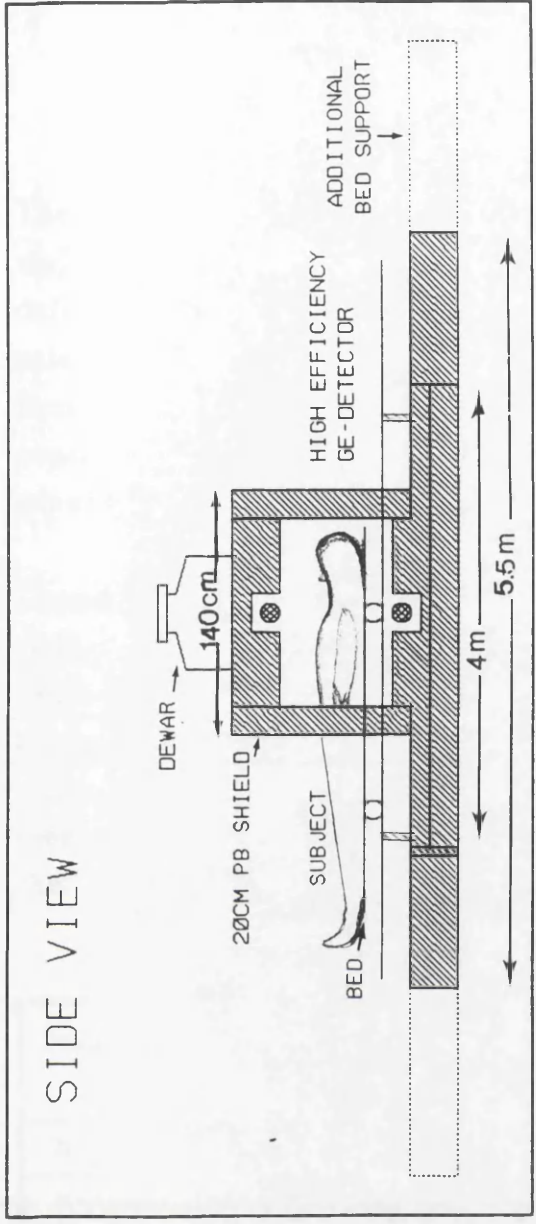
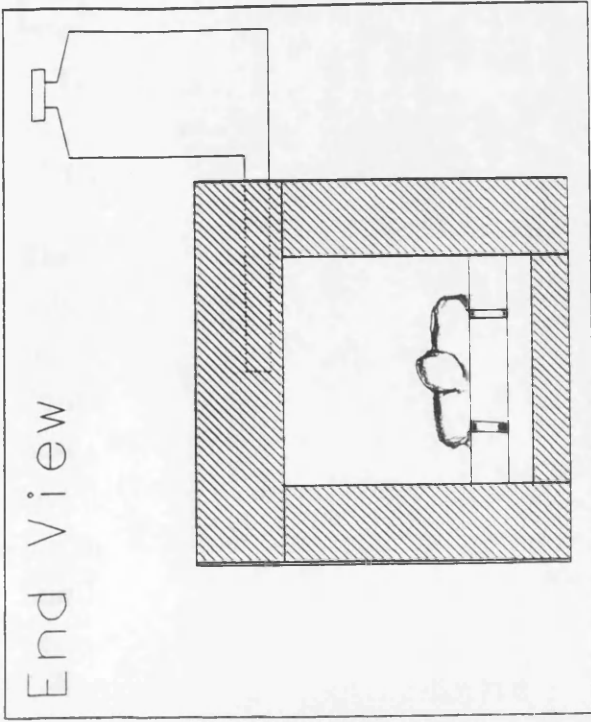


**Figure 6.1** Different views of the final shielding design and configuration suggested for the germanium whole-body monitor.

The first obvious difference is the shape and the highly resolved nature of the major background peaks from the Ge spectrum. These contrast with the ill-defined and poorly resolved peaks in the large volume NaI(Tl) detector. In the case of the Ge spectrum all the high yield background peaks are clearly separated from each other and from the Compton continuum in contrast to the Compton continuum-dominated NaI(Tl)  $\gamma$ -ray spectrum. This is a direct result of the superior energy resolution of the Ge detector.

Consequently, NaI(Tl) detectors are poor for measuring a mixture of different radionuclides when accurate quantification and positive identification of each radio-nuclide is required. This is because every additional peak compounds the background of all the other nuclides in the spectrum reducing the detection sensitivity. However it must be noted that, due to the smaller volume of the Germanium detector crystals their detection sensitivity is significantly lower than the NaI(Tl) detector crystals as demonstrated in Table 6.1.

Nuclide	$E_{\gamma}$ keV	Sens. cpm/Bq		$L_C$ Bq		$L_D$ Bq		$L_O$ Bq	
		NaI	Ge	NaI	Ge	NaI	Ge	NaI	Ge
$^{214}\text{Bi}$	351	0.639	0.04	4.0	3.0	57	45	779	1459
$^{214}\text{Bi}$	609	0.989	0.05	2.3	3.0	53	57	779	1887
$^{40}\text{K}^*$	1460	3.26	0.33	0.6	0.5	2.0	9.3	30	306

**Table 6.1 Comparison of the main detection parameters between the upper NaI(Tl) detector of the whole-body counter and the 127cm<sup>3</sup> Ge-detector using background spectra.**

\* Units: gramme of potassium.

These comparative data were obtained from measurements of the background using both types of detectors. They show that the calculated critical limits are similar for the main background  $\gamma$ -ray peaks. Also the minimum detectable limits are closely related for the two bismuth photon energies whereas for potassium-40 the level for NaI(Tl) is much lower, which makes it much superior.

At the same time the determination limits at 95% confidence are much higher for the germanium detector showing about a 10-fold difference.

Similarly it is useful also to compare the performance of the NaI(Tl) and germanium detectors for measuring thorium. The results obtained from

measurements on  $^{232}\text{Th}$  are presented in Table 6.2. It can be seen that in both detectors the  $L_C$  is about the same whereas  $L_D$  and  $L_Q$  are higher for the germanium detector.

As emphasised earlier these values are representative of the "ideal" geometry conditions. Therefore for more realistic counting geometries the actual performance achieved would probably be poorer in both cases. In relation to the quantities which it might be necessary to measure in the body these parameters are also very high and would need to be considerably improved.

$E_\gamma$ keV	Sen. NaI	cpm/mg Ge	$L_C$ NaI	mg Ge	$L_D$ NaI	mg Ge	$L_Q$ NaI	mg Ge
238	1.93	0.39	1.21	1.25	3.8	9.4	53	255
338	0.47	0.08	4.46	4.54	15	44.3	215	1299
583	0.88	0.13	2.38	2.03	7.8	25.6	116	794
727	0.28	0.03	6.66	7.46	23	123	364	4001

**Table 6.2** Comparison of the main detection parameters between the upper NaI(Tl) detector of the whole-body counter and the 127cm<sup>3</sup> Ge-detector using 60mg of  $^{232}\text{Th}$ .

To complete this comparison Table 6.3 presents the measured and the calculated detection parameters for the detection of uranium by each of the two detectors. It appears that the germanium detector has a much lower critical limit especially for the low energy 93 keV  $\gamma$ -ray peak; being about five times better. Also the detection limit is about half that obtained for the NaI(Tl) detectors.

$E_\gamma$ keV	Sen. NaI	cpm/mg Ge	$L_C$ NaI	mg Ge	$L_D$ NaI	mg Ge	$L_Q$ NaI	mg Ge
93	144	154	15	2.7	49	23	708	650
186	129	67	18	5.9	56	52	791	1495
766	131	5	19	37	58	686	779	22275
100	230	10	10	19	30	309	442	10011

**Table 6.3** Comparison of the main detection parameters for the upper NaI(Tl) detector of the whole-body counter and the 127cm<sup>3</sup> Ge-detector for a one-gramme uranium source.

However, the 95% confidence limit of determination is higher for the Ge-detector especially at higher energies. It is clear that under the present circumstances both detectors do not in any way meet the requirement for the detection of the natural uranium in the human body. In "Reference Man" the average mass of uranium is 90  $\mu\text{gm}$ .

However with the latest germanium crystal production technology present detectors have sufficient sensitivity to detect, identify and even quantify the above mentioned levels of radionuclides or a mixture of them in any matrix in a manner that cannot be matched by NaI(Tl) or phoswich detectors. Some newly developed germanium detectors have a relative efficiency of 80% which increases their detection capability tremendously.

For high sensitivity detection and measurement of low energy levels, NaI(Tl) detectors usually require a more complete type of shielding arrangement such as an expensive steel room or a highly massive shadow shield. In contrast, for germanium detectors, although shielding is still required the quantities necessary are not as extensive as those for NaI(Tl) detectors due largely to the fact that photomultiplier assemblies often have to be accommodated in the latter case.

### 6.3.2 Potassium-40

The contribution and effect of  $^{40}\text{K}$  gamma rays on the measured radiation background can not be overemphasised, because of its unavoidable influence on body measurements. The average adult male contains about 140gm of potassium, which means that the presence of potassium-40 will offset considerably the measured values of the minimum detectable activity. For this reason this gamma-ray energy peak has been thoroughly investigated under the different shielding conditions.

From Fig 6.2. which represents the observed count rate reduction along with the calculated ( $\pm$ ) standard deviation of the  $^{40}\text{K}$   $\gamma$ -ray energy peak and the different collimation thickness, it is seen that there was a minimal reduction of counts between 17-20mm of collimator thickness and no decrease at all in the measured counts between 20-22mm of collimation. It is also noted that there is a noticeable decrease of counts beyond 30mm but this is not an ideal length of collimation for the required conditions as the detector should preferably be as close as possible to the measured person.

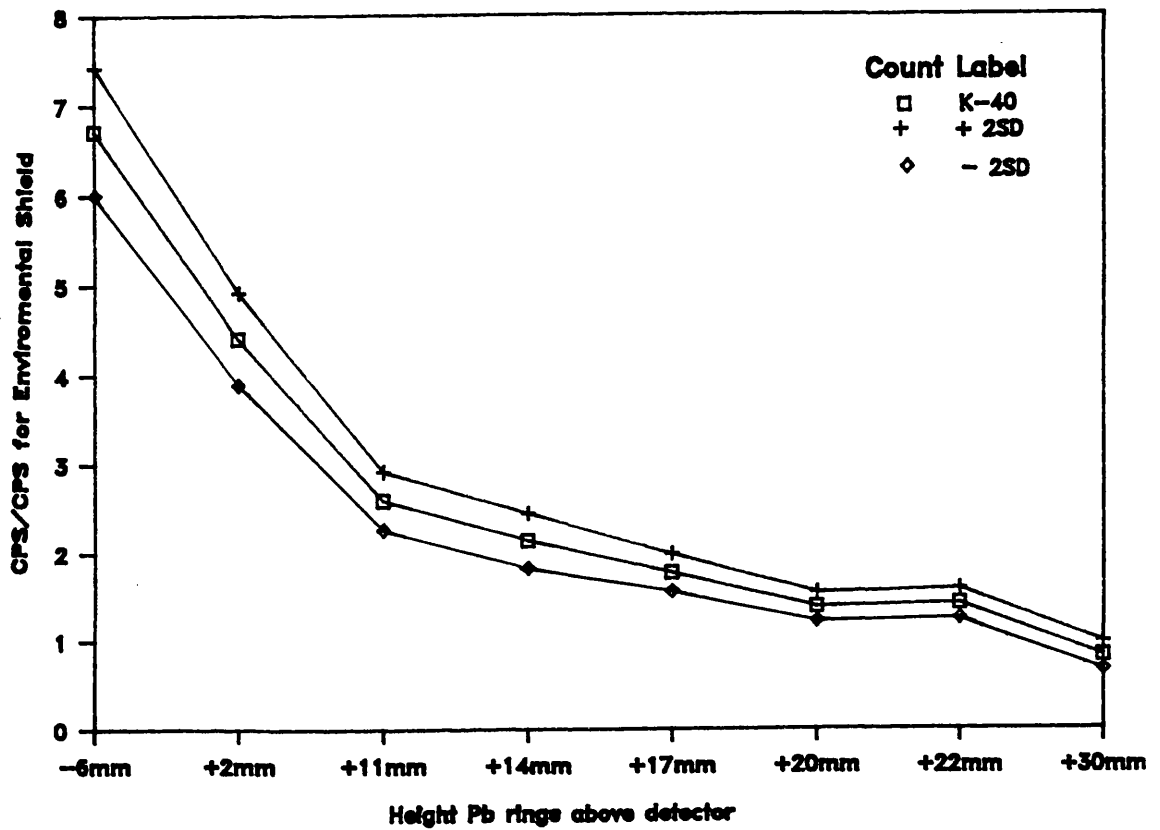


Fig 6.2  $^{40}\text{K}$  count rate vs collimation depth for the final shielding configuration.

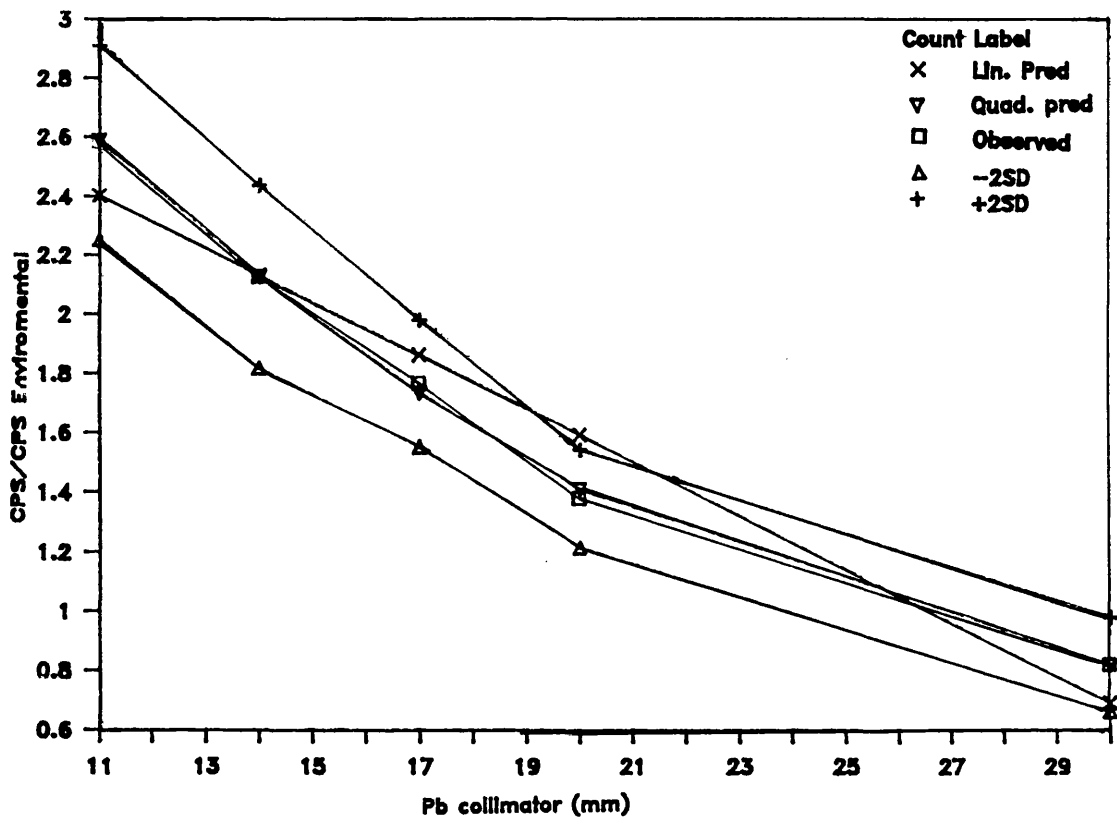


Figure 6.3  $^{40}\text{K}$  observed and mathematical prediction models for collimation thickness.

Using the computer program Lotus 1-2-3 (Lotus manual,1985) a regression analysis was performed on initial data points in terms of the ratios of counts observed at different collimator heights to those with the complete closed shielding arrangement. Linear, quadratic and cubic formulae were used and the slopes and intercepts of the best fitting lines were determined for the various measurement points. From these regression analysis it is seen that the linear and quadratic prediction regression analysis curves that the predicted reduction values for  $^{40}\text{K}$ , shown in Figure 6.3, coincides very well with the observed experimental decline in Figure 6.2. and within the 95% confidence limit ( $2\sigma$ ). Which indicates the good reliability of its statistical accuracy.

For the purpose of body monitoring therefore it was considered that collimation between 17mm and 22mm could be taken as a suitable operating condition, thus bringing the detector as close as possible to the measured part of the body.

In practice the detector would probably be collimated to some extent within the overall shield, one factor being that this would help to reduce the  $^{40}\text{K}$  background contribution from the measured subject by effectively shielding the extremities not immediately within the field of the detector.

In the Figure 6.3 the regression formula used was :

$$Y=B_0+B_1X+B_2X^2$$

Where;  $B_0 = 1.0106$  ,  $B_1 = 8.603.10^{-4}$  ,  $B_2 = 2.14.10^{-5}$ ,  
and X is the percent dead time used.

Use of the available computer summation program could make the measurement time on a human subject more acceptable and amenable, since short periods of measurement could be taken on the same subject and the separate spectra then could be summed together in order to get best sensitivity. Since the summed peak spectra contain a higher number of counts representing more information, the "signal-to-noise" ratio or peak-to-background ratio should be improved, over a signal spectrum, making the measurement of very small activities more feasible. The same program could be used on a large number of people in order to calculate the committed dose equivalent.

#### 6.4 The utilisation of the Planar Ge-detector.

From the data presented regarding the planar germanium detector, it seems that it is very efficient for the detection and identification of low energy radionuclides. Therefore it would be very useful to incorporate at least two detectors of this type in the new whole-body counter to give a practical counting arrangement. As mentioned in 5.8 ( page 92), bone seeking radionuclides such as  $^{241}\text{Am}$  a contaminant of plutonium which results from the  $\beta$ -decay of  $^{241}\text{Pu}$  ( $t_{1/2} = 14\text{a}$ ) can be best measured by counting over bony areas where the overlying tissue is minimised. Such areas where there is a bulk of bone are the skull, the tibia and the knees and semi-portable Ge-detectors could readily be positioned over these areas close to the surface. For incorporation into a shadow-shield body counting arrangement it is suggested that a lead "castle" could be built in such a way that the head of a supine subject on the main bed of the monitor could be positioned inside it with enough space for two planar detectors to be located around the skull. For measurement of the tibia the subject could be placed in a sitting position with the legs positioned inside the "castle" with the detectors placed over them.

From the detector data obtained in Table 5.11.1. the detection limit for  $^{241}\text{Am}$  is 11 Bq for a two hour counting time. With a second detector this could be reduced, roughly by a half or with larger counting times, obtained by summing repeated counts, several factors of reduction could be possible. The ability to measure  $^{241}\text{Am}$  in the Bq range, even with poorer statistics would be of considerable use for body monitoring in relation to environmental studies of this radionuclide and its association with plutonium.

#### 6.5 Conclusions and general remarks.

It has been shown that the components of the measured background radiation are 30% from cosmic radiation, 60% from the measured subject and 10% from unidentified sources. It follows that when measuring a human subject about two-thirds of the measured background is due to the presence of body potassium. Therefore, any further improvement of the shadow-shield arrangement will not increase significantly the sensitivity for the measurement of the low energy actinides e.g plutonium-239. It is also obvious when examining equation 3.5 of chapter 3, that the background parameter is an important factor in order to lower

the minimum detectable activity of gamma radiation detectors. The natural background peaks have range of energies and form a multi-peak spectrum due to the presence of several radionuclides. Therefore one of the primary concerns when using scintillation or germanium detectors is to lower the background levels seen by the detector crystal especially for NaI(Tl) detectors.

The low resolution of NaI(Tl) detectors causes complete masking of low energy peaks due to the high Compton continuum from the higher energy photopeaks.

The high energy resolution of the germanium detector allows a smaller region of the background to be used under the photopeak. In turn, this results in a greater sensitivity of detection and lower interference from high energy  $\gamma$ -ray peaks when measuring a multi-gamma-ray peaks or a mixture of radionuclides.

In addition to the drawback of low energy resolution, the signal-to-noise ratio for NaI(Tl) detectors is also high which results in a high background from Compton scattering especially at low energies or in a mixture of radionuclides with various photon energies. This effect can distort the energy resolution and even mask a number of low energy peaks.

From the previous discussion it appears that the only method to resolve the background is by using detectors of high energy resolution. With recent advances in detector production technology high energy resolution detectors such as the short coaxial germanium detectors "LOAX" have become commercially available at more favourable prices. They have resolution values of about 350eV for the 5.9keV of  $^{55}\text{Fe}$  and about 610eV for 122keV of  $^{57}\text{Co}$ . This improvement in the energy resolution is almost two times better than that of the detectors used in this study. This increased resolution could effectively reduce the background for measuring low energy photons by a factor of almost two and therefore increase the detection sensitivity and lower the minimum detectable activity accordingly by almost 30%. Also higher efficiency with larger (Ge-crystals) germanium detectors would enhance the detection capability even further.

Hence, it is recommended that a number of these "LOAX" and the high efficiency (80%) germanium detectors be purchased and used in a shadow-shield monitor similar to that described in these studies. Such a facility would possibly permit low-level measurement of activities in accordance with the latest national and international recommended levels for both classified workers and general public.

## **6.6 A proposed design for a high resolution whole-body monitor.**

The geometrical arrangement of the  $127\text{cm}^3$  germanium detector used for these experimental studies does not easily lend itself for use in a whole-body counter.

A better configuration would be for the detector to be mounted horizontally, so that it could be inserted into a suitable shield without having to utilise extra shielding to accommodate the liquid nitrogen container. Consequently a design based on this type of germanium detector monitoring is suggested and depicted in Figure 6.4. It can be seen that the detectors can easily be set up so as to be close to the subject either for static or scanning counting. Two or more detectors could be accommodated in the proposed shield but it is suggested that where only one detector is available this should be placed in the upper position, in order to obtain maximum shielding effect.

## REFERENCES

- Adams,E.; and Dams,R (1970). *Applied Gamma-Ray Spectrometry*,2nd Ed. 1970.
- Andreaco,M.S; Seymour,R.S and Zimmer,W.H.(1984). Evaluation of the Efficiency of HPGe Coaxial Detectors for Low Level In-Vivo Bioassay Applications, 6<sup>th</sup> International Congress of IRPA, Berlin, West Germany May 7-12,1984.
- ANSI N13.30;(1989). American National Standards Institute. 'Draft American National Standard for performance for radiobioassay'. New York. 1989
- Attix,F.H.(1986). *Introduction to Radiological Physics and Radiation Dosimetry*. Wiley, New York, NY 1986.
- Armantrout,G.A.; Bradley,A.E; Phelps, P.L. (1972). Sensitivity Problems in Biological and Environmental Counting *IEEE Tran.Nucl.Sci* 19(1)107, 1972.
- BEIR(1989)." Committee on the Biological Effects of Ionizing Radiations" , The Effects on Populations of Exposure to Low Levels of ionizing Radiation. National Academy press, Washington, 1989.
- Berger,C.D; Goans,R.E.(1981) A Comparison of the NaI-CsI Phoswich and a Hyperpure Germanium Array for In Vivo Detection of actinides' *Health. Phys.*40 (1981) 535.
- Cember, H 'Introduction to Health Physics' 2nd ed., Pergamon Press, Elmsford, NY 1983.
- Black,Sir Douglas Report (1984). Investigation of the possible increased incidence of cancer in West Cumbria. Report of the independent advisory group. HMSO, London, 1984
- Boddy,K.; Robertson,I.; Mahaffy,M.E; Holloway.I.(1975). A High Sensitivity Dual-detector Shadow-Shield Whole-Body counter with "Invariant".
- Response for Total Body in-vivo Neutron Activation Analysis. *Phys.Med.Biol.* Vol 20, No.20, pp 296-304, 1974.
- Cohen,N.; Spitz,B.; Wrenn,M., (1977) Estimation of skeletal burden of "bone seeking" radionuclides in man from *in vivo* scintillation measurements

of the head. *Health.Phys.* 33 (1977) 431.

Cooper,J.A (1970) 'Factors Determining the Ultimate Detection Sensitivity of Ge(Li) Gamma-ray Spectrometers' *Nucl.Instrum.Methods. Vol 82, pp 273-277, 1977.*

Cooper,J.A (1971) 'Figures-of-Merit Measurement for Ge(Li) Detectors,' *Nucl.Instrum & Methods. 94, pp 289-296, 1971.*

Currie,L.A. (1968). Limit for Quantitative Detectors and Quantitative Determination. *Analytical Chemistry, Vol. No.3, 586-693. 1986.*

Debertin,K and Helmer, R.G. (1988). Gamma and X-ray Spectrometry with Semiconductor Detectors. 1988.

East,B.W; Robertson,I (1989). Measurement of radioactivity from Chernobyl in population groups in Scotland. Doe Report: Doe/RW/88.103. 1989.

East,B.W (1992). Private communication.1992.

EG&G Ortec (1988) Minigam<sup>TM</sup>II A34-BI. Basic Gamma-ray spectrometry analysis software manual. Version 3.0. 1988.

Falk,R.B., Tyree,E.H.; Wood,C.B. and Lagerquist,C.R. (1979). A system of high purity germanium detectors for the detection and measurement of inhaled radionuclides. *Advances in Radiation Protection Monitoring(proc.Int. Conf.,Stockholm, (1978) IAEA, Vienna (1979) 445.*

Fisenne,F.M; Perry.P.M; Decker *et al.*. The daily intake of uranium-234,235,238, thorium-228,230,232, and radium by New York residents. *Health Physics 53:357-363, 1987.*

Gibbons,P.E and Owens,R.B.(1971) 'Calculated Figures Of Merit for Planar and Coaxial Germanium Detectors,' *Nucl.Instrum & Methods 95, pp 551-555, 1971.*

Grubbe,E.H.(1933). Priority in the Therapeutic use of X-ray, *Radiology, Vol.XXI 1 July, 1933.*

Griffith,R.V; Dean,P.N; Anderson,A.L.; Fisher,J.C., (1978). A tissue-equivalent torso phantom for inter-calibration of *in vivo*, transuranic-nuclide

counting facilities. *Advances in Radiation Protection Monitoring ( Pro.sympo. Stockhlo, 1987) IAEA.Vienna (1979) 493.*

- Halm,H.L., Watt,M.; Bostock,I.; Campbell,J.L. *et al*, (1984). Background reduction in germanium spectrometers: materials selection, geometry and shielding. *Nucl.Instrum & Methods. 223(1984)420.*
- Harris,I (1991) private communication. Scottish Universities Research & Reactor Centre. 1991.
- Hofman,W.; Katz,R and Ehnxiang,Z. (1986). Lung cancer risk at low doses of alpha particles. *Health.Phys. Vol.51 (1986) 475.*
- Hughes, J.S; Shaw, K.D and O'Riordan,M.C. The radiation exposure of the UK population-1988.
- IAEA (1970) Directory of whole-body radioactivity monitoring. International Atomic Energy Agency STI/PUB/213, Vienna.
- Keyser,R.M; Twomey,T.R; and Wagner,S.E (1990). The benefit of Using Super Large Germanium Gamma-ray Detectors for the Quantitative Determination of Environmental Radionuclides EG & G Ortec.(1990)
- King,A., Scott,P.N., Disney,J.I, (1987). Comparison of sodium iodide and solid state detectors for the measurement of Lung-stored uranium, *Health Physics. 34 (1978) 34.*
- Knoll,G.F. (1979). Radiation Detection and Measurement. John Wiley & sons, New York N.Y
- Lochamy, T.C. (1976). The Minimum Detectable Activity Concept NBS. Sp 456. 1976
- Lotus 1-2-3 reference manual(1985).
- Mariscotti,M.A., (1967). A method for automatic identification of peaks in the presence of background and its application to spectrum analysis. *Nucl.Inst & Methods 50 (1967) 309.*
- Medvedev,Z. (1990). The Legacy of Chernobyl, Blackwell. NRPB report R227 March 1989.
- Minnema,D.M and Hudson,C.G (1981). A Comparison of Ge(Li) Detectors with different efficiency for Low Level General Purpose Counting.

- Morgan,K.Z and Turner,J.E.(1967). 'Principles of Radiation Protection,' John Wiley & sons, Inc, New York
- Morgan,K,Z. (1970). 'Maximum Permissible Levels of Exposure To Ionizing Radiation ' Radiation Dosimetry Vol.1 Proceedings of the International Summer School on Radiation Protection,' Sep, 21-30 , 1970
- Morsy,S.M., El-Assaly,F.M., Aloush,A.A (1971). Direct methods for the Assessment of plutonium-239 and uranium-235 Body Burdens. " Assessment of Radioactive Contamination in Man" Proceedings of IAEA Symposium 22-26 Nov., 1972 WENN and Blachard ,1971
- NRPB-GS6 (1987). O'Riordan, M.C.; James, A.C.; Green, B.M.R; and Wrixon, A.D. Exposure to Radon Daughters in Dwellings. Jan 1987.
- Sikl,H. (1950). The Present Status of Knowledge About the Jachymou Disease (cancer of the Lungs in the Miners of Radium Mines),
- Spitz,H.B.; Buschbom,R.L.; Rieksts,G.A and Palmer, H.E (1990). A New Method for Analyzing High-Resolution Spectra from Whole-Body Counter in-vivo Measurements.*Health.Phys.Vol 49.No 6 pp 1085-1096, 1990.*
- Sumner,D.; Wheldon,T.; Watson,W., (1991) Radiation Risk, 3rd edition, The Tarragon press. Glasgow.
- Palmer,H.E; Rieksts,G.A and Lynch,T.P.,(1991). Performance of an Array of Large-Volume Germanium Detectors for Whole-body Counting.*Health Phys. Vol. 61. No.5(Nov) pp 595-600, 1991.*
- Palmer,H.E.; Rieksts,G.A. (1984). Ge Detectors for measurement of photon emitters. *Health Phys. 47, 569-578. 1984.*
- Palmer,H.E.; Rieksts,G.H. (1985). High purity Planar Germanium detectors for in-vivo measurement of Uranium and Transuranium Radionuclides. " Assessment of Radioactive Contamination in Man 1984. Proceedings of a symposium, Pari, 19-23 November 1984. IAEA.

RWMAC Report (1990). Radioactive waste management advisory committee annual report. 1990.

Traub,P.J and Robinson,A.V. The Sources of uncertainties associated with internal dose calculation.

Toohy,R.E.; Keane,A.T; Rundo,J.(1983) Measurement techniques for radium and actinides in man at the centre for human radiobiology.*Health Phys. Vol. 44, supp. No1. pp 323-341, 1983.*

ICRP2(1959) International Commission on Radiobiological Protection (ICRP) "Recommendation of the International Commission on Radiological Protection," *Health Phys.,Vol.3, P.1* (ICRP Publication 2, Report of Committee II on permissible Dose for internal Radiation, Pergamon Press, New York (1959)). 1960.

ICRP23 (1975) International Commission on Radiological Protection (ICRP) 1975, "Report of the Task Group on Reference Man", ICRP Publication 23, Pergamon press, Oxford.

ICRP30 (1979) International Commission on Radiological Protection (ICRP), 1979. "Limits for Intake of Radionuclides By Worker" ICRP Publication 30, Part I. Pergamon press.Oxford.

ICRP26 (1977). International Commission on Radiological Protection (ICRP) 1977. "Recommendations of the International Commission on Radiological Protection ICRP Publication 26 , Pergamon Press, Oxford

Urquhart,J.O; Black,R.J; Nuirhead;M.J; Sharp,L; Maxwell,M; Eden,O.b; Jones, D.A. Case-control study of Leukaemia and non-Hodgkin's Lymphoma in children in Caithness near the Dounreay nuclear installation. *Br.Med.J. 302;687-692; 1991.*

UNSCEAR (1986),(1988). " United Nations Scientific Committee on the Effects of Atomic Radiation", Reports to the General Assembly, United Nations, New York. N.Y

Zimmer,W.H. Whole Body Counting with a Gamma Detectors, EG & G Ortec/PSD#16 Zimmer, W.H. (1977). System Application Studies-Minimum Detectable Activity and Peak Background Correction,

EG&G Ortec/PSD#4 December 1977. Zimmer, W.H. What Effects A  
Gamma Spectrum EG&G Ortec/PSD#9.